

Echo statistics associated with discrete scatterers: A tutorial on physics-based methods

Timothy K. Stanton, Wu-Jung Lee, and Kyungmin Baik

Citation: *The Journal of the Acoustical Society of America* **144**, 3124 (2018); doi: 10.1121/1.5052255

View online: <https://doi.org/10.1121/1.5052255>

View Table of Contents: <https://asa.scitation.org/toc/jas/144/6>

Published by the [Acoustical Society of America](#)

ARTICLES YOU MAY BE INTERESTED IN

[A mathematical model of bowel sound generation](#)

The Journal of the Acoustical Society of America **144**, EL485 (2018); <https://doi.org/10.1121/1.5080528>

[Macroscopic observations of diel fish movements around a shallow water artificial reef using a mid-frequency horizontal-looking sonar](#)

The Journal of the Acoustical Society of America **144**, 1424 (2018); <https://doi.org/10.1121/1.5054013>

[Multiplicative and min processing of experimental passive sonar data from thinned arrays](#)

The Journal of the Acoustical Society of America **144**, 3262 (2018); <https://doi.org/10.1121/1.5064458>

[Performance comparisons of array invariant and matched field processing using broadband ship noise and a tilted vertical array](#)

The Journal of the Acoustical Society of America **144**, 3067 (2018); <https://doi.org/10.1121/1.5080603>

[An Empirical Mode Decomposition-based detection and classification approach for marine mammal vocal signals](#)

The Journal of the Acoustical Society of America **144**, 3181 (2018); <https://doi.org/10.1121/1.5067389>

[Putting Laurel and Yanny in context](#)

The Journal of the Acoustical Society of America **144**, EL503 (2018); <https://doi.org/10.1121/1.5070144>



CAPTURE WHAT'S POSSIBLE
WITH OUR NEW PUBLISHING ACADEMY RESOURCES

Learn more 



Echo statistics associated with discrete scatterers: A tutorial on physics-based methods

Timothy K. Stanton^{a)}

Department of Applied Ocean Physics and Engineering, Woods Hole Oceanographic Institution,
Mail Stop #11, Woods Hole, Massachusetts 02543, USA

Wu-Jung Lee

Applied Physics Laboratory, University of Washington, 1013 Northeast 40th Street, Seattle,
Washington 98105, USA

Kyungmin Baik

Center for Medical Convergence Metrology, Division of Chemical and Medical Metrology,
Korea Research Institute of Standards and Science, Daejeon 34113, Republic of Korea

(Received 8 August 2017; revised 7 August 2018; accepted 11 August 2018; published online 6 December 2018)

When a beam emitted from an active monostatic sensor system sweeps across a volume, the echoes from scatterers present will fluctuate from ping to ping due to various interference phenomena and statistical processes. Observations of these fluctuations can be used, in combination with models, to infer properties of the scatterers such as numerical density. Modeling the fluctuations can also help predict system performance and associated uncertainties in expected echoes. This tutorial focuses on “physics-based statistics,” which is a predictive form of modeling the fluctuations. The modeling is based principally on the physics of the scattering by individual scatterers, addition of echoes from randomized multiple scatterers, system effects involving the beampattern and signal type, and signal theory including matched filter processing. Some consideration is also given to environment-specific effects such as the presence of boundaries and heterogeneities in the medium. Although the modeling was inspired by applications of sonar in the field of underwater acoustics, the material is presented in a general form, and involving only scalar fields. Therefore, it is broadly applicable to other areas such as medical ultrasound, non-destructive acoustic testing, in-air acoustics, as well as radar and lasers. © 2018 Author(s). All article content, except where otherwise noted, is licensed under a Creative Commons Attribution (CC BY) license (<http://creativecommons.org/licenses/by/4.0/>). <https://doi.org/10.1121/1.5052255>

[JFL]

Pages: 3124–3171

TABLE OF CONTENTS

LINKS TO SOFTWARE USED TO CREATE FIGURES.....	3125
I. INTRODUCTION	3126
II. KEY ELEMENTS OF ECHO STATISTICS.....	3127
A. Interfering signals.....	3128
B. Stochastic scattering from a single scatterer.....	3128
C. Beampattern effects	3129
III. EXPLOITING ECHO STATISTICS FOR VARIOUS APPLICATIONS	3129
A. Inferring information on scatterers.....	3129
1. Inferring number of scatterers.....	3130
2. Discriminating between echo from scatterer of interest and background.....	3130
3. Removing beampattern effects to isolate properties of resolved scatterer.....	3130
4. Discriminating between different types of aggregations of scatterers	3131
5. Further considerations.....	3131

a. Directionality of sensor beam improves inference techniques.....	3131
b. Noise and “tail” of echo PDF.....	3131
B. Predicting error or uncertainty in signal magnitude.....	3131
IV. KEY EQUATIONS FOR SCATTERING AND ASSOCIATED STATISTICAL PROCESSES... ..	3131
A. Deterministic scattering.....	3131
1. Single scatterer	3132
2. Multiple scatterers.....	3132
B. Probability density function and related quantities	3133
1. Definitions and equations.....	3133
2. Calculating PDFs: Directly and from Monte Carlo simulations	3133
3. Non-uniform spacing of bins.....	3134
4. Normalization.....	3134
a. Vertical scale.....	3134
b. Horizontal scale.....	3134
C. Fundamental statistical processes relevant to echo statistics	3134
1. Randomizing the deterministic scattering equations.....	3134

^{a)}Electronic mail: tstanton@whoi.edu

2. Function of a single random variable....	3135	4. Beampattern PDF for entire beam (axisymmetric transducer, uniformly distributed scatterer)	3149
3. Function of two random variables	3135	5. Beampattern PDF for 2D and 3D distribution of scatterers	3150
4. Product of two random variables	3136	6. Echo PDF for different types of individual scatterers in axisymmetric beam	3151
5. Sum of random variables	3136	a. Point scatterer; main lobe only.....	3151
a. Method of characteristic functions. ..	3136	b. Rayleigh scatterer; mainlobe only...	3151
b. Monte Carlo simulations.....	3136	c. Complex scatterer; entire beam.	3152
6. Sum of infinite number of random variables (central limit theorem; Rayleigh PDF).....	3137	7. Beampattern PDF for non-axisymmetric beampattern, non-uniform distribution of scatterer.....	3152
V. IN-DEPTH TREATMENT OF ECHO STATISTICS: OVERVIEW	3137	a. Non-uniformly distributed scatterer..	3153
A. How to use this material for realistic signals/environments, and advanced signal/ beam processing	3138	b. Uniformly distributed scatterer.....	3153
B. Peak sampling, pulsed signals with boundaries, and beyond	3138	B. Multiple identical scatterers randomly located in beam	3153
VI. IN-DEPTH TREATMENT OF ECHO STATISTICS: NO BEAMPATTERN EFFECTS	3138	C. Multiple scatterers of different types and sizes.....	3156
A. Addition of random signals (generic signals; not specific to scattering)	3139	1. Split aggregation of type A and B scatterers—mixture PDF	3156
1. Arbitrary cases.....	3139	2. Interspersed aggregation of type A and B scatterers—coherent phasor sum	3157
2. Sine wave plus noise (Rice PDF).....	3139	3. Comparisons between echo PDFs from split and interspersed two-type aggregations	3157
3. Special distributions of N or a_i (K PDF).	3140	4. Many types of scatterers (general formulations)	3157
4. Adding independent realizations of the complex signal A	3142	VIII. SYSTEMS AND ENVIRONMENTS WITH MORE COMPLEXITY.....	3159
B. Complex scatterers with stochastic properties	3142	A. Pulsed signals (partially overlapping echoes)	3160
1. Point scatterer	3142	B. Object near a rough boundary.....	3161
2. Rayleigh scatterer	3142	C. Object(s) in a random waveguide.....	3162
3. Randomized prolate spheroid	3142	1. Some simple formulations	3163
a. Smooth boundary, fixed orientation. .	3142	2. Closed form solutions for limiting cases involving a saturated waveguide.....	3164
b. Smooth boundary, random orientation.....	3143	a. Small patch of scatterers.	3164
c. Rough boundary, random orientation.	3144	b. Extended patch of scatterers.	3165
4. Randomly rough objects with full range of roughness and circumferential/internal waves.....	3145	IX. DISCUSSION AND CONCLUSIONS	3165
a. Circumferential and internal waves (smooth boundary).....	3145	ACKNOWLEDGMENTS	3165
b. Front interface only: Small-to- intermediate roughness, Rice PDF. ..	3145	APPENDIX: GENERIC OR COMMONLY USED STATISTICAL FUNCTIONS	3166
c. Randomized circumferential and internal waves added to front interface echo; nulls and attenuation effects.....	3146	1. Rayleigh PDF.....	3168
VII. IN-DEPTH TREATMENT OF ECHO STATISTICS: WITH BEAMPATTERN EFFECTS	3146	2. Rice PDF.....	3168
A. Single scatterer randomly located in beam..	3147	3. K PDF.....	3168
1. Accounting for beampattern effects in echo PDF	3147	4. Weibull PDF.....	3168
2. PDF of spatial distribution of scatterer ..	3147	5. Log normal PDF	3168
3. Beampattern PDF for mainlobe only (axisymmetric transducer, uniformly distributed scatterer)	3148	6. Nakagami-m PDF (and related chi-squared and gamma PDFs).....	3169
a. Exact solution.....	3148	7. Generalized Pareto PDF.....	3169
b. Power law approximation for beampattern PDF.	3149		
		LINKS TO SOFTWARE USED TO CREATE FIGURES	
		The software used to produce all predictions in the fig- ures is in the supplementary material at https://doi.org/	

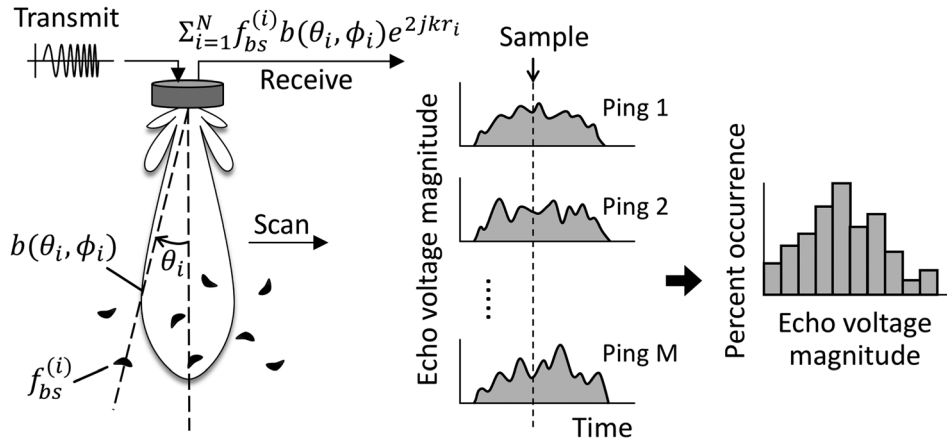


FIG. 1. Echoes fluctuate from ping to ping as the sensor beam scans across the scatterers. The resultant ensemble of echoes can be formed into a histogram, related to the probability density function of the echo magnitude. A simple direct-path geometry involving a homogeneous medium with no boundaries is illustrated. Key elements to echo statistics are illustrated—stochastic scattering ($f_{bs}^{(i)}$) from a single scatterer, random angular location (θ_i, ϕ_i) of scatterer within the sensor beam causing random modulation of the echo due to the beam pattern (b), and randomized interference caused by overlap of echoes from multiple random phase scatterers ($\sum \dots$). The statistics is formed over M pings to form a histogram of echo magnitudes in the far right graph. All of these terms are defined in Sec. IV.

10.1121/1.5052255. The software is also stored online (Lee and Baik, 2018), where it is subject to future revisions.

I. INTRODUCTION

Echoes, as measured through the receiver of an active monostatic sensor system, will typically fluctuate from ping to ping as the beam emitted from the system scans across a volume containing scatterers or as the scatterers in that volume move through the beam (Fig. 1). It is essential to understand the echo statistics for accurate interpretation of the scattering and for modeling system performance. Toward that goal, understanding the underlying physical processes that give rise to the fluctuations allows one to accurately predict and interpret the echo statistics. In the simplest case in which the propagation medium is homogeneous and there are no boundaries present (i.e., a “direct path” geometry), the fluctuations are due to a combination of several statistical processes: the interference between overlapping echoes when multiple scatterers are present, the random nature of the echoes from individual scatterers (not including beam-pattern effects), and the modulation of the echo due to the random location of the scatterer in the beam. Once the geometry is further complicated by heterogeneities in the medium and/or the presence of boundaries, the propagated signals will become refracted and/or rescattered, giving rise to more propagation paths that are potentially random and, in turn, also contributing to the fluctuations. This tutorial presents key concepts and formulations associated with predicting the echo fluctuations over a wide range of scenarios in terms of the physics of the scattering, system parameters, and signal theory.

The statistical behavior of echoes is important across a diverse range of active sensor systems and applications involving the use of either acoustic waves (such as with sonar, medical ultrasonics, or non-destructive testing) or electromagnetic waves (such as with radar or light) to study individual discrete scatterers, assemblages of scatterers, or rough interfaces that cause scattering. Understanding echo

statistics has been integral in interpreting radar clutter (Watts and Ward, 2010) and sonar reverberation and clutter (Ol’shevskii, 1978; Gallaudet and de Moustier, 2003; Abraham and Lyons, 2010), sonar classification of marine life and objects on the seafloor (Stanton and Clay, 1986; Medwin and Clay, 1998), medical ultrasound classification of human tissue (Eltoft, 2006; Destremes and Cloutier, 2010, 2013; Oelze and Mamou, 2016), and non-destructive ultrasound testing of materials (Li *et al.*, 1992). Within each of these areas, echo statistics are used in the detection and classification of scatterers, discriminating between scatterers of interest from clutter (i.e., unwanted echoes), estimating numerical density of scatterers, and determining the performance of sensor systems for use in detection and classification of scatterers. The studies of clutter involve characterizing the statistics of unwanted echoes from features or objects in the environment that have properties resembling the target of interest. The clutter may be due to the sea surface (radar/sonar/laser), marine life or seafloor (sonar), human tissue (medical ultrasound), or grains in solids (non-destructive testing).

The above applications have many elements of statistical theory in common. Those common elements are treated formally in Goodman (1985) and Jakeman and Ridley (2006). There are also notable differences between interpreting echoes from acoustic and electromagnetic systems, such as the presence of shear waves and polarization, respectively, which are summarized in Le Chevalier (2002). Differences in echo statistics between scalar fields (both acoustics and electromagnetic, ignoring shear waves and polarization, respectively) and those fields with polarization effects (electromagnetic only) are summarized in Jakeman and Ridley (2006).

While there has been much work conducted in the area of echo statistics, the focus has generally involved describing the variability of echoes through use of generic statistical functions whose parameters need to be determined from experimental data. Here, “generic” refers to those functions generally devoid of a physical basis and derived solely from

random signal theory, such as a Gaussian process. These generic functions include the Rayleigh, Rice, K, Weibull, log normal, and Nakagami-m distributions (App). Only under a narrow range of conditions can some of the generic functions be connected to the physics. There has been a much smaller set of studies in which the statistics were modeled from first principles, and hence being predictive, through a combination of the physics of scattering, sensor system parameters, and signal theory. To date, there has been no text or tutorial with a comprehensive coverage of physics-based phenomena.

This tutorial presents the fundamentals of echo statistics associated with an active monostatic sensor system, written in a manner that is readable by a wide audience. While much of the material is motivated by the use of sonar in underwater applications, the material is broadly applicable to other types of active acoustic systems used in various media including air, solids, and biological tissue, as well as to radar and lasers. Because of the generality of the treatment, the system used to transmit waves and receive the echoes will heretofore be referred to as a “sensor system” regardless of application and whether it involves acoustic or electromagnetic waves. The formulations describe scalar fields, which can be directly applied to either acoustic or electromagnetic signals in the absence of the presence of shear waves or polarization effects, respectively. Only brief reference is made to those latter effects.

The emphasis in this tutorial is on describing the statistics of the magnitude of the complex echo (or echo envelope) in terms of the physics of the scattering, sensor system parameters, and signal processing. More specifically, the emphasis is on *physics-based* methods, in contrast to the generic approaches referenced above. The methods are focused solely on “first-order statistics” which concern statistical properties of the signal at a single instant in time. Also, the material can apply to single beam (fixed or scanning) and multi-beam systems where the scatterer(s) in each case are randomly located in each beam.

Since there are too many combinations of types of systems, signal processing, and environments to adequately describe in a single paper, the material is focused on the fundamental aspects of echo statistics due to discrete scatterers that are not specific to any particular system, signal processing, or environment. The range of beamwidths, types of scatterers, and number of scatterers in the predictions illustrate the corresponding range of statistical behavior of the echoes from a wide range of system parameters and distributions of scatterers. However, the formulations are completely limited to (1) first-order statistics as described above, and are mostly limited to (2) narrowband signals that are long enough so that the echoes from the scatterers overlap significantly, (3) direct path geometries where there are no boundaries present, and (4) a homogeneous medium. Beyond those limited scenarios, examples are presented of more complex cases involving pulsed signals in which the echoes from the scatterers only partially overlap and the presence of boundaries and/or heterogeneities, including waveguide effects. There are also many more important cases not covered explicitly, but that can be described using these formulations as a basis, including advanced signal processing and complex environments.

A common theme of the material involves predicting the degree to which the statistics of the echo magnitude deviate from the classic Rayleigh distribution (described in more detail later), with a focus on the “tail” of the echo distributions. Experimental observations of echo statistics, particularly in the limit of a large number of scatterers, tend toward the Rayleigh distribution and deviations from that distribution contain information on the scatterers. The tail corresponds to the highest values of echo magnitude and will typically be the part of the echo that is detected above the background noise or reverberation. This tail is shown to contain valuable information as it is a function of the numerical density of scatterers, type of scatterer, bandwidth, and beamwidth.

The tutorial is organized as follows: Secs. II–IV provide qualitative descriptions and illustrations of concepts that are important to echo statistics, a summary of the range of applications that exploit echo statistics, and equations specific to scattering and random processes (not specific to scattering) that are common to many formulations in echo statistics. Sections V–VIII draw from the material in Secs. II–IV in a presentation of echo statistics formulations for a wide range of important physical scenarios. These scenarios include beampattern effects associated with main lobes of various width, narrowband and broadband signals, completely overlapping echoes (long signal) and partially overlapping echoes (short signal), single scatterers and mixed assemblages of scatterers, elongated and randomized scatterers, and geometries involving either a direct path and a homogeneous medium or ones involving the presence of boundaries and/or heterogeneities. Sections VI and VII include a progression of cases, all involving a direct path geometry with a homogeneous medium using narrowband signals that are long enough so that the echoes from the scatterers overlap significantly. The two sections begin with the case involving no beampattern effects (omni-directional beam) (Sec. VI), and then later incorporating beampattern effects (directional beam) (Sec. VII). Section V, besides providing an overview of the material of the rest of the tutorial, outlines how the results in Secs. VI and VII can be extended to more complex cases, such as the ones given in Sec. VIII. Section VIII draws from Secs. VI and VII for selected complex cases involving partially overlapping echoes and the presence of boundaries and/or heterogeneities. Although many details of the derivations are not given in Secs. VI–VIII, references to the concepts and equations in Secs. II–IV are given, as well as references to previously published papers.

II. KEY ELEMENTS OF ECHO STATISTICS

Fundamental to the echo statistics are the (1) various types of interference between overlapping echoes from multiple scattering features from a single scatterer, multiple scatterers, and/or multiple propagation paths in a heterogeneous medium or a medium containing boundaries, (2) stochastic nature of scattering by individual scatterers (not including sensor system effects), and (3) random modulation due to random location of the scatterers in the sensor beampattern (Fig. 1). These elements are first discussed qualitatively with

important aspects illustrated. Formal mathematical treatments based on the physical processes, sensor system, and signal types are presented later. All processes are described quantitatively in terms of the probability density function (PDF), which is the probability of occurrence of a random variable for each of its values. The PDF and related quantities are defined formally in Sec. IV B 1.

A. Interfering signals

Echoes from one or more scatterers can be decomposed into the sum of the echoes from multiple scattering highlights from each individual scatterer, echoes from multiple scatterers when more than one scatterer is present, and echoes from multiple propagation paths when the medium is heterogeneous and/or there are one or more boundaries present. Regardless of scenario, because of randomness generally associated with the scatterer or environment, the echoes will tend to interfere randomly with each other, causing fluctuations from ping to ping.

In order to understand this interference phenomenon, we first examine the simple case of a single sinusoidal signal whose amplitude (i.e., envelope) does not vary in time. This signal corresponds to the echo from a point scatterer fixed in the beam of a narrowband system. In this case, the amplitude of the signal is constant [Fig. 2(a)]. The PDF describing this

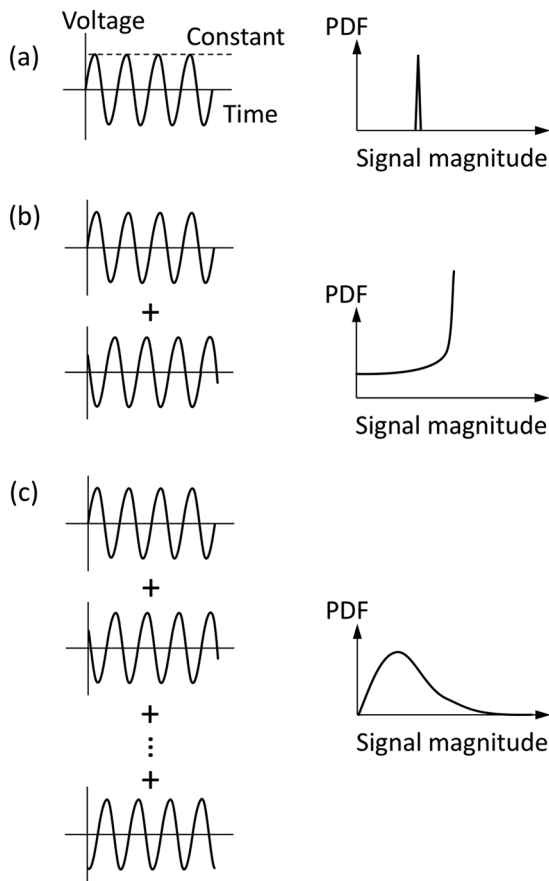


FIG. 2. PDFs of magnitude of sums of random phase sinusoidal signals: (a) The magnitude of one sine wave is single valued, which is described by the delta function PDF; (b) two sine waves results in a PDF skewed toward the value associated with complete constructive interference; and (c) the sum of many sine waves tends to the Rayleigh PDF.

single-valued quantity is the delta function [Fig. 2(a)]. Note that when expressing the signal as a complex variable (which is the case for most of this tutorial), then it is the *magnitude* of the signal that is of interest which is equal to the amplitude of the sine wave in this example.

The statistics change dramatically once another signal with the same magnitude but of random phase is added. This second signal corresponds to the echo from a second identical scatterer (or scattering feature or ray path) whose echo overlaps with that of the first. Now, the PDF of the magnitude of the sum is spread over a range of values, depending on whether the signals added constructively, destructively, or something in between [Fig. 2(b)]. As more signals of equal magnitude and random phase are added, the PDF continues to change and, in the limit of an infinite number of signals of random phase, the PDF converges to the Rayleigh PDF [Fig. 2(c)].

This example involved single-frequency signals of infinite extent. This idealized signal can be used to approximate pulsed (or “gated”) sine wave signals used in many sensor systems where echoes from scatterers significantly overlap. The same principles also apply, although with more complexity, to pulsed signals (narrowband and broadband) of much shorter extent where the multiple signals generally overlap only partially as presented in Sec. VIII A.

B. Stochastic scattering from a single scatterer

The simplest of scatterers is a point scatterer, as it gives the same echo regardless of orientation. In this case in which effects from the sensor system are ignored (i.e., omnidirectional beam) and when using a sinusoidal signal, the echo magnitude from a single point scatterer is constant with a delta function PDF [Fig. 3(a)]. For more realistic scatterers of finite extent, such as elongated ones whose orientation and/or shape may change in time, the echo magnitude will vary from ping to ping. Now, the PDF is significantly broadened and the echo statistics are more complex [Fig. 3(b)].

There is some correspondence between this and the former case involving sinusoidal signals. The echo from a point

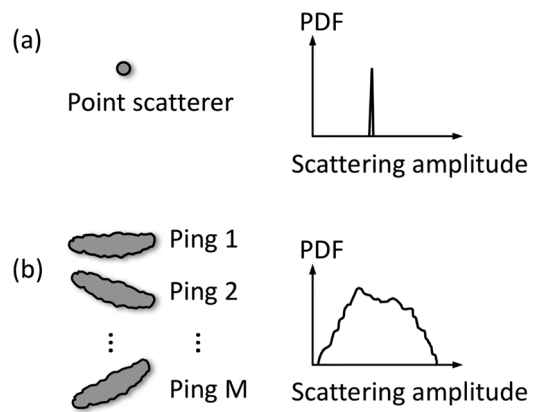


FIG. 3. Echo statistics of the magnitude of scattering amplitude for (a) a simple point scatterer and (b) a randomly oriented irregular elongated scatterer. This does not account for beampattern effects of the sensor system. The echo is shown to have a singular value for the point scatterer and is distributed over a range of values for the elongated scatterer.

scatterer corresponds to a single sine wave with a constant magnitude. In some cases, an echo from an irregular finite-sized scatterer can be decomposed into echoes from different parts of the body of the scatterer, which corresponds to the addition of multiple random-phased sinusoidal signals. Also, there are conditions under which the echo PDF from a complex scatterer can be the Rayleigh PDF, which corresponds to the sum of an infinite number of randomly phased sine waves.

C. Beampattern effects

The echo measured through the receiver of the sensor system depends, in part, on the location of the scatterer in the two-way beampattern. The beampattern will modulate the echo according to the location, with stronger values being associated with the scatterer being near the center of the main lobe and weaker values corresponding to locations well away from the center. For a randomly located scatterer, the modulation will correspondingly be random, adding to

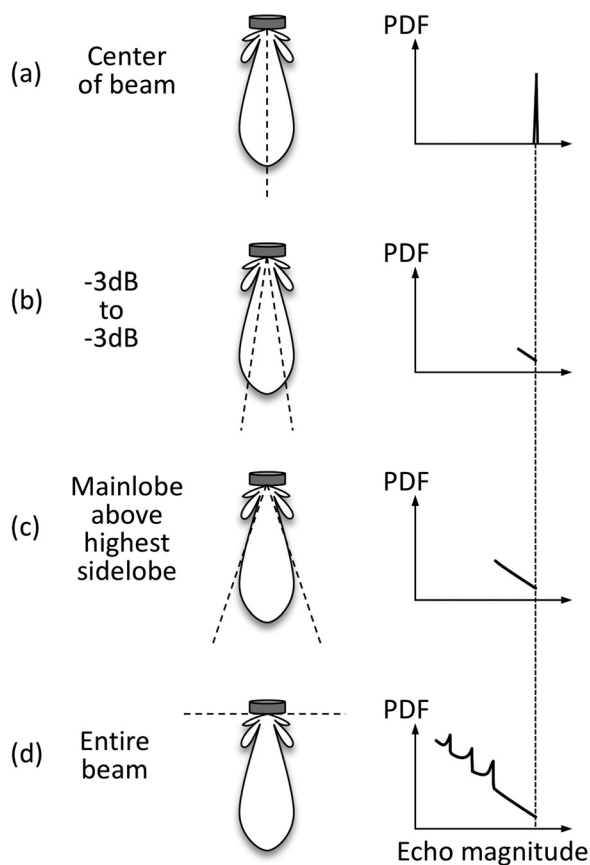


FIG. 4. PDF of echo magnitude from point scatterer in the sensor beam, randomly and uniformly located within different solid angles and at constant range. As illustrated in (a), the echo is delta-function-distributed when the scatterer is fixed in the center of the beam. Once it is randomly distributed across all angles as illustrated in (d), the trend of the echo PDF is roughly a power-law, with some strong structure associated with the sidelobes. The PDFs in (b) and (c) are monotonic functions and closely approximate a power law (corresponding to contributions solely from the main lobe) and are from segments of the near power law (monotonic) portion of the tail of the PDF in (d). All curves reach a maximum value corresponding to the center of the beam, as indicated by the vertical dashed line. The PDF is plotted on a logarithmic-logarithmic scale to illustrate the near constant slope for large echo values.

the variability of the echo. The distribution associated with this random modulation is referred to as the “beampattern PDF.”

The randomizing effects of the beampattern on the echo from a randomly located object can be illustrated by varying the solid angle within which the object is allowed to move (Fig. 4). In this simple example, a circular piston transducer is used to both send and receive the signal and the solid angle is centered about the axis of symmetry of the transducer (which is the center of the main lobe). A point scatterer is allowed to move randomly within the solid angle at a fixed distance from the transducer. In the first case, the solid angle is 0 and the scatterer is restricted to remain fixed in the center of the beam where the response is maximum [Fig. 4(a)]. The corresponding echo is single valued from ping to ping and its PDF is the delta function [right panel of Fig. 4(a)]. As the solid angle increases from zero allowing the scatterer to randomly move a greater amount across the beam, the ping-to-ping variability in the echo increases correspondingly [Figs. 4(b)–4(d)]. When only the portion of the main lobe above the highest sidelobe is involved in the motion [Figs. 4(a)–4(c)], then the echo PDF is either single valued or approximately power-law-distributed. However, once sidelobes are involved, then the echo PDF is more complex, as a non-monotonic characteristic is present due to the sidelobe structure [“spiky” section of curve in Fig. 4(d), where values of echo are lower].

These effects will be shown in Sec. VII A 4 to be qualitatively similar over a wide range of beamwidths. In essence, regardless of beamwidth (several degrees or several tens of degrees), if the scatterer is randomly located within a solid angle containing at least most of the main lobe of the beampattern, then the echo will correspondingly be modulated over a wide range of values of the beampattern.

III. EXPLOITING ECHO STATISTICS FOR VARIOUS APPLICATIONS

Understanding and quantifying the statistical variability of a signal is useful in a diverse range of applications. Below are described two common uses of echo statistics, one in which the variability of the observed signal is used to infer important information regarding the scatterers, and the other in which the degree to which the signal varies for a given scenario is predicted to understand the error or uncertainty regarding the expected signal. Specific examples are given in Sec. III A where echo statistics are used as an inference tool spanning use of sonar, radar, and medical ultrasound.

A. Inferring information on scatterers

Regardless of the field and type of sensor system, one can exploit properties of the variability of the echo to make inferences of important quantities such as number of scatterers, scatterer characteristics, discriminating between and classifying different types of scatterers, and probability of false alarm when detecting a scatterer of interest that is interspersed with other unwanted scatterers. Key to the success

of the inference is using a model of the echo statistics whose parameters can be linked to the physical properties of interest. The description of such models is the focus of this tutorial.

Once the statistics model is determined for the particular application, there are numerous methods to infer parameters of modeled echo statistics from data including use of least squares, maximum likelihood estimators (MLE) (Azzalini, 1996), and method of moment estimators (MME) (Joughin *et al.*, 1993). Performance of an unbiased estimator can be evaluated formally through the Cramer-Rao lower bound (CRLB) method which estimates a lower bound of the variance of the estimator (Hogg and Craig, 1978). Abraham and Lyons (2002b) provides an example of use of MLE, MME, and CRLB for inference of modeled parameters from data (Appendix B of that paper).

Many applications using echo statistics as an inference tool are described in citations given in Sec. I. Selected examples spanning three types of sensor systems—sonar, radar, and medical ultrasound—are briefly summarized below.

1. Inferring number of scatterers

The shape of the echo PDF can be used to infer the number of scatterers. This topic has especially seen much attention spanning many applications, with attempts to connect parameters of either physics-based or generic PDFs, such as the K PDF, to numerical density of scatterers. Stanton *et al.* (2015) used physics-based methods (such as described in this tutorial in Sec. VII B) to relate the shape of the PDF of the magnitude of the echo to the number of scatterers in a sonar beam in the ocean. The inferences were conducted for several different types of scatterers (“bottom-like,” “compact stationary,” and “compact non-stationary”) that ranged in densities from resolved to unresolved. Lee and Stanton (2015) used similar physics-based methods with a sonar beam to infer the numerical density of fish (more details on this broadband method given in Sec. VIII A). Other studies have related a parameter of a generic PDF to numerical density of scatterers. For example, Abraham and Lyons (2002b) analytically related the shape parameter of the K PDF to numerical density of scatterers (for certain conditions; general and not specific to sonar) and applied the results to using sonar to estimate numerical density of scatterers on the seafloor. Tunis *et al.* (2005) performed a controlled laboratory experiment with various dilute solutions containing cancerous cells (acute myeloid leukemia and prostate adenocarcinoma) to empirically relate a parameter of the gamma distribution of the medical ultrasound echo to numerical density of the cells.

For the general case in which there is a mixture of different sized scatterers, Lee and Stanton (2014) have formulated the echo PDF based on various physical parameters—sensor beampattern, scattering amplitudes, and numerical density of each type of scatterer. This method is not specific to any type of sensor system (and is described in Sec. VIIC) and the simulations demonstrated conditions under which the number of scatterers (especially within the type that

dominated the echo) could be inferred (see Figs. 6 and 7 of that paper).

2. Discriminating between echo from scatterer of interest and background

For a single scatterer of interest interspersed within an aggregation of other unwanted scatterers (in a volume or on a surface), echoes from the scatterer of interest can be discriminated from those containing only the surrounding unwanted or “background” scatterers. Here, the echo containing the scatterer of interest will also be contaminated with echoes from the background. Ferrara *et al.* (2011) conducted an experimental study on the ocean involving use of radar to detect and classify echoes from ships and oil rigs. In their data, there were echoes from two types of regions containing (1) both the scatterers of interest (ships or oil rigs; one at a time) and the sea surface and (2) only the sea surface. The experimental radar-echo statistics data were fit to the generalized K PDF. They demonstrated that combinations of generalized K parameters (such as ratios of the parameters) could be used to unambiguously distinguish between echoes involving the scatterers of interest (ships and oil rigs) and the background (sea surface) scattering from those due to the surrounding sea surface alone. There was only one false alarm out of 229 detected targets.

3. Removing beampattern effects to isolate properties of resolved scatterer

While the previous case in Sec. III A 2 involves classifying a scatterer of interest when its echo is confounded with that of the surrounding background, the case simplifies once the echo is resolved from the background. This can occur when the scatterer is suspended in the volume away from any boundary or other neighboring scatterer. In this case, through inversion methods, variability due to the scatterer’s random location in the beampattern can be removed to isolate echo variability due to the target alone. The target echo variability (with no beampattern effects) contains information on the scatterer, such as its size and degree to which it is elongated or rough.

For example, in Clay (1983), the PDF of the echo (as described in Sec. VII A 1 of this tutorial), which is a function of both the beampattern PDF and the PDF of the scattering amplitude of the scatterer, is formulated in terms of a convolution involving each of those individual PDFs. Through knowledge of the beampattern properties, the effects of the beampattern are removed from the echoes through deconvolution, leaving only the PDF of the scattering amplitude. The statistics of the scattering amplitude are then used to classify the scatterer in terms of its size and type. Although the paper was intended for use of sonar to detect and classify echoes from fish, the equations are general and applicable to any sensor system. Clay’s method was refined in Stanton and Clay (1986).

4. Discriminating between different types of aggregations of scatterers

Oelze and Mamou (2016) reviewed a number of previously published studies concerning use of medical ultrasound to detect and classify *in vivo* soft tissue. One such study (Fig. 3 of that paper) combined the spectral content of the broadband echo [to estimate effective scatterer diameter (ESD)] with echo statistics data fit to the homodyned K distribution. The feature analysis plot of ESD versus two parameters of the homodyned K distribution provided strong discrimination (with no overlap) between echoes from three different types of cancerous tumors (mammary) in rodents (rat fibroadenomas, mouse carcinomas, and mouse sarcomas).

5. Further considerations

In order for the echo statistics to best be exploited, there are further considerations in using echo statistics as a tool with a practical sensor system.

a. Directionality of sensor beam improves inference techniques. The degree to which the echoes are non-Rayleigh contains valuable information such as numbers of scatterers that can be inferred, as summarized above. Once the echoes are Rayleigh distributed, the amount of information to be inferred is limited. The beampattern causes echoes that may be otherwise Rayleigh-like to be non-Rayleigh through reducing the effective number of scatterers that are “seen” by the narrow mainlobe of the system. Furthermore, echoes that are non-Rayleigh before beampattern effects will deviate even more from the Rayleigh PDF once the beampattern is accounted for. The process of inferring information from the field of scatterers can therefore be enhanced or even optimized through varying, when possible, the width of the main lobe of the beampattern so that the echoes will be non-Rayleigh over the range of expected values.

b. Noise and “tail” of echo PDF. In any practical sensor system, there will be various sources of noise (including electronic noise) and background reverberation that will normally dominate the lower values of echoes. Thus, any information to be inferred must generally come from the higher portion of the echo PDF—that is, the “tail.” Many analyses focus solely on properties of the tail that is above the detection threshold of the system.

B. Predicting error or uncertainty in signal magnitude

In many applications, it is desired to predict the magnitude of the signal after it has propagated through an environment. The applications can deal with ones such as those described above in which one wishes to infer properties of the environment or scatterers from the signal or other types of applications in which the performance of the sensor system is being studied. Ideally, one wants to know all key parameters of the environment and scatterers so that the properties of the signal that propagates through the environment can be known to 100% certainty. However, due to a

combination of the uncertainties of the values of the many parameters of the environment [e.g., roughness of surface(s), material properties, etc.] and scatterers (e.g., number, type, orientation, etc.) as well as random variations of those same quantities due to naturally occurring processes, the predicted signal in a natural environment is normally a random variable.

To quantify the degree to which the signal varies (that is, predict what is commonly called its error or uncertainty), the random variables associated with parameters of the environment and scatterers must first be estimated. Using these random variables, the variability of the signal can then be predicted through use of physics-based equations as described below. Regardless of the approach used, there are different degrees of variability. First, predicting the variability of the signal due to random variations in the environment and scatterers from the expected mean properties. A higher order variability would be due to errors in those estimates of the random variations in the environment and scatterers and associated deviations from the predicted variability of the signal (that is, an error in a prediction of a signal PDF).

Beyond the above considerations in which there is no noise in the system, there is also uncertainty in the predictions associated with random noise. This noise can be due to a combination of ambient noise in the environment and electrical system noise. Also, diffuse background reverberation is sometimes considered to be part of the noise. Although this topic is outside the scope of this tutorial, it is an important consideration in modeling practical systems. The noise can be accounted for through various methods which include (1) modeling the noise as an additive random complex variable to the (complex) echo signal (Jones *et al.*, 2017) and (2) modeling the echo magnitude PDF as a “mixture” PDF, which is the sum of the noise-free echo magnitude PDF and the noise-only PDF (Stanton and Chu, 2010; Abraham *et al.*, 2011).

IV. KEY EQUATIONS FOR SCATTERING AND ASSOCIATED STATISTICAL PROCESSES

Fundamental equations are first given describing deterministic scattering such as for a fixed location or orientation of the scatterer. In order to describe the scattering for a randomized case such as when the location or orientation vary randomly, general equations describing statistical processes that occur in such scenarios are given, which are then incorporated into the equations for deterministic scattering to describe randomized scattering. All of the below equations relate the echo and its fluctuations directly to the physical properties of the scatterers and sensor system. This type of treatment is referred to as “physics based.”

A. Deterministic scattering

The scattering described in this section is from a single ping or statistical realization. This deterministic description will then be randomized for use in predicting the statistics of the echoes. The scattering geometry involves use of an active monostatic sensor system where the transmitter and receiver are collocated (Fig. 1). The scattering can involve

one or multiple scatterers. Also, all analyses involve scatterers distributed within a thin shell of constant radius with the sensor system at the center. The thickness of the shell is much smaller than its radius.

This (shell) geometry is for modeling a long narrowband signal in which echoes from all of the scatterers within the shell completely overlap. For a sensor system that uses short pulses to detect a more broadly distributed set of scatterers (such as in many practical applications), the thickness of this thin shell can be related approximately to the duration of the pulse. A rigorous approach to modeling pulsed systems where the echoes generally only partially overlap is given in Sec. VIII A.

1. Single scatterer

The voltage V_s received by the sensor system due to the echo from a single scatterer is

$$V_s = V_T G_T G_R \frac{r_0}{r^2} e^{-j\omega t} e^{2jkr} e^{-2\alpha r} b(\theta, \phi) f_{bs}, \quad (1)$$

where V_T is the voltage applied to the transducer, G_T is the transmitter response (conversion factor of applied voltage to acoustic or electromagnetic field) which is equal to the acoustic or electromagnetic signal, respectively, at reference distance r_0 per unit applied voltage V_T , G_R is the receiver sensitivity (conversion of acoustic or electromagnetic field to voltage) which is equal to the voltage signal at the output of the transducer per unit acoustic or electromagnetic signal, respectively, incident at the transducer, r is the distance between the transducer and scatterer, $j = \sqrt{-1}$, ω is the angular frequency of the sinusoidal signal, k is the acoustic or electromagnetic wavenumber ($= 2\pi/\lambda$, where λ is the wavelength), α is the absorption coefficient of the medium so that $e^{-2\alpha r}$ is the two-way loss due to absorption, and $b(\theta, \phi)$ is the two-way beampattern of the sensor system whose values lie in the range $[0,1]$. The term $b(\theta, \phi)$ is the product of the beampatterns of the transmitter and receiver and the terms θ and ϕ are the angular coordinates of the scatterer. Specifically, $b(\theta, \phi) = b_T(\theta, \phi)b_r(\theta, \phi)$, where b_T and b_r are the transmitter and receiver beampatterns, respectively. The term f_{bs} is the backscattering amplitude of the scatterer and is a complex variable.

In this formulation, the signal is assumed to be at a single frequency (i.e., narrowband) of infinite temporal extent. Also, the acoustic and electromagnetic fields associated with G_T and G_R are assumed to be scalar quantities. For acoustics, this scalar quantity is pressure, the compressional component of the field, and assumes no shear component in the medium (although conversion of compression to shear wave can take place within the scatterer). For the electromagnetic field, the scalar quantity is one polarization component of the electric or magnetic field. This assumption in this latter case treats each polarization component independently and ignores coupling between the components [Chap. 4 of Goodman (1985); Chap. 4 of Jakeman and Ridley (2006)].

The target strength of the scatterer can be expressed in terms of the backscattering amplitude and differential backscattering cross section σ_{bs} as

$$TS = 20 \log |f_{bs}| \quad (2)$$

$$= 10 \log \sigma_{bs}, \quad (3)$$

where $\sigma_{bs} = |f_{bs}|^2$ and the units of f_{bs} (m) and σ_{bs} (m^2) are suppressed. Note that the term σ_{bs} should not be confused with a similar representation for backscattering cross section, σ , that is commonly used where $\sigma = 4\pi\sigma_{bs}$ and $TS = 10 \log(\sigma/4\pi)$.

For simplicity in the analysis, all parameters of the system and measurement are assumed to be constant and will be suppressed in the following equation. From Eq. (1), the magnitude of the echo voltage due to a single scatterer as received through the monostatic active sensor system is now given by

$$\tilde{e} = |f_{bs}|b(\theta, \phi), \quad (4)$$

where V_T , G_T , G_R , r , and α in Eq. (1) have been suppressed and $r_0 = 1m$. Here, the magnitude of the signal is based simply on the absolute value of the signal.

2. Multiple scatterers

The voltage received by the sensor system due to the echo from an aggregation of N scatterers is

$$V_s = V_T G_T G_R r_0 e^{-j\omega t} \sum_{i=1}^N \frac{e^{2jkr_i}}{r_i^2} e^{-2\alpha r_i} f_{bs}^{(i)} b(\theta_i, \phi_i), \quad (5)$$

where r_i , $f_{bs}^{(i)}$, and (θ_i, ϕ_i) are the range, backscattering amplitude, and angular location of the i th scatterer, respectively. As with Eq. (1), the signal is assumed to be at a single frequency of infinite temporal extent. With this type of signal, there is 100% overlap between the echoes from all individual scatterers. The simple summation of echoes from individuals reflects the assumption that only single-order scattering is being considered and higher-order scattering (i.e., re-scattering of echoes between individuals) is assumed to be negligible.

From Eq. (5), and suppressing the constants of the system and measurement in a manner similar to that with the individual scatterer described above, the magnitude of the echo voltage due to N scatterers as received through the sensor system is given by

$$\tilde{e} = \left| \sum_{i=1}^N \tilde{e}_i e^{j\Delta_i} \right|, \quad (6)$$

where the magnitude of the echo voltage from the i th scatterer as received through the sensor system is

$$\tilde{e}_i = |f_{bs}^{(i)}|b(\theta_i, \phi_i). \quad (7)$$

The assumption that all parameters of the sensor system and measurement are constant requires the range from the sensor system to each scatterer to be approximately the same so that the differences in losses due to spreading and absorption in the r_i^{-2} and $e^{-2\alpha r_i}$ terms, respectively, in Eq. (5) associated with each scatterer are negligible (i.e., $r_i^{-2} \sim r^{-2} = \text{constant}$

and $e^{-2\alpha r_i} \sim e^{-2\alpha r} = \text{constant}$). Specifically, all scatterers are assumed to be located within a thin shell whose thickness is small compared with the radius of the shell. However, minor differences in range within the shell can still lead to significant changes in phase of the echo from individual scatterers, especially when the acoustic or electromagnetic wavelength is comparable to or smaller than the shell thickness. For simplicity in the formulation, all phase shifts associated with the i th scatterer are in the term Δ_i , which includes phase shifts due to differences in range within the shell (i.e., $2kr_i$) and due to the scatterer and beamformer. For acoustic/electromagnetic wavelengths that are small compared with the shell thickness, Δ_i will generally vary randomly and uniformly in the range $[0, 2\pi]$ for randomly distributed scatterers.

B. Probability density function and related quantities

1. Definitions and equations

The statistics described herein involve the probability of occurrence of random variables. This is in contrast to other types of statistics such as statistical tests (e.g., the t- and Kolmogorov-Smirnov tests). The principal statistical quantities used are the probability density function (PDF or p), cumulative distribution function (CDF), and probability of false alarm (PFA), which are interrelated from the following expressions for one-dimensional continuous random variables (Ol'shevskii, 1978; Papoulis, 1991; and Goodman, 1985). Expressions involving multi-dimensional random variables will appear later in context. While the below expressions are general, the integration limits associated with echo magnitude statistics later will reflect the fact that the magnitude (x) is always positive and $p = 0$ for $x < 0$.

Note that the CDF is rigorously referred to as the “distribution” or “distribution function.” However, the PDF is also commonly referred to as a “distribution” as well as “frequency function” throughout the literature. While “PDF,” “distribution,” and “distribution function” are commonly interchanged with no change in meaning (in context), the term “PDF” will be principally used herein.

The infinitesimal probability dP_X of a random variable X occurring in the differential interval $[x, x + dx]$ is expressed in terms of the probability density function $p_X(x)$ of X ,

$$dP_X(x \leq X \leq x + dx) = p_X(x)dx. \quad (8)$$

For a finite interval $[a, b]$, the probability is calculated through the following integral:

$$P_X(a \leq X \leq b) = \int_a^b p_X(x)dx \quad (\text{probability}). \quad (9)$$

Once a and b are extended to $-\infty$ and $+\infty$, respectively, the integral over all values of X is equal to unity.

The probability of a random variable occurring for all values of X up to an arbitrary point x is determined from the integral in Eq. (9) and is referred to as the cumulative distribution function,

$$CDF_X(x) = \int_{-\infty}^x p_X(u)du \quad (\text{cumulative distribution function}). \quad (10)$$

As stated above, once these equations are applied to echo magnitude statistics, $p_X(u) = 0$ for $u < 0$, thus the lower limit of this integral would be zero.

The PDF can be determined from the CDF simply by taking the derivative of the above expression,

$$p_X(x) = \frac{d}{dx}[CDF_X(x)] \quad (\text{probability density function}). \quad (11)$$

The probability of false alarm PFA is commonly used to determine the probability of occurrence of a random variable occurring for any value higher than an arbitrary value (Chap. 7 of Ol'shevskii, 1978). From Eq. (9), the PFA of X for all values above x can be related to the integral of the probability density function as

$$PFA_X(x) = \int_x^{\infty} p_X(u)du \quad (\text{probability of false alarm}). \quad (12)$$

Using the fact that the integral of the PDF over all values of its argument is equal to unity, Eqs. (10) and (12) can be used to express the PFA in terms of the CDF,

$$PFA_X(x) = 1 - CDF_X(x). \quad (13)$$

The PFA presented in this tutorial is mathematically equivalent to the probability of detection (PD). The nomenclature varies depending on the context of application. For example, when the PDF is used to describe the unwanted background echoes or “noise,” the PFA gives a measure of the probability that the source of scattering is *not* from the target of interest. Conversely, when the PDF is used to describe the anticipated echo from a scatterer (or “target”) of interest, the PD gives a measure of the probability of detecting the target of interest. The limit, x , in Eq. (12) is the threshold above which the PFA and PD are calculated (Chap. 7 of Ol'shevskii, 1978).

2. Calculating PDFs: Directly and from Monte Carlo simulations

Some PDFs are, conveniently, closed-form analytical solutions that can be calculated directly. For example, the Rayleigh and K PDFs given later, as well as the Gaussian PDF are in a simple analytical form and are straight forward to calculate. Other analytical solutions, such as those given in integral form, are also straight forward to calculate through numerical integration. However, PDFs for many realistic cases are generally not in closed form and require numerical simulations involving the scattering equations to estimate them. For example, once parameters of the sensor system and scatterers are specified, models of the echo at the *signal* level (not PDF level) such as in Eq. (6) are simulated to create the statistics of the echo.

A common method to estimate PDFs is through use of Monte Carlo simulations which generally involves making

calculations of many statistical realizations of the signal to form an ensemble from which the PDFs are estimated. For example, in Eqs. (6) and (7), each i th scatterer will have a distribution of scattering amplitudes $f_{bs}^{(i)}$ and locations (θ_i, ϕ_i) . Each realization involves randomly selecting one of those scattering amplitudes and locations for each scatterer, then calculating the signal using Eq. (6). The process is repeated many times, with each selection of random values being statistically independent (when independence is required) from the other selections.

Use of Monte Carlo simulations tends to be more general than analytical methods as there are fewer assumptions and, hence, limitations. For example, the scatterers can be arbitrarily correlated in space (such as being in a thin layer or small patch) and can have arbitrary phase-shift distributions. While many analytical models are restricted to cases involving independently distributed scatterers whose phases are uniformly distributed over $[0, 2\pi]$, use of the Monte Carlo simulations do not have such restrictions.

Once the many simulations have been completed, the PDF is commonly estimated by putting the realizations of the signal into “bins” to form a histogram. For an analysis of echo magnitude statistics in the example described above, the result of each calculation is put into a magnitude bin (i.e., quantized value of echo magnitude) so that a histogram can be formed. These simulations require many realizations so that there can be correspondingly many narrow bins in order to produce a histogram that is an accurate representation of the actual PDF.

This binning approach is intuitive and is a method used in this paper, when appropriate, due to its simplicity. Conditions under which this method are used depend upon a combination of the type of structure in the PDF and corresponding number of realizations required to model that structure. In some cases, such as for a smoothly varying PDF, the computation time is reasonable. Calculations of PDFs for other applications where there is structure such as the presence of narrow peaks or nulls in the PDF curve may require more realizations and correspondingly significant computer time. When making too few calculations in this latter case, there can be artifacts in the result, such as smoothed or completely missed peaks or nulls. Thus, when there is the presence of narrow peaks or nulls in the PDF, a closed-form analytical method is used in this paper to determine the PDF, when possible. Beyond these approaches, the kernel density estimation (KDE) method was used to reduce the number of realizations needed to produce a reliable estimate of the echo PDF (Botev *et al.*, 2010; Lee and Stanton, 2015; Scott, 1992). The calculations illustrated in this paper typically involve 10^7 realizations.

Finally, for applications that extract information from the tail of the PDF, estimation methods such as importance sampling can be used to reduce the variance in the estimate and to increase the efficiency of the Monte Carlo process through selectively sampling the more desired (tail) samples (Agapiou *et al.*, 2017).

3. Non-uniform spacing of bins

Depending upon the types of features one is investigating in a PDF, the curves will either be plotted on a linear

linear or logarithmic-logarithmic scale. While the former scale may be more intuitive, the latter is especially useful when examining the tail of the PDF which typically has low values relative to the maximum. Choice of type of scale influences how the bins are determined. For linear-linear plots of PDFs, equally-spaced bins for the horizontal axis are normally used. However, when plotting PDFs on a logarithmic-logarithmic scale, the width of the bins should be equal on a log scale, which is non-uniform on a linear scale. Otherwise, if the bins were equal on a linear scale, but plotted on a log scale, the density of points on the plots would increase throughout the plot, and not fully characterize the shape of the PDF.

4. Normalization

a. Vertical scale. The probability of a variable occurring over *any* of the values of the random value x over the entire range is, by definition, unity. Therefore, the integral over x of any PDF over all values is unity. PDFs are commonly derived with a constant factor introduced that is determined through normalizing the area under the PDF curve to unity. From this property, it follows that the CDF will begin at a value of 0 for the smallest value of x and reach its maximum value of unity at the largest value of x . Similarly, the PFA will begin at unity and decrease to the value of 0 for the corresponding smallest and largest values of x , respectively.

b. Horizontal scale. In some applications, it is also important to normalize the (horizontal) scale associated with the random variable. This can be the case when the calibration of the system is not known accurately, the propagation loss of the signal in the medium is not known accurately, or when only the shape of the PDF, CDF, and PFA are of interest regardless of the echo strength. Through normalization, only the relative values of the random variable will be considered. One convenient approach is to normalize the random variable by its root-mean-square (*rms*) value $\langle x^2 \rangle^{1/2}$ and plot the PDF, CDF, and PFA versus the random variable divided by $\langle x^2 \rangle^{1/2}$, where $\langle \dots \rangle$ is the average over a statistical ensemble of values. In this case, the area under the PDF curve (with an argument normalized by $\langle x^2 \rangle^{1/2}$) is preserved under the transformation and is unity.

Regardless of the type of scale (linear-linear or logarithmic-logarithmic) or uniformity of spacing of bins, all normalizations are first calculated on a linear-linear scale. For example, an equation such as Eq. (9) is on a linear-linear scale and can be used to normalize the PDF to unity while accounting for non-uniform spacing in the integral.

C. Fundamental statistical processes relevant to echo statistics

1. Randomizing the deterministic scattering equations

Random fluctuations of echoes involve several fundamental statistical processes. For example, in Eq. (1), the beampattern is shown to be a function of the angular coordinates. In general, the scatterer will be randomly located in the beam, making the angular coordinates of the

scatterer random variables. Since the beampattern is a function of the random angular coordinates, then the beampattern function is, in turn, a random variable for a randomly located scatterer. The scattering amplitude in Eq. (1) is also generally a randomly variable due to the random nature of the scatterer. Since the echo \tilde{e} in Eq. (4) as measured through the receiver of the sensor system is the product of the two random variables, the beampattern function and scattering amplitude, then \tilde{e} is also a random variable. Finally, once there are multiple scatterers in the beam of the sensor system, the resultant echo \tilde{e} [Eq. (6)], as measured through the receiver, will be the sum of the random individual echoes [Eq. (7)] and will, in turn, be a random variable.

These statistical processes—function of a random variable(s), multiplication of two random variables, and addition of random variables—are of wide applicability, are not specific to sensor systems or scattering, and appear in standard textbooks on statistics. Formulas summarizing these general processes are given below for later reference in the scattering problem. While only the simplest of cases involving one or two random variables are given, formulas involving more random variables are given in the references and/or later in context of the application.

2. Function of a single random variable

If the function Z is a function of the random variable X , then $Z(X)$ is also a random variable. The formulations relating the PDF of Z to the PDF of X are based on the fundamental principle that the probability of occurrence of an event in one space (X in this case) is the same as that in the transformed space (Z in this case). The resultant PDF $p_Z(z)$ is then given by one of two equations depending upon whether $Z(X)$ varies monotonically or non-monotonically with respect to X . Specifically, $Z(X)$ is monotonic with X if it either solely increases or solely decreases over the range of X such that for any value of Z , there is only one (unique) value of X . Conversely, for the non-monotonic case, $Z(X)$ both increases and decreases over the range of X so that there can be multiple values of X for a given value of Z [both of these cases and the below equations are described on pp. 23–27 of Goodman (1985)].

For the case in which $Z(X)$ varies monotonically with respect to X over the entire range of X , then the following expressions can be written where the differential probabilities in the two spaces are equated to each other,

$$dP_Z(z \leq Z \leq z + dz) = dP_X(x \leq X \leq x + dx) \quad (\text{monotonic}). \quad (14)$$

From Eq. (8), this can be expressed in terms of the PDFs of X and Z ,

$$p_Z(z)dz = p_X(x)dx \quad (\text{monotonic}). \quad (15)$$

Rearranging terms yields an expression for the PDF of Z in terms of the PDF of X for this monotonic case,

$$p_Z(z) = \left. \frac{p_X(x)}{\left| \frac{\partial z}{\partial x} \right|} \right|_{x(z)} \quad (\text{monotonic}), \quad (16)$$

where the absolute value sign is used to keep the expression for the PDF positive.

In the more complex case in which $Z(X)$ varies *non-monotonically* with respect to X over the range of X , the PDF is described by a similar equation, but summed over M contiguous segments where $Z(X)$ varies monotonically within each segment,

$$p_Z(z) = \sum_{m=1}^M \left. \frac{p_X(x_m)}{\left| \frac{\partial z}{\partial x_m} \right|} \right|_{x_m(z)} \quad (\text{non-monotonic}). \quad (17)$$

Here, $x(z)$ and $x_m(z)$ in Eqs. (16) and (17) are the inverse functions $z^{-1}(x)$ and $z^{-1}(x_m)$, respectively. In practice, these inverse functions can be determined numerically from the forward analytical function, plots, or tables of $z(x)$ and $z(x_m)$.

3. Function of two random variables

The above analysis involving a function of one random variable is extended to the case of a function of two random variables. In this case, if the function Z is a function of the random variables X and Y , then $Z(X, Y)$ is also a random variable. Relating the PDF of Z to the PDF(s) of X and Y involves the same process as in the previous case of one random variable in which the probability of occurrence of an event in one space is set equal to that of the other space. This process generally involves first determining the Jacobian of the transformation relating the two spaces, although that will not be shown explicitly below (Papoulis, 1991).

From Eq. (6-35) of Papoulis (1991), the probability of Z occurring for any value below z is given in terms of x and y as

$$P_Z(Z \leq z) = \iint_{D_z} p_{X,Y}(x, y) dy dx, \quad (18)$$

where $P_Z(Z \leq z)$ is also the CDF_Z . Here, $p_{X,Y}(x, y)$ is the joint probability density function of the random variables X and Y , and D_z is the region or regions in the xy plane containing values of x and y where $Z(X, Y) \leq z$ (D_z is illustrated in Fig. 6-7 of Papoulis, 1991). This equation for $P_Z(Z \leq z)$ is a two-dimensional form of Eq. (10). The PDF of z can be expressed by taking the differential of $P_Z(Z \leq z)$ above,

$$p_Z(z)dz = dP_Z(z \leq Z \leq z + dz) = \iint_{dD_z} p_{X,Y}(x, y) dy dx, \quad (19)$$

where dD_z is now the differential region or regions(s) in the xy plane whereby the values of x and y are bounded by the differential area determined by the range $z \leq Z \leq z + dz$ [Eq. (6-36) and Fig. 6-7 of Papoulis, 1991].

This equation is complex to solve and depends upon the characteristics and form of $p_{X,Y}(x, y)$. For simple forms such as $Z = XY$ and $Z = X + Y$, where X and Y are independent

random variables, then the solution for $p_Z(z)$ in each case is in closed form. Since those two cases are used throughout this tutorial, they are treated separately in Secs. [IV C 4](#) and [IV C 5](#). The more complex case in which Z is a general function of X and Y is used only once later in the tutorial and the solution will be given in the context of that application (Sec. [VII A 7](#)).

4. Product of two random variables

If X and Y are random variables, then the product $Z = XY$ is also a random variable as described in Sec. [IV C 3](#). If X and Y are independent of each other, then $p_{X,Y}(x, y) = p_X(x)p_Y(y)$ in the integrand in Eq. (19), where $p_X(x)$ and $p_Y(y)$ are the PDFs of the random variables X and Y , respectively. Inserting this product of the two PDFs into the integrand in Eq. (19), the PDF $p_Z(z)$ of the product $Z = XY$ can be shown to be

$$p_Z(z) = \int_{-\infty}^{\infty} \frac{1}{|x|} p_X(x) p_Y\left(\frac{z}{x}\right) dx. \quad (20)$$

This equation is from Eq. (6-74) in [Papoulis \(1991\)](#). In that book, the equation is derived through a method involving use of a Jacobian of the transformation to map one coordinate system to another. However, this equation can also be derived directly from Eq. (19) of this tutorial [which is Eq. (6-36) of [Papoulis \(1991\)](#)] using the change of variables method illustrated in [Papoulis](#) for the ratio of two random variables (p. 138 of the book). Using that method in this case for the *product* of two random variables ($Z = XY$), the change in variables $y = z/x$ is used, and the area $dx dy$ for dD_z is mapped to the area $(1/|x|) dx dz$. Through this mapping, the double integral for dD_z is replaced with a single integral over x . Replacing $dx dy$ in Eq. (19) with $(1/|x|) dx dz$, the dz drops out of both sides of the equation and the integral is only over dx as shown. The absolute value sign is used for the variable x so that the differential area will be positive for all values of x . Note also that the term $|x|$ in the factor $(1/|x|)$ for the area is equal to the absolute value of the Jacobian of the transformation in the derivation of Eq. (6-74) in [Papoulis \(1991\)](#).

Once Eq. (20) is used in physical applications, the range over which one or more of the physical parameters may be constrained and its corresponding PDF will be zero outside of that range. The integration limit(s) may reflect that constraint by only spanning the range over which the PDF is non-zero as shown later.

5. Sum of random variables

There is a variety of methods to evaluate the PDF of the sum of independent random variables, ranging from purely analytical to purely numerical. Sometimes, a “purely” analytical method still requires numerical evaluation, such as when an integral or series summation are involved and numerical integration or summation are performed, respectively. Two common methods are discussed below: the method of characteristic functions and Monte Carlo simulations.

a. Method of characteristic functions. A commonly used analytical method involves use of characteristic functions (CFs) where the CF of a random variable is the Fourier

transform of its PDF ([Goodman, 1985](#)). Addition of an arbitrary number of independent random variables involves first taking the product of their corresponding CFs. This product is the CF of the sum of the random variables. The PDF of that sum is then the inverse Fourier transform of the CF product.

This CF approach can be derived from Eq. (18) for the case of $Z = X + Y$ where Z , X , and Y are all random variables. Since the random variables, X and Y , are independent of each other, then $p_{X,Y}(x, y) = p_X(x)p_Y(y)$. Using this relationship in the integrand of Eq. (18), the PDF of Z , $p_Z(z)$, can be shown to be the convolution of the two functions, $p_X(x)$ and $p_Y(y)$. This convolution can then be shown to be equivalent to the product of the Fourier transforms of $p_X(x)$ and $p_Y(y)$. Since these Fourier transforms are, as defined above, the CFs of the two functions, then the method of characteristic functions follows as described above ([Goodman, 1985](#); [Papoulis, 1991](#)). The method is extendable to the sum of an arbitrary number (N) of independent random variables by first expressing the convolution integral by formulating the sum of two random variables where one of the random variables is the sum of $N-1$ random variables and the other random variable is the remaining variable. The PDF of the sum of the $N-1$ random variables is determined through a similar process involving the sum of $N-2$ random variables, and so on. After completing this iterative process, the PDF of the summed N random variables is related to the product of the Fourier transforms of the PDFs of the N random variables.

Acoustic and electromagnetic signals are complex and normally constructed of a real and imaginary term, making them two dimensional. Since the method of characteristic functions is extendable to multi-dimensional variables, this method can be applied to determine the PDF of the sum of complex signals. For the case in which the phase of the summed signal is uniformly distributed $[0, 2\pi]$ and each component of the signal has a zero mean (i.e., a “circularly symmetric signal” in the complex plane), then the CF and PDF of the signal magnitude are a Hankel transform pair. Application of the CF to calculate the PDF of the magnitude and magnitude squared of complex signals is summarized in [Jakeman and Ridley \(2006, Chap. 4\)](#), including an extension to signals where the phase is not uniformly distributed. Methods to numerically evaluate the PDF for circularly symmetric signals (via the CF and Hankel transform) are given in [Drumheller \(1999\)](#).

[Barakat](#) used a broadly similar approach to the Hankel transform method by extending the 1D CF method to circularly symmetric complex signals through constructing an orthogonal component of the sum, equal in magnitude to the original single component of the sum, resulting in an exact, analytical expression for the PDF of the magnitude of the sum of complex random variables ([Barakat, 1974](#)). However, our experience in applying the Barakat approach has resulted in convergence issues due to truncation of the infinite series summation that must be evaluated ([Chu and Stanton, 2010](#); [Lee and Stanton, 2014](#)).

b. Monte Carlo simulations. The method of Monte Carlo simulations is discussed in more general terms in Sec. [IV B 2](#) and will only be briefly summarized here in the context

of adding random variables. This is a commonly used numerical approach that involves simulating a statistical ensemble of a large number of realizations of the process of interest so that the PDF can be formed. Performing Monte Carlo simulations to evaluate the sum of random variables in predictions of scattering will provide a stable and accurate solution (see, for example, [Stanton et al., 2015](#)). When using this method to simulate signals associated with a sensor system, random variables are normally added through (1) a phasor addition in the frequency domain of single frequency or narrowband signals of long enough extent that the echoes are completely overlapping [such as with Eq. (6)] or (2) addition in the time domain of short signals when the echoes are only partially overlapping and/or when broadband signals of any duration are used (Sec. VIII A). In the case of phasor addition, the signals are first represented in complex form and then the real and imaginary components are added separately before being recombined to calculate the signal magnitude.

6. Sum of infinite number of random variables (central limit theorem; Rayleigh PDF)

In the limit of the sum of an infinite number of independent complex random variables, drawn from identical distributions with uniformly distributed phases, each of the two independent components of the sum tends to a Gaussian PDF, with zero mean and equal variance. This is referred to as the central limit theorem (CLT) and is integral to many treatments of random variables ([Goodman, 1985](#); [Jakeman and Ridley, 2006](#)). The statistics of the magnitude of the sum can be shown to be the Rayleigh PDF,

$$p_{Ray}(x) = \frac{2x}{\lambda_R} e^{-x^2/\lambda_R}, \quad x \geq 0 \quad (\text{Rayleigh PDF}). \quad (21)$$

where $\lambda_R = \langle x^2 \rangle$ is the mean square magnitude.

From Eqs. (10) and (13), the CDF and PFA associated with the Rayleigh PDF are

$$CDF_{Ray}(x) = 1 - e^{-x^2/\lambda_R}, \quad x \geq 0 \quad (\text{Rayleigh CDF}), \quad (22)$$

$$PFA_{Ray}(x) = e^{-x^2/\lambda_R}, \quad x \geq 0 \quad (\text{Rayleigh PFA}), \quad (23)$$

where the lower bound in the integral in Eq. (10) is zero since $p_{Ray}(x) = 0$ for $x < 0$.

The Rayleigh PDF is widely used in describing echo statistics. It is commonly used as the “starting point” in describing the statistics of the echo magnitude, especially when there are many scatterers or many highlights from an individual scatterer contributing to the echo. When the statistics do not follow the Rayleigh PDF, deviations of the statistics from the Rayleigh PDF are frequently described. The deviations in the higher values of the echo magnitude, i.e., the “tail” of the distributions, are of particular interest. The term “non-Rayleigh statistics” is commonly associated with those distributions that deviate from the Rayleigh PDF. The Rayleigh PDF and associated CDF and PFA are illustrated (Fig. 5).

V. IN-DEPTH TREATMENT OF ECHO STATISTICS: OVERVIEW

As discussed in Sec. I, various important aspects of echo statistics will now be examined in detail. The treatment will draw from the concepts and equations given in Secs. II–IV. Generally, deterministic equations for the echo magnitude [Eqs. (4) and (6)], which are based on solutions to the wave equation, are randomized with respect to various physical quantities such as random location in beampattern and random orientation of scatterer. They are randomized using fundamental statistics equations given in Sec. IVC. This approach differs from other approaches such as first randomizing parameters of the governing differential equation before solving the equation [see, for example, the summary in Sec. 12.6 of [Jakeman and Ridley \(2006\)](#), and references therein].

In Sec. VI, the treatment begins with the simplest of cases—single-frequency signals of infinite extent in which echoes from all scatterers completely overlap and direct path

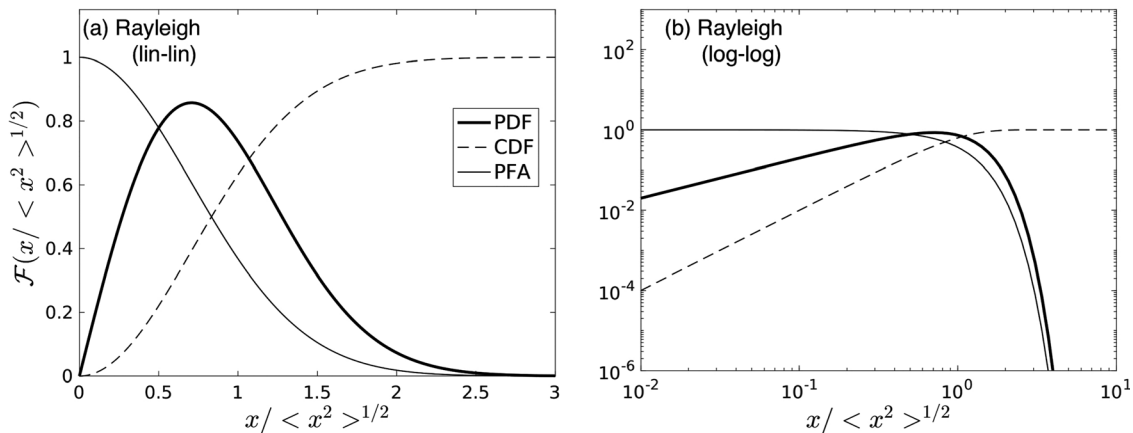


FIG. 5. Rayleigh PDF and associated CDF and PFA. The curves were calculated with the analytical solutions given in Eqs. (21), (22), and (23), respectively. Each function is denoted by the term \mathcal{F} . The functions are plotted on both linear-linear and logarithmic-logarithmic scales in (a) and (b), respectively. With each function plotted on a normalized scale, the curves are independent of the mean square magnitude of the signal (also, there is no shape parameter). The normalization of the horizontal scale here and throughout this paper involves dividing the argument (x) of the distribution by its *rms* level [$\langle x^2 \rangle^{1/2}$] where $\langle \dots \rangle$ represents an average over an ensemble of values. The software used to produce this figure is in the supplementary material at <https://doi.org/10.1121/1.5052255>. The software is also stored online ([Lee and Baik, 2018](#)), where it is subject to future revisions.

propagation in a homogeneous medium without the complicating effects due to reflections from boundaries. These idealized signals approximate gated sine waves where the echoes overlap significantly. In addition, given the importance of the random modulation effect of the beampattern on the echo when a scatterer is randomly located in the beam, the echo statistics are first described without those effects. This is equivalent to the sensor system having an omnidirectional beam. In Sec. VII, beampattern effects are then incorporated into the analysis. In Sec. VIII, the work is further extended into more realistic and complex cases involving pulsed signals (narrowband and broadband) in which echoes may only partially overlap, the presence of a boundary near a scatterer, and propagation and scattering in a waveguide with a heterogeneous medium.

A. How to use this material for realistic signals/ environments, and advanced signal/beam processing

The number of combinations of types of systems, signals, signal processing and beamforming algorithms, and environments is limitless and cannot be adequately described within this tutorial. The material is therefore aimed toward the more fundamental aspects of echo statistics that are not specific to any particular system or environment, but that many applications either have in common or could use as a basis. For example, most material involves the following: (1) *Signal type*: Long, narrowband signals are used in which the echoes from all scatterers completely overlap (in all cases in Secs. VI and VII, and some cases in Sec. VIII). (2) *Signal processing*: The magnitude of the signal as measured at a single instant in time is measured—that is, “first-order statistics” is modeled (in all cases in Secs. VI–VIII). The instant in time may be fixed or randomly selected, but it is not adaptively chosen according to a particular echo magnitude. (3) *Processing of beam data and/or beamforming*: Echoes from a single beam are modeled (fixed or scanning; or one selected from a multi-beam system) in which the scatterers are randomly distributed in space (in all cases in Secs. VII and VIII). The echo is sampled from a single beam for a random spatial distribution of scatterers and the beam is not steered adaptively to select or focus on a particular scatterer. (4) *Environment*: direct path geometries in which the medium is homogeneous and there are no reflecting boundaries (in Secs. VI and VII; and one case in Sec. VIII).

The following cases for systems, signals, and environments of greater complexity are examined in Sec. VIII: (1) *Signal type and signal processing*: pulsed signals are modeled in one example in which the echoes from the scatterers only partially overlap (Sec. VIII A). In Sec. VIII A, the pulse is further shortened through use of matched filter processing. (2) *Environment*: in two examples, geometries in which there are one or more boundaries present and there are heterogeneities in the medium (Secs. VIII B and VIII C, which cover boundary interaction and waveguide effects).

The several cases modeled in Sec. VIII, while far from spanning the many possible complex scenarios, provide examples for how the fundamental formulations involving

the more simple cases can be applied to the more complex cases. For example, the case involving a pulsed signal shows how a time series can be constructed due to the interference between the partially overlapping echoes from the scatterers (Sec. VIII A). The examples involving the presence of one or more boundaries and/or heterogeneities in the medium show the different types of effects associated with the boundaries and medium heterogeneities. For a single boundary near a scatterer, it can provide an added source of interference due to the interaction of the incident signal and the boundary and scatterer (Sec. VIII B). For two parallel boundaries and/or a medium with a local minimum in wave speed, a waveguide is formed and the signal can propagate along multiple paths that are guided by the boundaries or local minimum (Sec. VIII C). These multiple paths represent additional sources of fluctuations in the echoes.

B. Peak sampling, pulsed signals with boundaries, and beyond

There are many more important cases not covered explicitly in this tutorial, but that can be described using these formulations. For example, there are systems that use peak sampling signal processing, such as recording the maximum echo magnitude in a time window or adaptively steering a beam toward the scatterer with the largest echo. When multiple scatterers are present, the process of peak sampling in both cases (time and angle/space) will bias the statistics toward higher values than the magnitudes modeled with first-order statistics and a fixed beam. This process involves “extremal” statistics (Stanton, 1985), which is outside the scope of this tutorial. However, for the time-based peak sampling, the method in Sec. VIII A that produces a time series could then serve as a basis of the time series with which a peak sampling algorithm could be applied. As shown in Stanton (1985), the bias in this case increases with the ratio of window duration to ping duration of the signal. For the case of a scanning beam or multi-beam system adaptively focusing on the peak echo in a field of multiple scatterers, this extremal statistics formulation can be adapted from a time series to a space series of echoes scanned across angles. The bias here will increase as the angular window is increased.

Another important case involves use of pulsed signals in the presence of boundaries in which the echoes from the scatterers are only partially overlapping. Here, the method given in Sec. VIII A to produce a time series can be incorporated into the formulations in Secs. VIII B or VIII C that involve the presence of boundaries. Furthermore, advanced signal processing such as peak sampling can also be incorporated into this case as described above.

VI. IN-DEPTH TREATMENT OF ECHO STATISTICS: NO BEAMPATTERN EFFECTS

Given the complex effects of the beampattern on the echo statistics (Fig. 4), fluctuations of the echoes without the influence of the beampattern are first examined separately. This is equivalent to a sensor system with an omnidirectional beam so that the echo value is the same

regardless of angular location (at constant range) in the beam. In this simplified case, fluctuations can be due to a combination of interference between overlapping echoes and scattering effects. Fluctuations due to those effects are treated separately below.

A. Addition of random signals (generic signals; not specific to scattering)

This initial treatment solely involves analyses of generic random signals, devoid of explicit representation of the sensor system and field of scatterers. This analysis forms the foundation for the more complex analyses given later that first involve scattering from objects and, eventually, system effects. The case of an arbitrary number of arbitrary signals is first presented, which is then followed by some commonly used special cases, including the Rice and K PDFs.

1. Arbitrary cases

When N arbitrary complex signals completely overlap, the resultant signal A is the coherent sum

$$A = \sum_{i=1}^N a_i e^{j\Delta_i}, \quad (24)$$

where a_i and Δ_i are the amplitude and phase of each individual signal, respectively, and are both considered arbitrary random variables. Since this equation models sinusoidal signals, all with the same frequency, the term $e^{-j\omega t}$ that each signal has in common, has been suppressed as in the previous formulations.

Since a_i and Δ_i are random variables, then so is A . The fluctuations of A from realization to realization depend strongly on the statistical properties of a_i and Δ_i . The phase shifts Δ_i play a major role in the fluctuations. For example, for the simple case in which a_i is constant for all i (i.e.,

$a_i = a$) and Δ_i is randomly and uniformly distributed over the range $0-2\pi$, A will fluctuate greatly from realization to realization due to variability in constructive and destructive interference effects associated with phase variability alone (Figs. 2 and 6). In one realization, there may be complete constructive interference and A is at a maximum. In another realization, there may be complete destructive interference and A is at a minimum. And, generally, A will take on intermediate values due to partial interference.

The characteristics of the fluctuations in this case also depend greatly on N as illustrated. When there is only one signal ($N = 1$), the signal is single valued and the PDF of the signal magnitude $|A|$ is the delta function (Fig. 2). In the other extreme in which there are an infinite number of signals ($N = \infty$), the PDF of $|A|$ is the Rayleigh PDF as given in Eq. (21) (Fig. 2). The PDF of $|A|$ takes on other shapes for intermediate values of N (Fig. 6). In the more general case in which a_i is a random variable (not equal), the curves will fluctuate in a similar fashion and, in the limit of $N = \infty$, the PDF of $|A|$ will become Rayleigh via the CLT.

Equation (24) is broadly applicable to the scattering problem as it could represent the summation of scattering highlights from within a single scatterer or the summation of echoes from multiple scatterers. Characteristics of the scatterer, sensor system, and scattering geometry can be incorporated into N , a_i , and Δ_i .

2. Sine wave plus noise (Rice PDF)

Equation (24) can be manipulated to model the important case of a signal in the presence of noise. In this case, one of the amplitudes a_i is held fixed while the others are

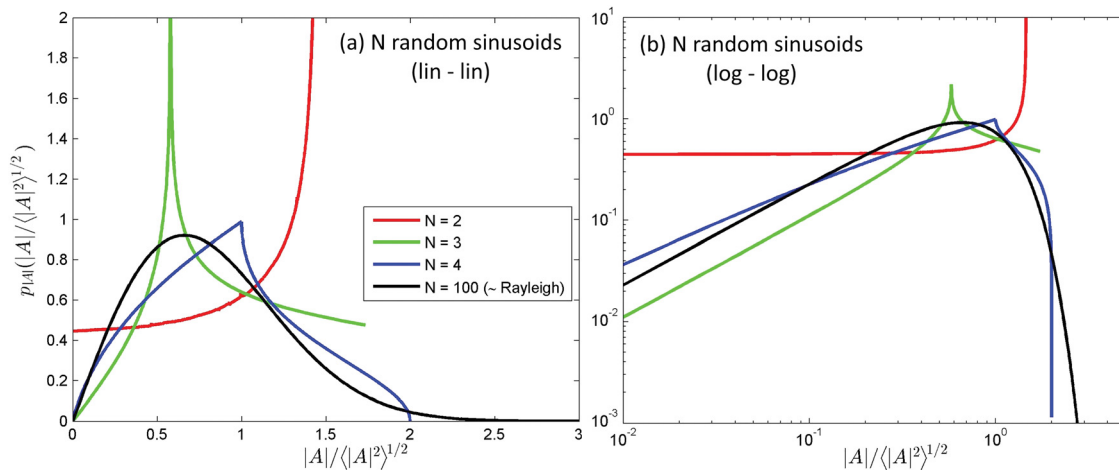


FIG. 6. (Color online) PDFs of magnitudes of sums of N random phase sinusoids of identical amplitude. The phasor addition given in Eq. (24) was evaluated using Monte Carlo simulations (10^7 realizations) in which $a_i = \text{constant}$ and Δ_i are randomly and uniformly distributed over $[0, 2\pi]$. The curves are shown to vary significantly for small N and approach the Rayleigh PDF for high N . The PDFs are plotted on both linear-linear and logarithmic-logarithmic scales in (a) and (b), respectively. The curves for $N = 2$ and 3 in this figure are also presented in Jao and Elbaum (1978) using an analytical approach involving characteristic functions (noise-free, $r = \infty$ curves in Figs. 2 and 4, respectively, of Jao and Elbaum). Note that Figs. 2 and 4 of Jao and Elbaum also show those curves to become rounded once noise is added [similarly, Fig. 2 of Chu and Stanton (2010) illustrates (rounded) PDFs for N sinusoids in the presence of noise for a 20 dB signal-to-noise ratio]. The software used to produce this figure is in the supplementary material at <https://doi.org/10.1121/1.5052255>. The software is also stored online (Lee and Baik, 2018), where it is subject to future revisions.

randomly varied. Pulling the fixed-amplitude signal out of the summation, Eq. (24) is rewritten,

$$A = ae^{j\Delta} + \sum_{i=1}^N a_i e^{j\Delta_i}, \quad (25)$$

where the second term on the right-hand-side, representing noise, is the sum of a large number of random amplitude, random phase signals. The PDFs of the magnitudes of the fixed amplitude and summed signals are the delta function and Rayleigh PDF, respectively. Here, N must be sufficiently large so that the magnitude of the summation converges to a Rayleigh random variable. The PDF of $|A|$ is the Rice PDF (Rice, 1954),

$$p_{Rice}(|A|) = 2|A| \frac{(1+\gamma)}{\langle |A|^2 \rangle} e^{-[(1+\gamma)|A|^2 + \gamma\langle |A|^2 \rangle] / \langle |A|^2 \rangle} I_0(q) \quad (26)$$

(RicePDF),

where

$$q \equiv 2|A| \left[\frac{\gamma(1+\gamma)}{\langle |A|^2 \rangle} \right]^{1/2}, \quad (27)$$

and

$$\gamma = \frac{a^2}{\sigma_n^2}. \quad (28)$$

The term γ is the ratio of the mean squared values of the sine wave and noise (i.e., the power signal-to-noise ratio or SNR where the “signal” is the sine wave in this context), σ_n is the *rms* value of the noise term, $\langle |A|^2 \rangle$ is the mean square of the sine wave plus noise [i.e., mean square of Eq. (25)], and I_0 is the zeroth-order modified Bessel function of the first kind. Note that in the original derivation by Rice, the noise term in

Eq. (25) can also involve the summation of signals of different frequencies as well (i.e., more general than the single frequency case shown here).

The shape of the Rice PDF depends strongly on γ (Fig. 7). For example, in the limit as γ approaches infinity, the PDF is close to a Gaussian PDF. This corresponds to the limit of high SNR where the signal is dominated by the constant sine wave. In the other extreme, as γ approaches zero, the PDF approaches the Rayleigh PDF. This latter case corresponds to the limit of low SNR where the signal is dominated by the noise. The shape of the Rice PDF changes smoothly for all intermediate values of γ .

In addition to this formula being widely applicable in modeling noisy signals, it can also be applied to scattering problems where the “signal” [sine wave in Eq. (25)] is the mean scattered field and the “noise” [summation term in Eq. (25)] is the component of the scattered signal that fluctuates about the mean (Stanton and Clay, 1986; Stanton and Chu, 1992). For example, it could be used to model the fluctuations of the echo from a sphere near a rough interface where the individual echoes from the sphere and rough interface are delta-function- and Rayleigh-distributed, respectively. Or, rather than a rough interface, the sphere could be surrounded by a cloud of smaller scatterers whose individual echoes are of random phase. If the constant sine wave in Eq. (25) is considered to represent a single scatterer of interest (such as the sphere) and the noise term represents the background reverberation (such as from the rough interface or cloud of smaller scatterers), then the term γ is the signal-to-reverberation ratio.

3. Special distributions of N or a_i (K PDF)

A more complex, but commonly occurring, case is when N and/or a_i in Eq. (24) are random variables. This can be divided into two categories—one in which Δ_i is randomly and uniformly distributed over the range $0-2\pi$, and the other in which Δ_i is non-uniformly distributed. The former

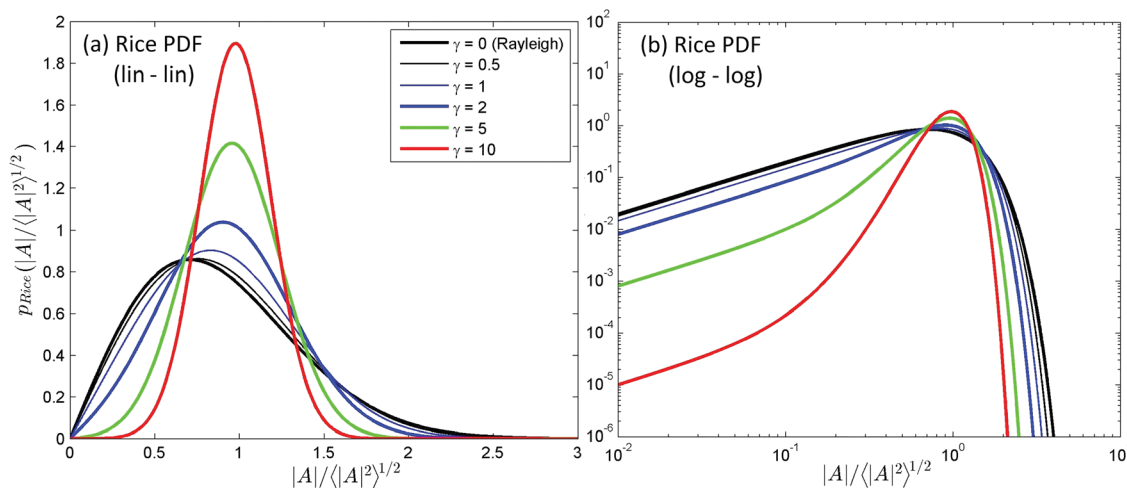


FIG. 7. (Color online) Rice PDF for various values of shape parameter γ . The curves were calculated with the analytical solution given in Eq. (26). The PDF approaches the Rayleigh and Gaussian distributions as γ approaches 0 and ∞ , respectively. The PDFs are plotted on both linear-linear and logarithmic-logarithmic scales in (a) and (b), respectively. With each function plotted on a normalized scale, the curves are independent of the mean square magnitude of the signal and only depend upon γ . The software used to produce this figure is in the supplementary material at <https://doi.org/10.1121/1.5052255>. The software is also stored online (Lee and Baik, 2018), where it is subject to future revisions.

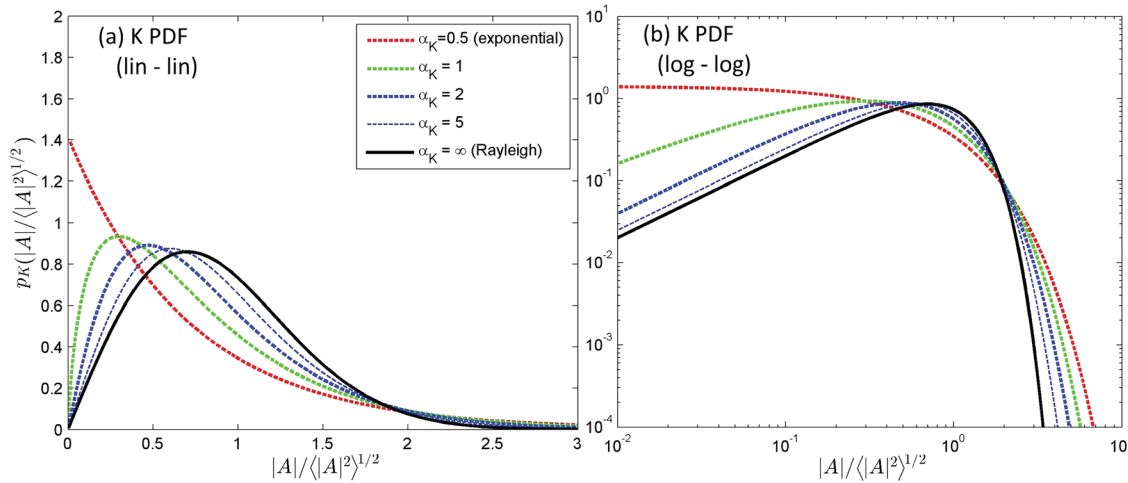


FIG. 8. (Color online) K PDF for various values of shape parameter α_K . The curves were calculated with the analytical solution given in Eq. (29). With each function plotted on a normalized scale, the curves are independent of the mean square magnitude of the signal and only depend upon α_K . The PDFs are plotted on both linear-linear and logarithmic-logarithmic scales in (a) and (b), respectively. The software used to produce this figure is in the supplementary material at <https://doi.org/10.1121/1.5052255>. The software is also stored online (Lee and Baik, 2018), where it is subject to future revisions.

category will first be discussed. If N follows a negative binomial PDF and its average value tends to infinity, the statistics of $|A|$ in Eq. (24) for arbitrary a_i is described by the K PDF (Jakeman and Pusey, 1976; Abraham and Lyons, 2002b),

$$p_K(|A|) = \frac{4}{\sqrt{\lambda_K} \Gamma(\alpha_K)} \left(\frac{|A|}{\sqrt{\lambda_K}} \right)^{\alpha_K} K_{\alpha_K-1} \left(\frac{2|A|}{\sqrt{\lambda_K}} \right) \quad (\text{K PDF}), \quad (29)$$

where K is the modified Bessel function of the second kind (and served in the naming of the PDF), Γ is the gamma function, α_K is the shape parameter, and λ_K is a scale parameter equal to the mean square of the signal divided by α_K .

The K PDF has a single mode and varies smoothly with $|A|$ (Fig. 8). The distribution tends to the Rayleigh PDF in the limit of high α_K . Note that the function K also has other, less common names, including the Basset function and the modified Bessel function of the *third* kind.

The K PDF can also be derived in several other ways. For example, it has been shown that for finite N and if a_i follows an exponential PDF, then $|A|$ is K-distributed (Abraham and Lyons, 2002b). Beyond methods involving summing sinusoidal signals, the K PDF has been shown to be due to the product of two independent random variables: a Rayleigh-distributed term and one that is chi distributed (Ward, 1981). This product was later written in extended form as the product of a Rayleigh-distributed term and the square root of a term that is gamma distributed (Abraham and Lyons, 2002b). Here, the square root of the gamma-distributed term is related to the chi-distributed term through analytical continuation of the integer number of summed terms in the chi distribution to a non-integer number in the gamma distribution. In another derivation, the K PDF has also been shown to result from a Rayleigh PDF whose mean-square value is gamma distributed (Jakeman and Tough, 1987). Both of these latter derivations are referred to as a “compound representation.”

Equation (29) has been widely used to describe echo statistics in both acoustic and electromagnetic applications.

While there has generally not been a direct connection to the physics of the scattering, the tail of the distribution has generally followed those from experimental data after an empirical fit. As discussed above, through the interpretation of Abraham and Lyons (2002b), the number of scatterers has been related to the shape parameter of the K PDF for the specific case in which the amplitudes a_i of the individual echoes are exponentially distributed. Since a_i in this case is observed through the receiver of the sensor system, the exponential PDF includes the effects of both fluctuations from the stochastic nature of the scatterer and the variability due to the scatterer being randomly located in the beam. Details of those effects are given in Sec. VII. Also, in his expression of a K-distributed magnitude being due to the product of Rayleigh- and chi-distributed random variables, Ward (1981) attributed the Rayleigh term as being due to quickly varying interference between scatterers (such as from phase shift differences within a patch of scatterers) and the chi term being due to slowly varying changes in the echo from larger-scale variations in the “bunching” or patchiness of scatterers.

The above K PDF involves signals who phases are uniformly and randomly distributed over $[0 \ 2\pi]$. However, when the distribution of phases is non-uniform, then $|A|$ can be described by the *generalized* K-distribution (not shown) (Jakeman and Tough, 1987). This distribution is described by three parameters— λ_K and α_K as given above, plus a third that describes the non-uniform phase distribution. In addition, the generalized K PDF in Jakeman and Tough (1987) can also describe an n-dimensional random walk (generalized from the two-dimensional walk for the standard K PDF). For the case of a non-uniform phase distribution, this is a random walk with directional bias. Similar to the compound representation of the K PDF above being a Rayleigh PDF with its mean-square value being gamma distributed, with this directional bias, the generalized K PDF can be (compound) represented by a Rice PDF with the mean square noise and constant amplitude signal components each

being gamma distributed in a correlated way (Jakeman and Tough, 1987). The generalized K PDF can be applicable to the case in which one or several scatterers dominate the scattering from within a field of many scatterers, thus skewing the distribution of phases into one that is non-uniform (Ferrara *et al.*, 2011).

Another generalization of the K PDF is the *homodyned* K-distribution (not shown). Like the generalized K PDF, it is also a three-parameter distribution. And, like the generalized K PDF, it can also be (compound) represented by a Rice PDF, but with only the mean square noise component (but not the constant amplitude component) being gamma distributed (Jakeman and Tough, 1987).

The properties and potential relations to scattering of the K PDF, generalizations of the K PDF, and other generic PDFs are summarized in Destrepes and Cloutier (2010).

4. Adding independent realizations of the complex signal A

As discussed in Secs. IVC6 and VIA1, in the limiting case of the sum of an infinite number of random complex variables, the PDF of the magnitude of the sum is Rayleigh distributed (as per the CLT). Specifically, for Eq. (24) where the phase shifts Δ_i are randomly and uniformly distributed over the range $0-2\pi$, in the limit of $N = \infty$, $|A|$ is Rayleigh distributed. Now, consider the case in which there is an ensemble of statistically independent realizations of the complex signal A (in the limit of large N) where the magnitude of each realization of A is Rayleigh distributed and with the same mean square value. Then by extension of the CLT, the magnitude of the sum of those realizations of A is likewise Rayleigh distributed, even for a finite number of realizations. However, if each realization of A is modulated by a multiplicative term with a magnitude that is a random variable, the resultant magnitude of the sum of a finite number of these (complex) signals can possibly be strongly non-Rayleigh. As described in Sec. VIA3, such a modulation can be caused by patchiness of the scatterers, resulting in echo PDFs that can be derived through a compound representation. Also, when the scatterers are uniformly distributed (i.e., no patchiness effects), there can also be modulation caused by the beam pattern where the echo from the scatterer is randomly modulated by its random location in the beam, causing strongly non-Rayleigh echoes as described in Secs. VIIB and VIIC.

B. Complex scatterers with stochastic properties

Scatterers can range in complexity from the simplest of form, a point scatterer, in which the scattering amplitude is constant for all orientations, to an arbitrarily shaped object whose echo varies from orientation to orientation. In this section, the statistics of scattering by an individual are examined in a progression of complexity. The point scatterer, Rayleigh scatterer (defined below), and smooth and rough prolate spheroids with both fixed and random orientation are modeled. A summary of scatterers with other complexities are given at the end.

1. Point scatterer

The simplest case is the point scatterer or, more precisely, very small scatterer. The dimensions of this scatterer are sufficiently small compared with an acoustic or electromagnetic wavelength that the echo is constant for all orientations. It is constant because there is only one scattering highlight from this object and nothing else with which to interfere. The PDF of the echo magnitude is the delta function [Figs. 2(a) and 3(a)].

2. Rayleigh scatterer

At the other extreme from a point scatterer is a scatterer whose echo is Rayleigh distributed. This so-called “Rayleigh scatterer” can be in many forms. For example, it could be a small patch of many point scatterers, each with an echo whose phase is randomly and uniformly distributed over the range $[0, 2\pi]$. Or, it could be a single spherical scatterer whose surface is randomly rough and can be described as a collection of many scattering highlights bounded by the surface. The echo from each highlight has a phase that is randomly and uniformly distributed over the range $[0, 2\pi]$. In each case, from the central limit theorem, the echo from the patch or rough sphere is Rayleigh distributed [Fig. 2(c); Eq. (21)]. The fluctuations occur from ping to ping as the patch or rough sphere are rotated, or from realization to realization of a randomized spatial distribution of scatterers in the patch or randomized roughness of the rough sphere.

3. Randomized prolate spheroid

A sequence of formulations is presented, beginning with the deterministic description of the scattering by a smooth prolate spheroid at fixed orientation, then randomizing its orientation, and then further randomizing the spheroid by roughening its boundary. In contrast to the Rayleigh scatterer, the echoes from the randomized prolate spheroid are generally non-Rayleigh because of the elongated shape of the prolate spheroid. The degree to which the echoes are non-Rayleigh can be connected to various parameters of the scatterer through the physics-based formulas given below. The formulas given below are adapted from Bhatia *et al.* (2015).

a. Smooth boundary, fixed orientation. We begin with a deterministic description of the scattering by a smooth prolate spheroid at fixed orientation. The spheroid is modeled as being impenetrable (acoustically “hard” or “soft” or, with an electromagnetic signal, perfectly conducting). Also, the scattering is in the “geometric optics” or high frequency limit where the acoustic or electromagnetic wavelength is much smaller than any dimension of the spheroid. For simplicity, only echoes from the front interface are analyzed and waves that travel around the boundary (i.e., circumferential waves) are ignored. Using the Kirchhoff approximation and the stationary phase approximation, the magnitude of the backscattering amplitude of the spheroid is (Chap. 4 of Crispin and Siegel, 1968)

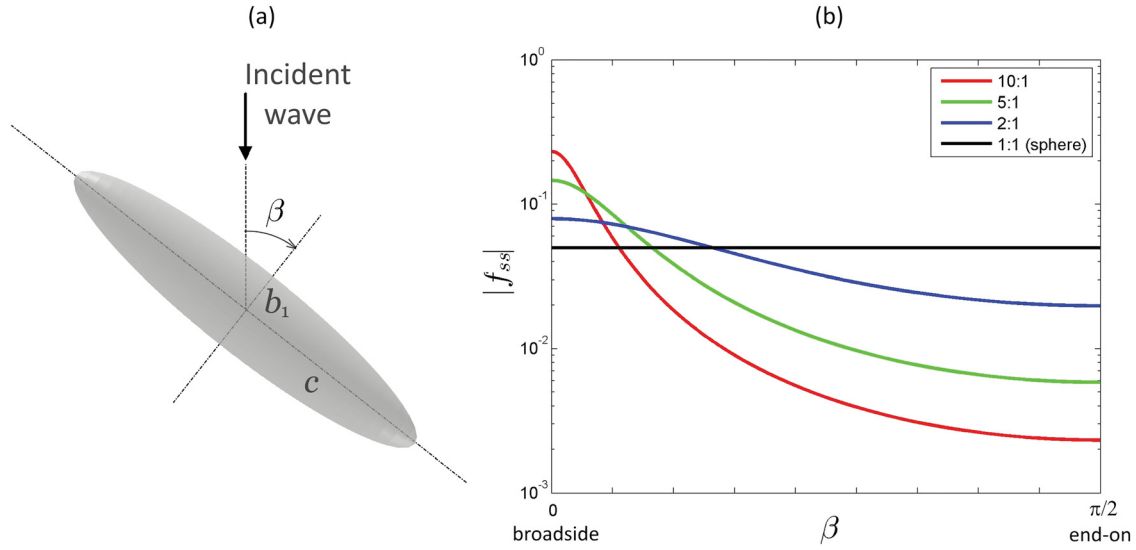


FIG. 9. (Color online) Backscattering by an impenetrable prolate spheroid. (a) Scattering geometry. The term β is the angle between the direction of the incident wave and the plane that is normal to the lengthwise axis of the prolate spheroid. For simplicity, this illustration is drawn in the plane containing the incident wave vector and the lengthwise axis. (b) Magnitude of scattering amplitude (backscatter direction) versus angle of incidence β for smooth prolate spheroids. The curves were calculated with the analytical solution given in Eq. (30). All spheroids, which span a range of aspect ratios from 1:1 (sphere) to 10:1 (most elongated), have the same volume equal to that of a sphere of radius 0.1 m. Adapted from Bhatia *et al.* (2015). The software used to produce panel (b) of this figure is in the supplementary material at <https://doi.org/10.1121/1.5052255>. The software is also stored online (Lee and Baik, 2018), where it is subject to future revisions.

$$|f_{SS}| = \frac{\frac{1}{2}cb_1^2}{b_1^2 \cos^2\beta + c^2 \sin^2\beta} \quad (\text{smooth boundary, fixed orientation}), \quad (30)$$

where the “SS” subscript to the scattering amplitude refers to “smooth spheroid” and β is the angle between the direction of the incident acoustic or electromagnetic wave and the plane that is normal to the lengthwise axis of the prolate spheroid [Fig. 9(a)]. Note that this equation is equivalent to Eq. (7) of Bhatia *et al.* (2015), but is in a form in which no terms have singularities. $\beta=0$ and $\beta=\pi/2$ correspond to broadside and end-on incidence, respectively, relative to the incident wave. The terms c and b_1 are the lengths of the semimajor and semiminor axes of the prolate spheroid, respectively (the length and width of the spheroid are $2c$ and $2b_1$, respectively). The spheroid is axisymmetric about the length-wise axis, leading to only one unique value of semiminor axis. The term b_1 is not to be confused with the beampattern b . The aspect ratio of the spheroid is defined to be the ratio c/b_1 (or, equivalently, length/width). The scattering is a strong function of the aspect ratio and orientation [Fig. 9(b)]. At broadside incidence, the above formula reduces to

$$|f_{SS}| = \frac{c}{2}. \quad (31)$$

b. Smooth boundary, random orientation. We now randomize the scattering by first randomizing the orientation. This is done by making β a random variable with an associated PDF $p_\beta(\beta)$. For simplicity, the prolate spheroid will only rotate in a single plane about its minor axis in a plane containing the direction vector of the incident plane wave [Fig. 9(a)].

Since the scattering amplitude f_{SS} is a function of the random variable β , then f_{SS} is a random variable as well. Inserting $|f_{SS}|$ and $p_\beta(\beta)$ into Eq. (16), the PDF of the magnitude of the scattering amplitude of a randomly oriented smooth prolate spheroid is

$$p_{SS}(|f_{SS}|) = \left. \frac{p_\beta(\beta)}{\left| \frac{\partial |f_{SS}|}{\partial \beta} \right|} \right|_{\beta(|f_{SS}|)} \quad (\text{smooth boundary, random orientation}). \quad (32)$$

Equation (16) was used because the scattering amplitude in Eq. (30) varies monotonically over the entire range of orientations. If the scattering amplitude varied non-monotonically, then Eq. (17) would have been required to calculate the echo PDF.

Inserting Eq. (30) into Eq. (32) gives the PDF of the magnitude of the scattering amplitude of a randomly oriented smooth prolate spheroid explicitly in terms of the dimensions of the prolate spheroid,

$$p_{SS}(|f_{SS}|) = p_\beta(\beta) \frac{(b_1^2 \cos^2\beta + c^2 \sin^2\beta)^2}{cb_1^2(c^2 - b_1^2) |\sin\beta \cos\beta|} \Big|_{\beta(|f_{SS}|)} \quad (\text{smooth boundary, random orientation}). \quad (33)$$

Calculation of the echo PDF requires knowledge of the orientation distribution. For the simple case in which the angles of rotation are uniformly and randomly distributed over the range $[0, 2\pi]$, the PDF of β is

$$p_\beta(\beta) = \frac{2}{\pi}, \quad 0 \leq \beta \leq \frac{\pi}{2} \quad (\text{rotation in one plane}), \quad (34)$$

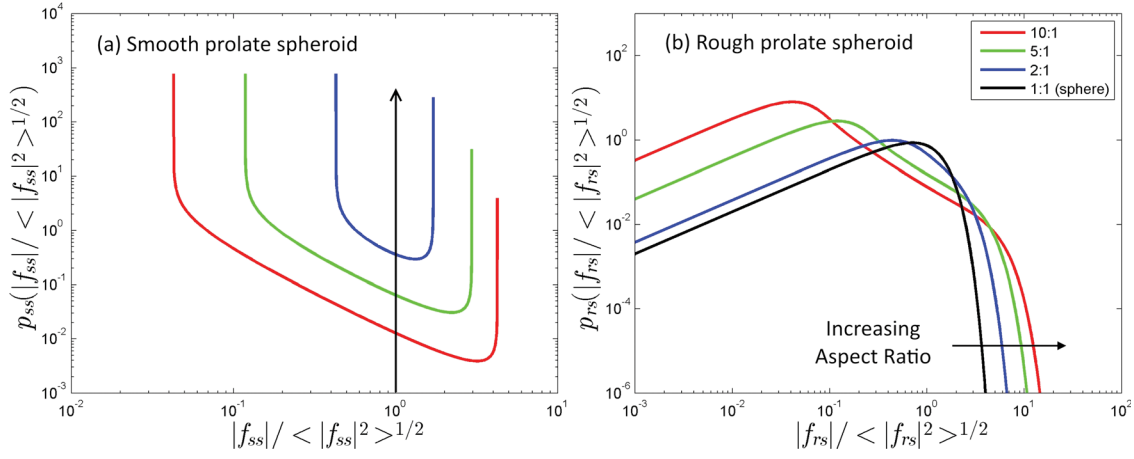


FIG. 10. (Color online) PDF of magnitude of backscattering amplitude for (a) smooth prolate spheroid and (b) rough prolate spheroid. Each spheroid is randomly and uniformly oriented in a single plane. The axis of rotation (a minor axis of the spheroid) is the normal to this plane, which contains the omnidirectional sensor system. Aspect ratio is varied from 1:1 (sphere) to 10:1 (most elongated). The curves in (a) (not including the sphere) and (b) are calculated using the analytical solutions given in Eqs. (33) and (35), respectively. Equation (34) was used in each case for the orientation distribution. Equation (33) for p_{ss} is used in the integrand in Eq. (35). The Rayleigh PDF [from Eq. (21)] in the integrand of Eq. (35) is normalized so that the rms amplitude is equal to unity. From Bhatia *et al.* (2015). The software used to produce this figure is in the supplementary material at <https://doi.org/10.1121/1.5052255>. The software is also stored online (Lee and Baik, 2018), where it is subject to future revisions.

where β only varies over the range $0-\pi/2$ because of the symmetry of the scattering over the other angles.

The echo PDF for the randomly oriented smooth prolate spheroid is calculated for a range of aspect ratios (not including the case of a sphere where the aspect ratio is unity) by inserting Eq. (34) into Eq. (33) [Fig. 10(a)]. For each (non-unity) aspect ratio, the echo PDF is characterized by a smoothly varying function for most magnitudes, but with strong narrow peaks at the end points. These peaks are attributed to the fact that the backscattering near broadside and end-on incidence varies slowly with orientation angle, which increases the probability of occurrence at those corresponding echo values. The range of echo values as well as probability of occurrence are both shown to be a strong function of aspect ratio of the spheroid. For the case of a sphere, the echo is constant for all β and the echo PDF is a delta function [Fig. 10(a)].

c. Rough boundary, random orientation. We further randomize the scattering by roughening the boundary of the prolate spheroid, where the roughness here is the deviation from the mean boundary. In this case, the boundary is randomly rough throughout the entire surface of the spheroid. Furthermore, it is assumed to be sufficiently rough compared with an acoustic or electromagnetic wavelength such that for any orientation, the magnitude of the scattering amplitude is Rayleigh distributed. For the randomly rough surface, the echoes are assumed to be independent of each other from orientation to orientation (or realization to realization). In this limiting case, we model the scattering by being equal to the product of the magnitude of the scattering amplitude $|f_{ss}|$ of the smooth prolate spheroid at a particular orientation and an independent “modulation” random variable that follows a Rayleigh PDF. This latter modulation term has a unity rms and, for each orientation, the term is statistically independent from its value at all

other orientations. For a randomly oriented prolate spheroid, $|f_{ss}|$ is also a random variable. Thus, the magnitude of the scattering amplitude for the randomly rough, randomly oriented prolate spheroid is the product of two random variables, $|f_{ss}|$ and the Rayleigh-distributed modulation term. The statistics of the echoes from randomly rough, randomly oriented prolate spheroids can be described using Eq. (20),

$$p_{rs}(|f_{rs}|) = \int_{|f_{ss}|_{\min}}^{|f_{ss}|_{\max}} \frac{1}{x} p_{SS}(x) p_{Ray}\left(\frac{|f_{rs}|}{x}\right) dx$$

(randomly rough boundary, random orientation), (35)

where the subscript “rs” refers to rough (randomly oriented) prolate spheroid and p_{Ray} is the Rayleigh PDF of the modulation term [Eq. (21)]. The terms $|f_{ss}|_{\min}$ and $|f_{ss}|_{\max}$ are the minimum and maximum values of the magnitude of the scattering amplitude of the smooth prolate spheroid, respectively, which correspond to end-on and broadside incidence. Those two terms replaced the limits $-\infty$ and $+\infty$, respectively, in the integral in Eq. (20) to reflect the fact that the magnitude of the scattering amplitude of the smooth prolate spheroid is within the range $[|f_{ss}|_{\min}, |f_{ss}|_{\max}]$ and that the corresponding PDF p_{ss} is zero for values of its argument outside that range. Without the above constraint, the integral still would have been constrained by the Rayleigh PDF whose argument is limited to only positive values, which would have led to integral limits of zero to infinity.

The resultant echo PDFs of the scattering by the randomly rough, randomly oriented prolate spheroid are significantly different from the smooth counterpart [Fig. 10(b)]. The curves for each aspect ratio are now smoothly varying, have a mode, and do not have any singularities.

4. Randomly rough objects with full range of roughness and circumferential/internal waves

There are many more important complexities of the scattering and associated echo statistics than described above and they are summarized briefly below. The above example involved the simplified case in which the boundary of the prolate spheroid was impenetrable, only the echo from the front interface was accounted for, and its roughness was sufficiently large so that the echo was Rayleigh distributed for any fixed orientation. However, it is not uncommon for an object to have circumferential and internally refracted/reflected waves and/or a boundary roughness that spans small-to-intermediate levels relative to a wavelength of the incident signal. Each of these latter cases can lead to statistics of the echo that are significantly different than that of the very rough impenetrable prolate spheroid discussed above and must be accounted for.

Given the complexity of predicting the scattering by objects with those various types of waves, the echo statistics will be summarized below according to a progression of complexity. In Sec. VIB 4a, effects on the scattering due to circumferential and internal waves for smooth objects are briefly reviewed. In Sec. VIB 4b, the object is roughened, and the statistics of the echoes from only the front interface are considered. This is similar to the case of the rough impenetrable prolate spheroid above but with the added complexity of accounting for small-to-intermediate roughness where the echoes are non-Rayleigh. In Sec. VIB 4c, circumferential/internal waves associated with penetrable materials are incorporated with boundary roughness included.

a. Circumferential and internal waves (smooth boundary). Objects with common material properties not only produce a significant echo from the front interface, but they also support various classes of circumferential and internally refracted/reflected waves due to incident signals (*acoustic*: Hackman, 1993; Marston, 1992; Numrich and Uberall, 1992; Uberall, 1973; *electromagnetic*: Chen, 1998; Crispin and Siegel, 1968; Moser *et al.*, 1981; Murphy *et al.*, 1980; Newton, 1982; *acoustic and electromagnetic*: Bowman *et al.*, 1987; Nussenzveig, 1969). For the case of impenetrable objects, such as infinitely dense materials for acoustics applications and perfectly conducting materials for electromagnetic applications, there is a weak signal that diffracts or “creeps” around the boundary and reradiates in all directions including back to the receiver. For the case of penetrable objects, such as elastic materials for acoustics applications and dielectric materials for electromagnetic applications, those diffracted waves also exist. In addition, with elastic objects, there can be strong surface elastic waves that are generated from the incident acoustic signal and will travel around the boundary (in addition to the diffraction boundary wave). Furthermore, other processes are also involved for the penetrable objects such as waves that refract into the interior of the object and reflect internally. Because of these various effects, the echo from a smooth symmetrical object such as a sphere or cylinder will generally be composed of the sum of echoes associated with the front-facing interface (sometimes

called the “specular” echo), internal transmission and reflections, and circumferential waves.

The total echo from these objects will vary according to the constructive and destructive interference between the individual echoes associated with each of the different scattering phenomena described above. For a smooth object such as a sphere or cylinder, the phase of the echo associated with each phenomenon will vary strongly with signal frequency (or more precisely, ka , where a is the radius of the object). Because of these frequency dependences, which also vary with each phenomenon, the pattern of echo vs frequency will contain a series of peaks and strong nulls associated with the constructive and destructive interference, respectively, between the different phenomena.

b. Front interface only: Small-to-intermediate roughness, Rice PDF. The following discussion concerns the echo from the front interface only, in isolation from the circumferential and internal waves.

When the roughness of the surface is smaller than the wavelength of the incident signal or, more precisely, when $k\sigma_B < 1$, where σ_B is the standard deviation of the boundary (or, equivalently, the *rms* deviation from the mean boundary), the magnitude of the echo from the front-facing surface of a rough object at normal incidence to that surface is generally not Rayleigh distributed. This is because the phases of the echoes from the individual scattering features of the surface are relatively narrowly distributed, in contrast to being uniformly distributed $[0, 2\pi]$ such as in the above case of the (very) rough spheroid. This effect has been studied mostly in the context of scattering by rough planar interfaces and, to a much lesser extent, for rough bounded objects. In either case, in the limit of small roughness (i.e., $k\sigma_B \ll 1$), the echo PDF will tend to the delta function. In the opposite limit (i.e., $k\sigma_B \gg 1$), the echo PDF will tend to the Rayleigh PDF (or at least be Rayleigh-like) as in the above example.

It has been shown that the echo statistics from the full range of roughness at normal incidence of a planar boundary can be described by the Rice PDF, as given above in Eq. (26) (Stanton and Clay, 1986). In this formulation, the scattered signal is decomposed into the sum of two components, the coherent mean (constant amplitude) and fluctuation component. The PDFs of the magnitudes of the two components are the delta function and Rayleigh PDF, respectively. The mean component is related to the reflection coefficient of the interface modified by the term $e^{-2k^2\sigma_B^2}$ —a term originally derived for rough planar interfaces by Eckart (1953). The fluctuation term is related to the scattering phenomena that cause deviations in the echo from this mean. These two scattering terms, the constant amplitude and fluctuation components, correspond to the sinusoidal signal and noise, respectively, in the original Rice formulation.

The Rice PDF shape parameter has also been explicitly connected to parameters of the roughness and sensor system for rough planar interfaces (normal incidence), as summarized in Stanton and Clay (1986). Parameters of the roughness are the *rms* deviations (σ_B) from the normal to the mean surface and the two-dimensional autocorrelation function (along the surface) of the surface. Parameters of the sensor

system are the frequency and beampattern. Although the studies summarized in [Stanton and Clay \(1986\)](#) are specific to underwater acoustic signals, the analysis involving the Rice PDF is formulated for scalar fields and could be applied to other types of sensor systems, such as radar, when scalar field representations are appropriate.

These formulations connecting the Rice PDF to fluctuations due to randomized scattering by a rough planar surface were extended to the case of acoustic scattering by rough elastic cylinders immersed in a fluid in [Stanton and Chu \(1992\)](#) and [Gurley and Stanton \(1993\)](#). Because of the complexity of the scattering by the elastic objects, the analysis in [Stanton and Chu \(1992\)](#) was divided into two formulations—a general one which described all echoes (i.e., including those associated with the front interface, the circumferential waves, and internally refracted waves) and a simple analysis involving only the front interface. The fluctuations of the echo from the rough front (curved) interface were related to the Rice PDF in the same manner as with the case of the rough planar interface involving a scalar field, but taking into account curvature of the surface. This simpler approach is clearly an approximation to the other, more general, case where the other waves played a major role in the fluctuations, especially near nulls due to interference effects (as discussed below). However, the Rice PDF, when used to model fluctuations of the echo from the front interface only, was demonstrated in these studies to predict the general trend of the fluctuations as parameters such as ka and $k\sigma_B$ were varied, where a is the mean radius of the rough cylinder.

An important element in the modeling of both the above simple and general cases was the fact that the Rice PDF assumes a noise term whose quadrature (i.e., real and imaginary) phase components have the same mean square values. However, the quadrature components of the random component of the scattered (scalar) signal from rough interfaces are generally not equal. Furthermore, the fluctuations of the scattered signal are sensitive only to the component of the “noise” (i.e., fluctuation component of scattered signal) that is *in phase* with the mean scattered field. These effects are quantified and accounted for in [Stanton and Chu \(1992\)](#) where the Rice PDF shape parameter is formulated in terms of the in-phase component of the fluctuation component of the scattered field.

c. Randomized circumferential and internal waves added to front interface echo; nulls and attenuation effects. The complexity is now increased by accounting for circumferential and internally refracting waves so that the echo consists of *all* waves—due to the front interface and circumferential/internal waves. As discussed above, in the case of the smooth penetrable object, these waves will interfere with each other and cause deep nulls in the pattern of echo magnitude versus frequency. When the penetrable object is roughened, the phases of the echoes associated with the various scattering phenomena will correspondingly vary, each in a different manner specific to the respective phenomenon. The total echo (sum of all components) will fluctuate from realization to realization due to the random roughness

in a manner broadly similar to that from an impenetrable rough object but with important differences. For example, the center frequency of the nulls from the destructive interference will vary from realization to realization. Because of the steepness of the null (typically 30 dB variation within a narrow band of frequencies), the echo at frequencies near that of the null will fluctuate significantly.

The fluctuations near the null for acoustic scattering by randomly rough elastic cylinders immersed in a fluid have been observed in both numerical ([Stanton and Chu, 1992](#)) and experimental ([Gurley and Stanton, 1993](#)) studies. In these studies, the shape parameter of the Rice PDF, when fit with the simulations or experimental data, is shown to vary dramatically at frequencies near each null. The shape parameter decreases by as much as two orders of magnitude near the null which corresponds to a similar increase in the degree to which the echo fluctuates.

The roughness not only affects the phase shifts of circumferential and internal waves, but also their magnitude. In one study, the dominant acoustic Lamb-wave (or “plate wave”) of a spherical elastic shell along all meridional paths was randomized due to the roughness. The variability in path length and, hence, phase of this circumferential wave was related to the roughness. The total Lamb wave echo summed from all paths was shown to be attenuated exponentially due to the decrease in coherence of the signal ([Stanton et al., 1998](#)).

Although the above two examples involved scattering of acoustic waves by elastic objects immersed in a fluid, the same principles apply to other sensor systems such as for medical ultrasound or radar applications. In general, when the phases of these different types of scattered signals vary randomly due to roughness, then the shape parameter of the echo PDF will vary significantly near any null in the echo versus frequency pattern. Similarly, any type of circumnavigating or internally refracting wave can experience attenuation due to the different ray paths adding incoherently.

VII. IN-DEPTH TREATMENT OF ECHO STATISTICS: WITH BEAMPATTERN EFFECTS

Beampattern effects are now added to the above treatment which involved the statistics of echoes from scatterers in the absence of beampattern effects (i.e., equivalent to an omnidirectional beam). Once the scatterers are placed in a directional beam of the sensor system, the echo received by the system becomes modulated by the beampattern. If the location of the scatterer is random, then the modulation is correspondingly random. In this case, the beampattern function is a random variable with a PDF referred to as the beampattern PDF.

The effect of the beampattern on echo statistics can be profound, as discussed in [Sec. II C](#) and illustrated ([Fig. 4](#)), and accounting for it can be complex. For example, in the simplest case of a point scatterer whose scattering amplitude is delta function distributed, the resultant echo PDF due to the scatterer being randomly located in a directional beam has a trend that is approximately power-law with strong structure superimposed [[Fig. 4\(d\)](#)].

The below treatment begins with a general formula for the echo PDF due to a single scatterer randomly distributed in a beam. The properties of the scatterer, spatial distribution, and beampattern are all arbitrary in this formula. Following the general formula is a progression of examples beginning with the simplest of cases—a point scatterer randomly and uniformly distributed within only the mainlobe of the beam of an axisymmetric transducer (i.e., excluding sidelobes). The analysis then extends to complex scatterers and the entire beam (including sidelobes) and, finally, to the case involving a beampattern from an arbitrary transducer in which the beampattern is not axisymmetric and a spatial distribution of scatterers that is not uniform. After the treatment of single scatterers, the echo statistics associated with multiple scatterers in the beam is presented. In the first set of examples, all scatterers are identical, which is then followed by the more general case of assemblages of scatterers of varying types.

The formulations can be applied to single beam (fixed or scanning) and multi-beam systems, provided that the scatterer(s) are randomly located in the beam. The formulations are general and are not specific to any particular system. Although specific types of signal processing or adaptive beamforming that some systems incorporate are not modeled, the formulations presented herein can serve as a basis for the modeling as discussed in Secs. V A and V B.

A. Single scatterer randomly located in beam

1. Accounting for beampattern effects in echo PDF

For the case in which a single scatterer is randomly located in the beam of the sensor system at approximately constant range, its angular coordinates (θ, ϕ) are random variables. Since the beampattern is a function of these random variables, the beampattern function $b(\theta, \phi)$ is also now a random variable (Sec. IV C 3) and can be described by the *beampattern* PDF, $p_b(b)$. Consider now a scatterer whose scattering properties are random (such as a randomly rough and/or randomly oriented elongated scatterer). The scattering amplitude is now a random variable and its magnitude can be described by the PDF $p_s(|f_{bs}|)$ (Secs. II B and VI B). The magnitude of the echo \tilde{e} received by the system is equal to the product of the magnitude of the scattering amplitude $|f_{bs}|$ and the beampattern $b(\theta, \phi)$ [Eq. (4)]. With both of these latter two terms being random variables, then \tilde{e} is also a random variable (Sec. IV C 4). Using Eq. (20), the PDF of \tilde{e} can be written in terms of p_s and p_b as [Ehrenberg (1972)]

$$p_e(\tilde{e}) = \int_{\tilde{e}}^{\infty} \frac{1}{x} p_s(x) p_b\left(\frac{\tilde{e}}{x}\right) dx, \quad 0 \leq b \leq 1, \quad (36a)$$

where x is used to denote $|f_{bs}|$. The term $b (= \tilde{e}/x)$ is implicitly the argument of p_b . Using the same procedure, $p_e(\tilde{e})$ can be expressed in an alternate, but equivalent form

$$p_e(\tilde{e}) = \int_0^1 \frac{1}{b} p_b(b) p_s\left(\frac{\tilde{e}}{b}\right) db, \quad 0 \leq b \leq 1. \quad (36b)$$

where now $|f_{bs}| (= \tilde{e}/b)$ is implicitly the argument of p_s .

Equations (36a) and (36b) are equivalent because of the commutative nature of the product of the two random variables in Eq. (20). The limits of $\pm\infty$ in the integral in Eq. (20) are reduced to the ranges $[\tilde{e} \infty]$ and $[0 1]$ in Eqs. (36a) and (36b), respectively, since the values of the beampattern b only span the range $[0 1]$ and the corresponding beampattern PDF p_b is zero outside that range. Finally, the range $0 \leq b \leq 1$ is used in each equation as they apply to the *entire* beampattern, whereas some applications later will involve only portions of the beampattern, such as for values of the mainlobe only above the highest sidelobe. In those cases, the limits in the integrals are modified accordingly.

These expressions, originally derived by Ehrenberg (1972) [using Eq. (20)] for echo intensity with identical form, are given for echo magnitude (i.e., not intensity) in Ehrenberg *et al.* (1981) and are also described in reviews in Stanton and Clay (1986) and Ehrenberg (1989). While use of one form over the other [Eq. (36a) vs Eq. (36b)] was not explained in the early papers, it is possible that one form may be more conducive for evaluation, such as in numerical integration (Bhatia *et al.*, 2015).

The above integral relationship in Eqs. (36a) and (36b) between the echo PDF $p_e(\tilde{e})$ and the PDFs of the magnitude of the scattering amplitude and beampattern function is completely general, as it applies to an arbitrary stochastic scatterer that is randomly located (at approximately constant range) in an arbitrary beampattern over an arbitrary spatial distribution. The constraint of the scatterers being at approximately constant range is consistent with Eq. (4) as these equations apply to the scatterers distributed within a thin shell at a nearly constant distance from the sensor system. This eliminates the range-dependent effects in analysis of the echo fluctuations.

2. PDF of spatial distribution of scatterer

The beampattern PDF depends not only on the beampattern function $b(\theta, \phi)$, but also the PDF, $p_{\theta,\phi}(\theta, \phi)$, of the angular location of the scatterer in the beam. This probability, in combination with the beampattern function, determines the degree to which the echo is randomly modulated by the beampattern. For example, if the scatterer were fixed in the center of the beam, then $p_{\theta,\phi}$ is a delta function peaked at $(\theta, \phi) = (0, 0)$ and the echo is multiplied by unity for all realizations [Fig. 4(a)]. In the other extreme, if the scatterer were randomly located throughout the entire half-space, then $p_{\theta,\phi}$ is finite for all θ and ϕ . In this latter case, the echo is randomly modulated by all values of the beampattern resulting in a wide range of echo values, even for a point scatterer [Fig. 4(d)].

Two simple examples are treated here involving the scatterer being randomly and uniformly distributed in a half-plane (2D) and half-space (3D) at approximately a constant range. The 2D and 3D cases apply to geometries in which the sensor system is detecting scatterers that are distributed throughout a thin semicircular arc and a thin hemispherical shell, respectively. The 2D case may apply to geometries where (1) the transducer is a line with a beampattern that only varies in one plane, (2) the sensor system is located within a thin layer of scatterers and is looking along the layer

from within that layer, or (3) the system is in a waveguide and long-range echoes only vary with respect to one dimension (such as in the plane parallel to the waveguide boundaries as described in Sec. VIII C). In all of these cases, only a half-plane or half-space are considered as the transducer is assumed to be baffled sufficiently so that there is no “back” radiation.

In each example, $p_{\theta,\phi}$ (which reduces to p_{θ} in some cases) is calculated using Eq. (8), where $p_X(x)$ in that equation is used to represent the probability of occurrence of the scatterer per unit volume at angular location (θ, ϕ) and x represents the volume V (Chap. 10 of Medwin and Clay, 1998). The term $dP_X (= dP_V)$ in Eq. (8) is the differential probability of occurrence of the scatterer in the differential volume dV at location (θ, ϕ) . For the case of the scatterers being located within a thin hemispherical shell of constant radius, which is the 3D geometry in most examples in this tutorial, then $dx = dV = r^2 \sin \theta d\theta d\phi \Delta r$, where r is the radius of the hemispherical shell, θ is the spherical polar angle, ϕ is the spherical azimuthal angle, and Δr is the thickness of the shell. For the case of the scatterers being located within a thin-shelled semi-circular arc of constant radius r , which is the 2D geometry sometimes used in this tutorial, then $dx = dV = rd\theta \Delta w \Delta r$, where Δw is the (thin) width of the circular arc (strip). The total volume of the thin shell in each of these two cases is $2\pi r^2 \Delta r$ and $\pi r \Delta w \Delta r$, respectively.

For a scatterer uniformly distributed within the volume, then the differential probability of occurrence dP_V per unit differential volume dV is held constant (i.e., $dP_V/dV = p_v = \text{constant}$). Using that constraint, and the fact that the integral of dP_V over the total volume that the scatterer can occupy is unity [and, hence, $dP_V/dV = p_v = (\text{total volume})^{-1}$], then $p_v = (\pi r \Delta w \Delta r)^{-1}$ and $p_v = (2\pi r^2 \Delta r)^{-1}$ for the 2D and 3D cases, respectively. Through these changes in variables, Eq. (8) becomes $dP_V = p_{\theta} d\theta$ and $dP_V = p_{\theta,\phi} d\theta d\phi$ for these two cases, respectively, where expressions for p_{θ} and $p_{\theta,\phi}$ are given below.

For the 2D case in which the scatterer is randomly and uniformly distributed in a half-plane at approximately constant range, the probability density function of the angular location of the scatterer in spherical coordinates is determined using the above approach,

$$p_{\theta} = \frac{1}{\pi}, \quad -\frac{\pi}{2} \leq \theta \leq \frac{\pi}{2}, \text{ fixed } \phi \quad (2\text{D}; \text{half-plane}). \quad (37)$$

There is no dependence upon θ since, at approximately constant range, the scatterer is uniformly distributed within a thin arc of nearly constant radius in that plane. There is no dependence upon ϕ as it is fixed in this geometry. Note that although the polar angle θ is normally restricted to the range $0 \leq \theta \leq \pi/2$, it is varied over the range $-\pi/2 \leq \theta \leq \pi/2$ for fixed ϕ . For the case of an axisymmetric beam centered at $\theta=0$ which is typically the major response axis (MRA) of the beam, the expression $p_{\theta} = 2/\pi$ for $0 \leq \theta \leq \pi/2$ has been used to eliminate redundant calculations (Bhatia et al., 2015).

For the 3D case in which the scatterer is randomly and uniformly distributed in a half-space at approximately constant range, the probability density function of its angular

location is determined using the above approach (Medwin and Clay, 1998),

$$p_{\theta,\phi} = \frac{1}{2\pi} \sin \theta, \quad 0 \leq \theta \leq \frac{\pi}{2}, \quad 0 \leq \phi \leq 2\pi \quad (3\text{D}; \text{half-space}). \quad (38)$$

Although the scatterers are located throughout all values of ϕ , $p_{\theta,\phi}$ still does not depend upon ϕ (as in the 2D case above). However, now $p_{\theta,\phi}$ depends upon θ because in this 3D polar-spherical coordinate system, the scatterer is randomly and uniformly distributed within a thin hemispherical shell in the range $0 \leq \theta \leq \pi/2$. Calculations in this coordinate system involve annular rings (at constant spherical radius), each located at some angle θ with a width of $d\theta$ and spanning all values of ϕ . Since the scatterer is randomly and uniformly distributed across all values of ϕ within each ring, then the probability $p_{\theta,\phi}$ only depends upon the area of each ring, which is proportional to $\sin \theta$ (which appears in the expression for dV above). Accounting for the uniform distribution across all ϕ $[0, 2\pi]$ for a given value of θ yields a factor $(2\pi)^{-1}$ in Eq. (38).

For the case in which the beampattern is symmetrical about the $\theta = 0$ axis, $p_{\theta,\phi}$ in Eq. (38) can be integrated over all ϕ $[0, 2\pi]$ for the simplified result

$$p_{\theta} = \sin \theta, \quad 0 \leq \theta \leq \frac{\pi}{2} \quad (3\text{D}; \text{half-space axisymmetric transducer}). \quad (39)$$

3. Beampattern PDF for mainlobe only (axisymmetric transducer, uniformly distributed scatterer)

a. Exact solution. Calculating the PDF of the beampattern function depends upon the complexity of the beam. The

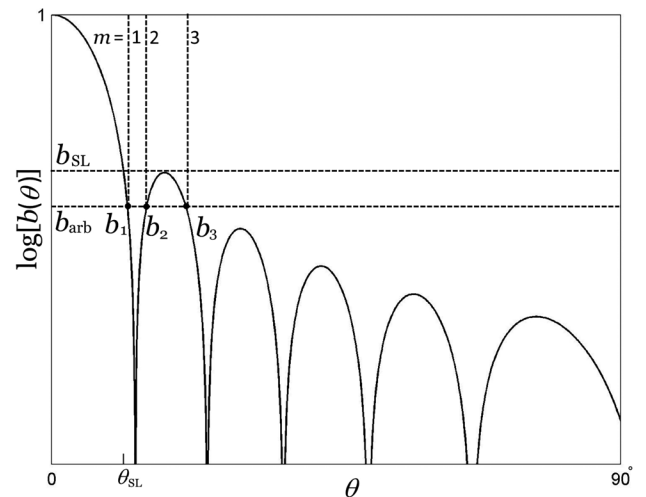


FIG. 11. Diagram illustrating different conditions considered when calculating beampattern PDF. The portion of b greater than the highest sidelobe, b_{SL} , varies monotonically with θ and Eq. (40) is used to calculate the PDF. Once the entire beampattern is used, the beampattern varies non-monotonically and Eq. (46) is used. For the arbitrary value of b_{arb} , the beampattern takes on that value three times in this example (b_1 , b_2 , and b_3 for $m = 1, 2$, and 3 , respectively, and correspondingly θ_1 , θ_2 , and θ_3 which are not shown). The vertical axis is on an arbitrary logarithmic scale to better illustrate the sidelobe structure.

simplest case is first examined involving an axisymmetric beam (i.e., due to a circular planar transducer) in which only the portion of the mainlobe above the value of the highest sidelobe is used [Figs. 4(c) and 11]. This results in the beampattern only being dependent upon a single random variable (spherical polar angle, θ) and furthermore varying monotonically with respect to this angle. Using only the values of the mainlobe above that of the highest sidelobe is not only easier to calculate, but it also generally relates to the highest values of the echoes, which have a higher chance of being detectable above the system noise levels. With these simplifications, Eq. (16) can be used to describe the beampattern PDF for the case in which the beampattern is monotonic and dependent upon only a single random variable,

$$p_b(b) = \frac{p_\theta(\theta)}{\left| \frac{\partial b}{\partial \theta} \right|} \Bigg|_{\theta(b)}, \quad b_{SL} \leq b \leq 1, \quad (40)$$

where b_{SL} is the value of the highest sidelobe of the beampattern and the notation $p_\theta(\theta)$ represents $p_{\theta,\phi}$ for this case where the scatterer distribution does not depend upon ϕ . This corresponds to the scenario where a scatterer is uniformly and randomly distributed either in 2D or 3D as shown in Sec. VII A 2, but with the restriction that $-\theta_{SL} \leq \theta \leq \theta_{SL}$ (fixed ϕ) and $0 \leq \theta \leq \theta_{SL}$ (all ϕ) for the 2D and 3D cases, respectively, where θ_{SL} corresponds to b_{SL} [Figs. 4(c) and 11]. With this restriction, $p_\theta(\theta) = 1/(2\theta_{SL})$ and $p_\theta(\theta) = \sin \theta / (1 - \cos \theta_{SL})$ for the 2D and 3D cases, respectively. These two latter expressions are calculated in a similar manner as for Eqs. (37) and (39), respectively, except that they involve use of a smaller volume, subtended by the angle θ_{SL} , over which dP_V is integrated for normalization.

The beampattern function for a circular planar transducer is (Kinsler *et al.*, 2000)

$$b(\theta) = \left[\frac{2J_1(ka_T \sin \theta)}{ka_T \sin \theta} \right]^2, \quad (41)$$

where a_T is the radius of the transducer and J_1 is the Bessel function of the first kind of order 1. The square of the brackets corresponds to the fact that this is a composite, or two-way beampattern, being produced by the product of the transmit and receive beampatterns which are identical to each other.

Using $p_\theta(\theta) = \sin \theta / (1 - \cos \theta_{SL})$ from above and Eq. (41) in Eq. (40), the beampattern PDF for an axisymmetric beam and associated with the values of the mainlobe above the highest sidelobe is

$$p_b(b) = \frac{\sin^2 \theta}{4\sqrt{b} \cos \theta (1 - \cos \theta_{SL}) |J_2(ka_T \sin \theta)|} \Bigg|_{\theta(b)}, \quad b_{SL} \leq b \leq 1, \quad (42)$$

where J_2 is the Bessel function of the first kind of order 2. Here, the scatterers are assumed to be uniformly distributed at approximately constant range within the mainlobe for polar angles in the range $0 \leq \theta \leq \theta_{SL}$ (all ϕ) (i.e., a 3D case).

b. Power law approximation for beampattern PDF. The beampattern PDF, when plotted on a log-log scale, has been shown to have a negative and nearly constant slope for the higher values of beampattern (Ehrenberg, 1972) (Figs. 4 and 12 of this paper). This pattern corresponds to the portion of the mainlobe higher than the highest sidelobe and also occurs over a wide range of beamwidths (Ehrenberg, 1972). Under these conditions, the beampattern PDF can be approximated using the following equation (Ehrenberg *et al.*, 1981):

$$p_b(b) = k_0 b^{-\mu}, \quad b_{SL} \leq b \leq 1, \quad (43)$$

where the normalization constant k_0 ensures the integral of Eq. (43) over b is unity and is given by

$$k_0 = \begin{cases} \frac{(1-\mu)b_{SL}^{\mu-1}}{b_{SL}^{\mu-1} - 1} & (\mu \neq 1), \\ -\frac{1}{\ln b_{SL}} & (\mu = 1). \end{cases} \quad (44)$$

Using Eq. (42) in the limit of b approaching unity or $ka_T \sin \theta$ approaching zero (that is, for angles near the center of the beam), the exponent in Eq. (43) is (Chu and Stanton, 2010)

$$\mu = \frac{5}{6} + \frac{2}{(ka_T)^2}, \quad b \rightarrow 1 \quad \text{or} \quad ka_T \sin \theta \rightarrow 0, \quad (45)$$

which shows that the slope of the beampattern PDF on a log-log plot varies only with ka_T (related to beamwidth) and is independent of b under these limiting conditions. This equation was derived under the assumption that the scatterers are uniformly distributed at approximately constant range within the mainlobe for polar angles in the range $0 \leq \theta \leq \theta_{SL}$ (all ϕ) (i.e., a 3D case). Note that the power-law form in Eq. (43) applies to both an intensity-based analysis (Ehrenberg, 1972; Ehrenberg *et al.*, 1981) and magnitude-based analysis such as in this tutorial and in Chu and Stanton (2010).

4. Beampattern PDF for entire beam (axisymmetric transducer, uniformly distributed scatterer)

Once the entire beampattern is accounted for in the echo statistics, the sidelobes become a significant factor. In this case, there can be more than one angle at which the beampattern achieves a certain value [Figs. 4(d) and 11]. In this non-monotonic case, Eq. (17) is now used to calculate the beampattern PDF,

$$p_b(b) = \sum_{m=1}^M \frac{p_\theta(\theta_m)}{\left| \frac{\partial b}{\partial \theta_m} \right|} \Bigg|_{\theta_m(b)}, \quad 0 \leq b \leq 1. \quad (46)$$

Now, the full range of polar angles is used [$-\pi/2 \leq \theta \leq \pi/2$ (fixed ϕ) and $0 \leq \theta \leq \pi/2$ (all ϕ) for the 2D and 3D cases, respectively]. The summand of this equation is the same as Eq. (40) which corresponds to the portion of the mainlobe above the highest sidelobe level and which

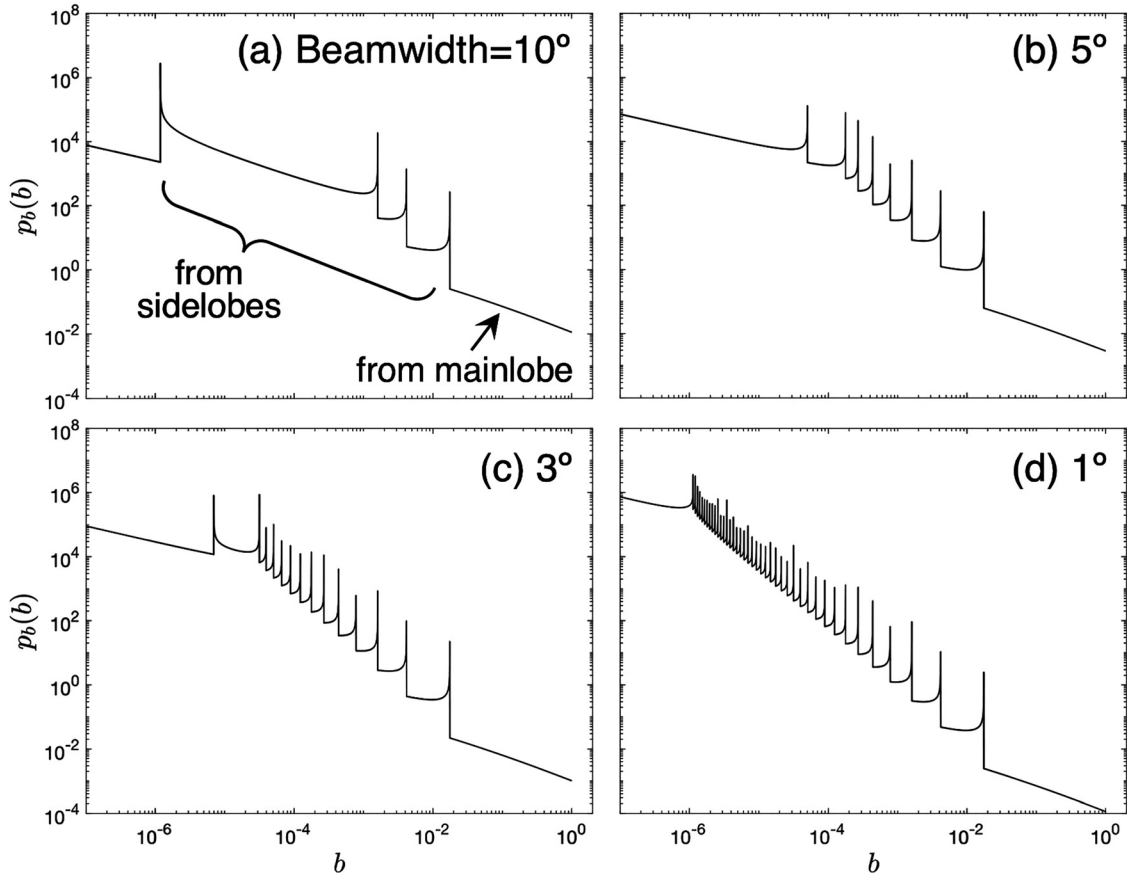


FIG. 12. Beampattern PDF associated with circular apertures of varying size and/or frequency (i.e., varying ka_T , where a_T is the radius of the aperture, k ($=2\pi/\lambda$) is the wavenumber, and λ is the wavelength). The width of mainlobe (-3 to -3 dB; defined in Table 1) of the composite (two-way) beampattern varies from 1° to 10° ($ka_T=132.74, 44.251, 26.556,$ and 13.291 for the widths of $1^\circ, 3^\circ, 5^\circ,$ and 10° , respectively). The sharp peaks are associated with singularities caused by the sidelobes, as indicated in (a). As ka_T increases, the number of sidelobes and, hence, singularities, increases. The curves were calculated using the analytical solution given in Eq. (46), where the numerator and denominator are evaluated separately, using Eqs. (39) and (41), respectively. These calculations assume the scatterer to be randomly and uniformly distributed in a thin hemispherical shell [as reflected in the use of Eq. (39)]. The software used to produce this figure is in the supplementary material at <https://doi.org/10.1121/1.5052255>. The software is also stored online (Lee and Baik, 2018), where it is subject to future revisions.

is a monotonic function. With this summation over m in Eq. (46), each value of m corresponds to a portion of the beampattern that is monotonic and is associated with the structure of the mainlobe and sidelobes (Fig. 11).

For a scatterer being uniformly distributed in a hemispherical shell, Eq. (39) is used for its spatial distribution $p_\theta(\theta)$. For the case of a circular planar transducer, Eqs. (39) and (41) are inserted into Eq. (46) to obtain the beampattern PDF for the entire beampattern,

$$p_b(b) = \frac{1}{4\sqrt{b}} \sum_{m=1}^M \frac{\sin^2 \theta_m}{\cos \theta_m |J_2(ka_T \sin \theta_m)|} \Big|_{\theta_m(b)}, \quad 0 \leq b \leq 1, \quad (47)$$

The summand of this equation is similar to Eq. (42), which describes the PDF of the portion of the mainlobe above the highest sidelobe, and differs only by the term in Eq. (42) containing θ_{SL} . By setting $\theta_{SL} = \pi/2$ in Eq. (42), thus allowing the polar angle to vary over the entire range $0 \leq \theta \leq \pi/2$ (all ϕ), Eq. (42) becomes identical to the summand in Eq. (47).

With the sidelobes accounted for in Eq. (47), the beampattern PDF has significant structure involving singularities

(Fig. 12). Each sharp peak in the PDF is associated with the peak of a sidelobe, while the smoothly varying portion with a nearly constant slope at the higher values of b is associated with the portion of the mainlobe above the highest sidelobe as discussed above. The beampattern PDF is also shown to vary with beamwidth (i.e., different ka_T). The narrower the beam, the more sidelobes are present, which leads to correspondingly more structure in the PDF. There is also some similarity in the occurrence of the sharp peaks as beamwidth is varied.

5. Beampattern PDF for 2D and 3D distribution of scatterers

For any distribution of scatterers containing at least most of the main lobe of the beampattern, the beampattern PDF will generally be qualitatively similar for all distributions of scatterers. Specifically, the PDF will generally have a downward trend, such as with the (approximately) power law illustrated in Figs. 4 and 12. Naturally, there will be some differences associated with the different distributions. As shown in Fig. 4, if the scatterers are only in the main lobe of the beam and do not encounter sidelobes, then the

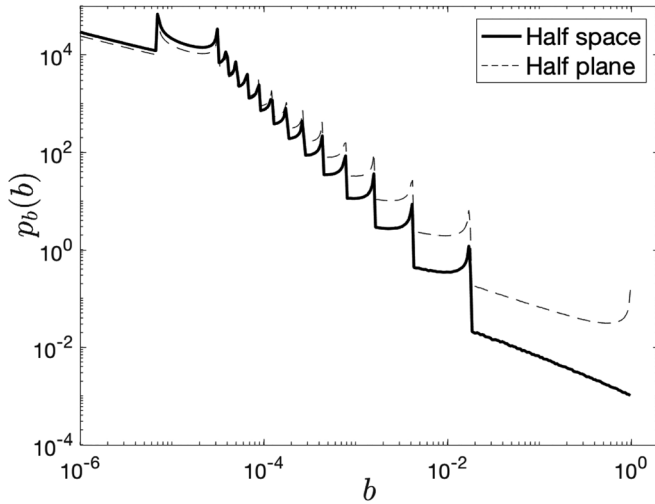


FIG. 13. Beam pattern PDF associated with a circular aperture for 3D and 2D distributions of scatterers. The scatterers are randomly and uniformly distributed within a thin hemispherical shell (half-space) in the 3D case and within a thin arc of constant radius in the half-plane containing the MRA of the beam in the 2D case. The curves were generated through Monte Carlo simulations (10^8 realizations) of the two-way beam pattern function given in Eq. (41) with random draws of (θ, ϕ) and θ (fixed ϕ) for the 3D and 2D cases, respectively. The width of mainlobe $[-3$ to -3 dB; as shown in Fig. 4(b) and defined in Table I] of the composite (two-way) beam pattern is 3° , corresponding to a value of $ka_T = 44.2511$. The numerically generated curve for the 3D case in this figure is to be compared with the analytically generated curve in Fig. 12(c). The software used to produce this figure is in the supplementary material at <https://doi.org/10.1121/1.5052255>. The software is also stored online (Lee and Baik, 2018), where it is subject to future revisions.

beam pattern PDF decreases monotonically with amplitude. Once the sidelobes are encountered, then there is structure superimposed on this decreasing trend. Furthermore, the beam pattern PDF will also vary depending upon whether or not the scatterers reside in a half-plane containing the MRA or the entire half space (Fig. 13). While the beam pattern PDF is shown to be generally similar between the two cases, there is a singularity associated with the 2D case at the maximum value of amplitude.

Beam pattern PDFs, such as those illustrated in Fig. 13, for 2D (half plane) and 3D (half space) distributions of scatterers at approximately constant range can be predicted analytically using Eqs. (37) and (39), respectively, with Eq. (41) used in Eq. (46). However, for the purpose of illustration and comparison with the analytical predictions in Fig. 12, the curves in Fig. 13 were produced through Monte Carlo simulations of Eq. (41) in which random draws of θ (fixed ϕ) and (θ, ϕ) were made for the 2D and 3D cases, respectively.

6. Echo PDF for different types of individual scatterers in axisymmetric beam

The above expressions for the beam pattern PDF in Secs. VII A 2–VII A 4 are now incorporated into the general expression in Eq. (36) to calculate the effects of the beam pattern on the echo PDF. The examples below give a progression of simple to complex scatterers, located either in

the main lobe of the beam only or anywhere in the entire beam (including sidelobes).

a. Point scatterer; main lobe only. In the simplest of cases in which a single point scatterer with a constant scattering amplitude (delta function PDF) is uniformly and randomly distributed in 3D at approximately constant range and its location is restricted to only the portion of the mainlobe of the beam that is above the highest sidelobe, the echo PDF is

$$p_e(\tilde{e}) = \begin{cases} k_0 |f_{ps}|^{\mu-1} \tilde{e}^{-\mu}, & \tilde{e} \leq |f_{ps}|, \\ 0, & \tilde{e} > |f_{ps}| \end{cases} \quad (b_{SL} \leq b \leq 1; \text{ point scatterer in mainlobe above highest sidelobe}), \quad (48)$$

where $|f_{ps}|$ is the magnitude of the scattering amplitude of the point scatterer. The echo PDF was calculated by inserting Eq. (43) for the beam pattern PDF and the delta function $\delta(|f_{bs}| - |f_{ps}|)$ for the PDF of the scattering amplitude into Eq. (36a) (where x denotes $|f_{bs}|$) with the upper limit of the integral \tilde{e}/b_{SL} , reflecting that the integral only involves values of the beam pattern above the highest sidelobe. The inequality involving b given after Eq. (48) explicitly indicates the range of b over which the equation applies, which also corresponds to the range in polar angles, $0 \leq \theta \leq \theta_{SL}$ (all ϕ).

This simple example illustrates the significance of the beam pattern in echo statistics. With the simplest case of a point scatterer with a constant scattering amplitude, the echo received through the receiver of a directional sensor system involving the main lobe only is approximately *power law distributed* as shown in Eq. (48) [Figs. 4(c) and 12(a)]. As demonstrated below, the echo PDF is further complicated once a more complex scatterer and the entire beam pattern (including sidelobes) are used.

b. Rayleigh scatterer; mainlobe only. The above example is now extended by replacing the constant-amplitude scatterer with a Rayleigh scatterer. As before, the scatterer is randomly and uniformly distributed in 3D at approximately constant range and its location is restricted to only the portion of the mainlobe above the highest sidelobe. Inserting Eq. (43) for the beam pattern PDF and Eq. (21) for the PDF of the Rayleigh scatterer into Eq. (36a) with the upper limit of the integral \tilde{e}/b_{SL} so that $b_{SL} \leq b \leq 1$, the echo PDF is

$$p_e(\tilde{e}) = k_0 \lambda_R^{(\mu-1)/2} \tilde{e}^{-\mu} \times \left[\Gamma\left(\frac{\mu+1}{2}, \frac{\tilde{e}^2}{\lambda_R}\right) - \Gamma\left(\frac{\mu+1}{2}, \frac{\tilde{e}^2}{b_{SL}^2 \lambda_R}\right) \right], \quad b_{SL} \leq b \leq 1 \quad (\text{Rayleigh scatterer in mainlobe}), \quad (49)$$

where $\Gamma(\alpha_g, \beta_g)$ is the upper incomplete gamma function, which is related to the gamma function $\Gamma(\alpha_g)$, but calculated with the lower limit in the integral form of $\Gamma(\alpha_g)$ set equal to β_g , rather than 0. Equation (49) is a corrected version of

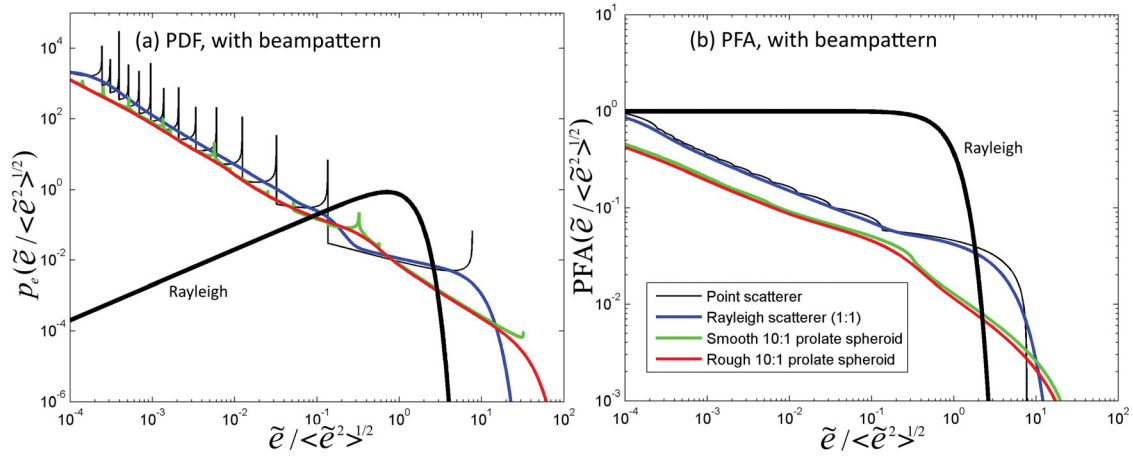


FIG. 14. (Color online) Distributions of magnitude of echo in backscatterer direction received by system (including beampattern effects) for several types of scatterers. The echo PDFs and PFAs are given in (a) and (b), respectively. The Rayleigh PDF and PFA are superimposed in those plots for comparison. The beampattern is due to a circular aperture with $ka_T = 44.2511$, where the width of mainlobe (-3 to -3 dB; defined in Table I) of the composite (two-way) beampattern is 3° . The scatterers are randomly and uniformly distributed in a thin arc of constant radius in the plane containing the MRA of the beam (i.e., 2D case). All curves were generated through evaluation of analytical solutions, not Monte Carlo simulations. All calculations involve use of Eq. (36a) and the beampattern PDF (2D case) calculated with Eq. (46), with Eqs. (41) and (37). In addition, the following equations are used—*point scatterer*: Using a delta function for the PDF, p_s of the magnitude of the scattering amplitude, Eq. (36a) reduces to the beampattern PDF; *Rayleigh scatterer*: p_s in Eq. (36a) is the Rayleigh PDF; *smooth prolate spheroid*: p_s in Eq. (36a) is given by Eq. (33) [using Eq. (34) for the orientation distribution]; and *rough prolate spheroid*: p_s in Eq. (36a) is given by Eq. (35) [using Eq. (33) for p_{SS} and Eq. (34) for the orientation distribution]. Both types of prolate spheroids (smooth and rough) are randomly and uniformly oriented in a single plane. The axis of rotation is the normal to this plane which contains the sensor system. Aspect ratios of scatterers are given. The software used to produce this figure is in the supplementary material at <https://doi.org/10.1121/1.5052255>. The software is also stored online (Lee and Baik, 2018), where it is subject to future revisions.

what appears in Ehrenberg *et al.* (1981) and has been confirmed with simulations over the entire range of echo magnitudes (not shown). The inequality involving b given after Eq. (49) explicitly indicates the range of b over which the equation applies, which also corresponds to the range in polar angles, $0 \leq \theta \leq \theta_{SL}$ (all ϕ).

c. Complex scatterer; entire beam. The analysis is further extended to more complex cases involving a point scatterer, Rayleigh scatterer, randomly oriented smooth prolate spheroid, and randomly oriented rough prolate spheroid, each randomly and uniformly located (one at a time) in a half-plane at approximately constant range involving the entire beam [mainlobe and all sidelobes; $-\pi/2 \leq \theta \leq \pi/2$ (fixed ϕ)] (Fig. 14). For each of those cases, the PDF of the magnitude of the scattering amplitude $p_s(|f_{bs}|)$ using $\delta(|f_{bs}| - |f_{ps}|)$, Eq. (21), Eq. (33), and Eq. (35), respectively, is inserted into Eq. (36a), where x denotes $|f_{bs}|$. For the case of using an axisymmetric beampattern due to a circular planar piston transducer, the beampattern PDF given in Eq. (46) is used in Eq. (36a) in which the entire beam is accounted for ($0 \leq b \leq 1$), while using Eq. (41) for the beampattern function and Eq. (37) for the 2D distribution of scatterers. Also, the prolate spheroids rotate in the plane and Eq. (34) is used for their orientation distribution.

As in Sec. VI in which beampattern effects are not included, predictions using these equations that now incorporate beampattern effects show dependence of echo PDF [and now also PFA through use of Eq. (12)] with type of scatterer (Fig. 14). However, the beampattern significantly alters the shape of the echo PDF over the counterpart cases not involving the beampattern: i.e., the delta function PDF for a point scatterer, Rayleigh PDF for a Rayleigh scatterer,

and the PDFs associated with a randomized prolate spheroid as illustrated in Fig. 10. Furthermore, the degree to which the PDFs deviate from the Rayleigh PDF increases once the beampattern is included. As with the examples excluding beampattern effects, the more elongated the scatterers become, the greater the degree to which the echo PDF is non-Rayleigh. As with the PDFs, the slope of the tail of all PFAs depends upon scatterer type. Note that these examples in Fig. 14 which involve a 2D distribution of scatterers are qualitatively similar to the corresponding examples involving 3D distributions in Sec. VII B for the single scatterer ($N = 1$) cases.

7. Beampattern PDF for non-axisymmetric beampattern, non-uniform distribution of scatterer

The above cases involve the simpler examples in which the beampattern is axisymmetric and the scatterer is randomly and uniformly distributed in a half-plane or half-space at approximately constant range. Those examples apply to many important scenarios. However, there are also important cases in which the beampattern may not be axisymmetric (such as a rectangular transducer or mills cross array) and where the location of the scatterer is non-uniformly distributed. In this more general scenario, the beampattern is now a function of two random variables— θ and ϕ . Furthermore, the PDF of the angular location of the scatterer is now a function of both of those variables. Below, the beampattern PDF for the most general case of non-axisymmetric beampattern and non-uniform distribution of scatterer is first given, which is followed by the simplified case of a non-axisymmetric beampattern with a uniformly distributed scatterer.

a. Non-uniformly distributed scatterer. For the case in which the beam pattern is non-axisymmetric and the angular distribution of the scatterer is non-uniform (but at approximately constant range), the beam pattern PDF is a more general version of Eq. (46) which now involves an integral over the azimuthal angle ϕ . Since the beam pattern function is a function of the two random variables, θ and ϕ , then Eq. (18) can be used to derive an expression for the beam pattern PDF. Beginning with Eq. (18), set $z = b$, $P_Z = P_B$ (where “ B ” is the random variable for the beam pattern function b), $x = \theta$, $y = \phi$, and $p_{X,Y}(x,y) = p_{\theta,\phi}(\theta, \phi)$. Differentiating P_B with respect to θ and rearranging terms gives the following expression for the beam pattern PDF (Ehrenberg, 1972):

$$p_b(b) = \int_0^{2\pi} \sum_{m=1}^M p_{\theta,\phi}(\theta_m, \phi) \left. \frac{1}{\left| \frac{\partial b(\theta_m, \phi)}{\partial \theta_m} \right|} \right|_{\theta_m(b)} d\phi, \quad 0 \leq b \leq 1. \quad (50)$$

As with the simpler case in Eq. (46), the summation over m accounts for the fact that the beam pattern function is not monotonic. Each segment within the integrand associated with a value of m is monotonic. These segments are related to the regions D_Z in Eq. (18) where the function b has the same value for multiple values of θ . This is illustrated specifically for the case of the beam pattern function in Fig. 11.

b. Uniformly distributed scatterer. For the simplifying condition of the scatterer being uniformly distributed in a half-space at approximately constant range (with a non-axisymmetric beam pattern), Eq. (38) is used for the PDF of the angular location of the scatterer and Eq. (50) reduces to

$$p_b(b) = \frac{1}{2\pi} \int_0^{2\pi} \sum_{m=1}^M \left. \frac{\sin \theta_m}{\left| \frac{\partial b(\theta_m, \phi)}{\partial \theta_m} \right|} \right|_{\theta_m(b)} d\phi, \quad 0 \leq b \leq 1, \quad (51)$$

where the integral over ϕ reflects the asymmetry in the beam pattern. Once the beam pattern becomes axisymmetric, this equation further reduces to Eq. (46) [with Eq. (39) used for $p_\theta(\theta)$ in Eq. (46)] in which there is no dependence upon ϕ in the beam pattern.

Given the complexity associated with the asymmetry of the sensor beam, both of the above two equations must generally be evaluated numerically. Equation (51) has been evaluated to predict the echo statistics associated with a rectangular transducer in which the one-way beamwidths in the two orthogonal planes were 5° and 20° (Stanton *et al.*, 2015). The beam pattern PDF of the two-way beam pattern, as illustrated in Fig. 2 in that paper, is qualitatively similar to the ones illustrated in this tutorial in that the PDF trends toward smaller values as the beam pattern value increases. However, the structure in the beam pattern PDF associated with the rectangular transducer is much different than that associated with the circular transducer in this tutorial because of the lack of axial symmetry in the beam pattern. Specifically, the sharp spikes shown in Fig. 12(a) of this

tutorial that are associated with the sidelobes for a circular transducer are much larger in magnitude, but fewer in number, than the corresponding spikes in the beam pattern PDF associated with the rectangular transducer. The beam pattern PDF for the rectangular transducer was used in Stanton *et al.* (2015) in interpreting experimental data, as summarized in Sec. III A 1 of this tutorial.

B. Multiple identical scatterers randomly located in beam

In this case, there are two or more scatterers present at the same time, each randomly, uniformly, and independently distributed in the beam at approximately constant range. The transmit signals are long enough so that the echoes from all scatterers are assumed to completely overlap. The scatterers are “identical” in that they possess the same statistical properties. For example, the magnitude of the scattering amplitude of each scatterer could be Rayleigh distributed with the same mean scattering cross section. Or, each scatterer could be a randomly rough, randomly oriented prolate spheroid with the same mean dimensions (and, hence, the same mean scattering cross section). Although the statistical properties are the same, the scattering amplitudes of the scatterers are generally different from each other for any given ping or realization since they are statistically independent of each other.

As discussed in Sec. IV C 5, there are various methods to calculate the echo statistics in this case in which the sum of multiple random variables (i.e., echoes from multiple scatterers) is calculated. The methods range from closed-form analytical to pure numerical approaches involving Monte Carlo simulations of summations of phasors. Because of its generality, the latter case is used in the below analysis.

In this simple “phasor summation” method, Eq. (6) is used in which a phasor (the summand) is calculated for each scatterer and each realization. For each realization, the phasors are added together coherently to form the total echo as measured by the sensor system. The echo PDF is estimated through forming a histogram of the total echo magnitude through the binning method or using the kernel density estimation (KDE) method described in Sec. IV B 2. The phase shift term Δ_i varies randomly and uniformly in the range $[0, 2\pi]$, reflecting the random location of the scatterers (range-wise) and high frequencies (short wavelengths) of the signal. All scatterers are distributed within a thin hemispherical shell so that there are no significant differences in the range-dependence of the losses due to spreading and absorption. The magnitude of the echo from each individual scatterer is given by Eq. (7). As discussed above, since the scattering amplitude and location of the scatterer in the beam are random variables (leading to the beam pattern function being a random variable), then this individual echo magnitude is a random variable as well.

Three sets of examples are investigated using three scatterer types from above—a point scatterer, Rayleigh scatterer, and randomly oriented rough prolate spheroid. For each phasor, the randomized terms (scattering amplitude, beam pattern function, and phase) are randomly drawn from

N Point Scatterers

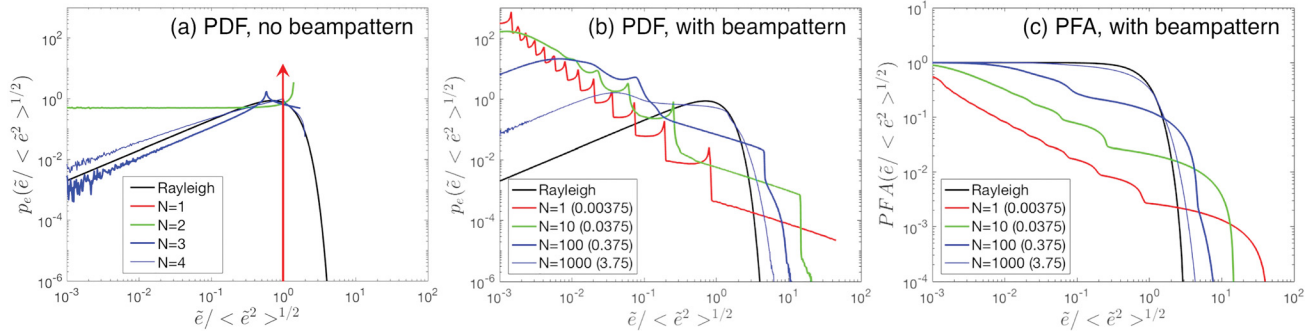


FIG. 15. (Color online) Distributions of magnitude of echo in backscatter direction from N point scatterers randomly and uniformly distributed in a thin hemispherical shell. (a) PDF of echo with no beam pattern effects (equivalent to having an omnidirectional beam), (b) PDF of echo with beam pattern effects, and (c) PFA of echo with beam pattern effects. Each scatterer is identical with a scattering amplitude that is constant. Except for the $N=1$ case, the curves in (a) are generated with Monte Carlo simulations using the same equations and parameters to generate Fig. 6(b), but with 10^8 realizations for this figure. The $N=1$ curve is also added to (a) (no simulations), which is the delta function. Monte Carlo simulations (10^8 realizations) of Eq. (6) are used in (b) and (c). The beam pattern is due to a circular aperture with $ka_T=44.2511$, where the width of mainlobe (-3 to -3 dB; defined in Table I) of the composite (two-way) beam pattern is 3° . The value given in parentheses after the value of N in the legend of (b) and (c) is the number of scatterers within the main lobe of the beam, as discussed in Table I. The Rayleigh PDF and PFA are superimposed in those plots for comparison. The software used to produce this figure is in the supplementary material at <https://doi.org/10.1121/1.5052255>. The software is also stored online (Lee and Baik, 2018), where it is subject to future revisions.

numerically generated statistical distributions. For the point scatterer, the magnitude of the scattering amplitude is simply a constant in Eq. (7). For the other two scatterers, the magnitude of the scattering amplitude is determined using random draws from numerically generated random variables. The magnitude of the scattering amplitude of the Rayleigh scatterer for each realization was randomly drawn from a numerically generated Rayleigh random variable [whose PDF is given in Eq. (21)]. Generating the magnitude of the scattering amplitude of the randomly oriented rough prolate spheroid began by randomly drawing an orientation angle β , which was then used to calculate the magnitude of the scattering amplitude of the smooth prolate spheroid from Eq. (30). That value, in turn, was multiplied by a Rayleigh distributed random variable (which was randomly drawn using the same method as for the Rayleigh scatterer). Note that the

prolate spheroid calculations could have used Eq. (35) directly to describe the statistics of the random variable scattering amplitude, from which a random draw could have been made. However, for the purposes of illustration, the scattering was described from the beginning (random draw of orientation angle), which would be the process used for a more general scatterer for which there is not a closed-form solution.

For each realization, the (axisymmetric) beam pattern is calculated for a random location (polar angle θ) with the scatterer angular (location) distribution PDF of $\sin \theta$ from Eq. (39), and the phase shift is sampled from a uniform distribution $[0, 2\pi]$. Also, for each realization, each of the above random variables is generated by employing inverse transform sampling, in which samples of any probability distribution is generated at random through its CDF (Devroye,

N Rayleigh Scatterers

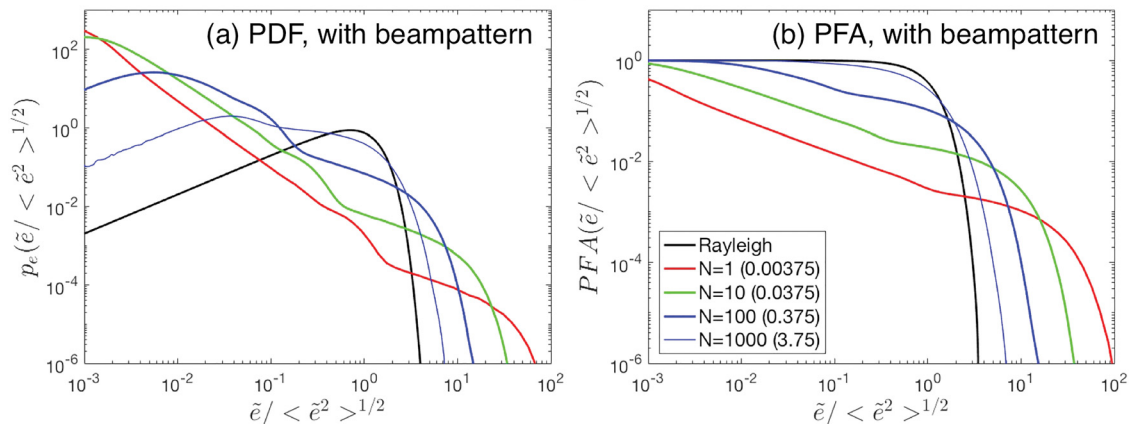


FIG. 16. (Color online) Distributions of magnitude of echo in backscatter direction from N identical Rayleigh scatterers randomly and uniformly distributed in a thin hemispherical shell. The PDFs and PFAs are given in (a) and (b), respectively. For the case in which there are no beam pattern effects (i.e., $b=1$), the echo magnitude PDF is Rayleigh for all N (not shown). Monte Carlo simulations (10^7 realizations) are used in each case using Eq. (6), where the scattering amplitude for each scatterer is Rayleigh distributed and with the same mean. The beam pattern is due to a circular aperture with $ka_T=44.2511$, where the width of mainlobe (-3 to -3 dB; defined in Table I) of the composite (two-way) beam pattern is 3° . The value given in parentheses after the value of N in the legend is the number of scatterers within the main lobe of the beam, as discussed in Table I. The software used to produce this figure is in the supplementary material at <https://doi.org/10.1121/1.5052255>. The software is also stored online (Lee and Baik, 2018), where it is subject to future revisions.

N Rough Prolate Spheroids

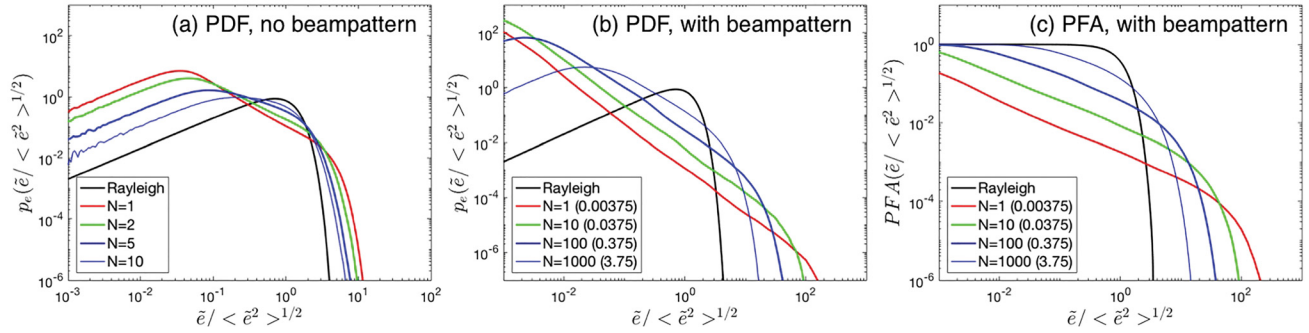


FIG. 17. (Color online) Distributions of magnitude of echo in backscatter direction from N randomly rough, randomly oriented prolate spheroids randomly and uniformly distributed in a thin hemispherical shell. (a) PDF of echo with no beam pattern effects (i.e., omnidirectional beam); (b) PDF of echo with beam pattern effects; (c) PFA of echo with beam pattern effects. This geometry is fully 3D as the spheroids are distributed within the hemispherical shell and the spheroid orientation varies randomly and uniformly in two planes of rotation of the spheroid. This is in contrast to Fig. 14 where the spheroid orientation follows a 2D distribution (spheroid distributed within thin arc and rotating in only one plane of rotation). The scatterers are identical in size and shape (10:1 aspect ratio), although statistically independent of each other. Monte Carlo simulations (10^7 realizations) are used in each case using Eq. (6), where the scattering amplitude for each scatterer is the product of Eq. (30) (smooth spheroid) and a Rayleigh distributed random variable (to simulate roughness effects). The beam pattern is due to a circular aperture with $ka_T = 44.2511$, where the width of mainlobe (-3 to -3 dB; defined in Table I) of the composite (two-way) beam pattern is 3° . The beam pattern b in Eq. (7) is set equal to unity in (a). The value given in parentheses after the value of N in the legend in (b) and (c) is the number of scatterers within the main lobe of the beam, as discussed in Table I. The software used to produce this figure is in the supplementary material at <https://doi.org/10.1121/1.5052255>. The software is also stored online (Lee and Baik, 2018), where it is subject to future revisions.

1986). Using these terms, the summand in Eq. (6) is calculated and summed over the N scatterers for each realization. The process is repeated for millions of realizations (typically 10^7) and a histogram is formed representing the statistics of the magnitude of the echo as received by the sensor system.

In each example, the echo PDFs are shown to vary significantly with type and number of scatterers (Figs. 15–17).

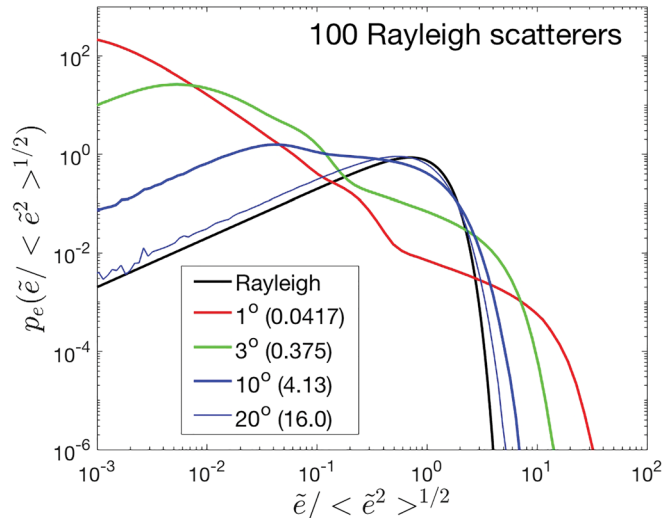


FIG. 18. (Color online) PDF of magnitude of echo from 100 identical Rayleigh scatterers that are randomly and uniformly distributed in thin hemispherical shell. The beamwidth (-3 to -3 dB; defined in Table I) of the composite (two-way) beam pattern is varied from 1° to 20° . The beam pattern is due to a circular aperture. Monte Carlo simulations (10^7 realizations) are used in each case using Eq. (6), where the scattering amplitude for each scatterer is Rayleigh distributed and with the same mean. The numbers of scatterers within the main lobe for the different directional beams are given in parentheses next to the corresponding beamwidth in the legend. Those numbers, as well as the respective values of ka_T , are summarized in Table I. The software used to produce this figure is in the supplementary material at <https://doi.org/10.1121/1.5052255>. The software is also stored online (Lee and Baik, 2018), where it is subject to future revisions.

As with the case of a single scatterer in the beam, the PDF is significantly different than when beam pattern effects are not accounted for. As expected, as the number of scatterers increases, the PDFs approach the Rayleigh PDF. In general, for a small number of scatterers, the echo PDF deviates significantly from the Rayleigh PDF, both in the small and large echo magnitude regions of the PDF. Echo PFAs are also illustrated, which also show significant dependences upon type and number of scatterer. The degree to which the PDF deviates from a Rayleigh PDF also varies with beamwidth (Fig. 18). For a fixed number of scatterers, the narrower the beam, the greater the deviation from a Rayleigh PDF. Note that the “noisy” characteristic in portions of some of the plots of PDF in Figs. 15–18 is due to the relatively low number of realizations in the Monte Carlo simulations that were

TABLE I. Average number of scatterers within the entire main lobe of a circular transducer (i.e., within solid angle defined by the first null of the beam pattern) for various beamwidths and various total number of scatterers, N , in the half space. The beam pattern $b (= b_T b_r)$ is the composite two-way beam pattern determined by the product of the transmit (b_T) and receive (b_r) beam pattern as given in Eq. (41). The beamwidth ($2\theta_0$) is the full width of the beam pattern between the -3 dB (half-power) points where $b(\theta_0) = 1/\sqrt{2}$. The parameters in this table correspond to various figures within this paper.

Beamwidth (-3 to -3 dB) (deg.)	ka_T	N (half space)	Average number within mainlobe
1	132.74	100	0.0417
3	44.2511	1	0.00375
3	44.2511	10	0.0375
3	44.2511	25	0.0937
3	44.2511	100	0.375
3	44.2511	250	0.937
3	44.2511	1000	3.75
3	44.2511	2500	9.37
10	13.2907	100	4.13
20	6.6707	100	16.0

within those particular log-spaced magnitude bins (i.e., when both p_e and $\bar{e}/\langle\bar{e}^2\rangle^{1/2}$ are low).

It is important to emphasize that the number of scatterers N is distributed uniformly in a thin hemispherical shell in a half-space. For a narrow beamwidth, the mainlobe occupies just a small fraction of that half-space. Since the mainlobe weights the echoes from the individual scatterers much more than the sidelobes, the scatterers within the mainlobe will generally contribute the most to the signal. In essence, the signal will be dominated by the *effective* number of scatterers—those that are within the mainlobe. The average number of scatterers within the mainlobe is indicated in parentheses after the value of N in the legends to these and later figures and are also given in Table I.

The echo statistics vary with beamwidth even though N is constant because the effective number of scatterers varies with beamwidth—that is, for fixed N , the number of scatterers within the mainlobe that contributes to the higher values of the scattering decreases with decreasing beamwidth (Fig. 18). For example, for $N=100$, the number of scatterers within a 1° -wide mainlobe is, on average, equal to 0.0417 (Table I). Before beampattern effects are included, the sum of 100 independent, random phase signals would be very close to Rayleigh distributed (Fig. 6). However, with such a narrow beam with only a small fraction of the 100 scatterers within the mainlobe, the resultant echo PDF will be strongly non-Rayleigh.

C. Multiple scatterers of different types and sizes

Once there is more than one type or size of scatterer present, the echo PDF will not only depend upon the type and number of scatterers, and sensor beamwidth, as in the above examples in Sec. VII B which involved one type of scatterer at a time, but will also depend upon the variability of values of mean scattering cross section and variability of numbers of scatterers across the different types of scatterers. Furthermore, the echo PDF will depend upon the differences in spatial distributions of the different types of scatterers. For example, consider two distinct cases: (1) a *split aggregation* in which scatterers of only one type reside in “monotype” patches and each echo contains contributions from only one type of scatterer and (2) an *interspersed aggregation* in which the different types of scatterers are uniformly

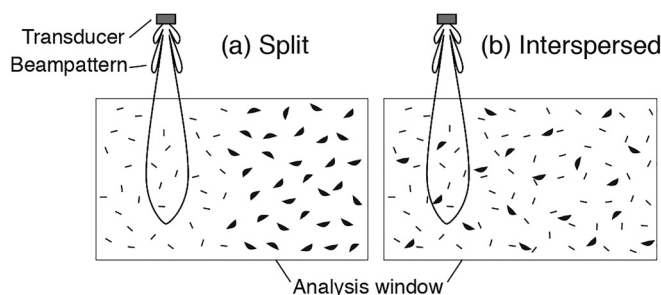


FIG. 19. Analysis windows involving two different spatial arrangements for aggregations composed of more than one type of scatterer. (a) Split aggregation where scatterers of different types are separated into their own sub-regions. (b) Interspersed aggregation where scatterers of different types are uniformly interspersed throughout the window. In each case, the resolution cell of the sensor system is much smaller than the analysis window and, in case (a), it is also much smaller than each sub-region. From Lee and Stanton (2014).

interspersed with each other so that each echo contains contributions from all of the types of scatterers (Fig. 19). In each case, the beam is much narrower than both the patch and analysis window containing the scatterers and the echoes from many pings or independent realizations are observed within each window (Fig. 19). The echo statistics will generally be significantly different for the two distributions, even when the same set of scatterers of varying types are involved in each distribution (Lee and Stanton, 2014). And, for each type of distribution, the echo PDF will vary as the number and mean scattering cross section of each scatterer type are varied.

Below, the echo PDF is formulated for each type of spatial distribution—first for cases involving two types of scatterers, then generalizing to an arbitrary number of scatterer types. For the split aggregation, a mixture PDF (to be defined below) involving separate phasor summations for the monotype patches is used and, for the interspersed aggregation, the phasor summation method is used to form the echo PDF from the echoes from all types of scatterers within the analysis window. Examples of echo PDFs from each type of distribution are given in Sec. VIIC 3 for the simple case involving two different sizes of scatterers, “weak” (type A) and “strong” (type B), for a range of numbers and sizes of scatterers. Both types of scatterers are Rayleigh scatterers, but with different mean scattering cross sections.

1. Split aggregation of type A and B scatterers—mixture PDF

Formulating the echo PDF for the split aggregation geometry [Fig. 19(a)] for two types of scatterers is intuitive and is done in two steps. First, the echo PDF is determined for each homogeneous patch of identical scatterers—the type A and type B patches. As discussed in Secs. IV C 5 and VII B, the PDF can be determined for each patch using a variety of methods, including the phasor summation method which uses Eqs. (6) and (7) for each patch separately. The patches are analyzed separately since the echoes from the different types of scatterers do not overlap in this case. Since the echo PDF from the sensor system scanning all scatterers is based on echoes accumulated from both patches, the echo PDF from the analysis window is simply the weighted sum of the PDFs from the two patches, which is known as a two-component “mixture” PDF,

$$p_e(\tilde{e}) = w_A p_e^{(A)}(\tilde{e}) + w_B p_e^{(B)}(\tilde{e}) \quad (\text{mixture PDF; split aggregation}). \quad (52)$$

Here, the weighting factors w_A and w_B represent the fractional volume occupied by the type A and type B scatterers, respectively. For example, if the patch of type A scatterers occupies 60% of the analysis window and the patch of type B scatterer occupies 40% of the window, then $w_A = 0.6$ and $w_B = 0.4$. Since, by definition, the two patches collectively occupy 100% of the analysis window, then $w_A + w_B = 1$ and Eq. (52) can be simplified,

$$p_e(\tilde{e}) = w_A p_e^{(A)}(\tilde{e}) + (1 - w_A) p_e^{(B)}(\tilde{e}) \quad (\text{mixture PDF; split aggregation}). \quad (53)$$

2. Interspersed aggregation of type A and B scatterers—coherent phasor sum

In contrast to the above case of a split aggregation, the echoes from the two types of scatterers in the interspersed aggregation overlap with each other [Fig. 19(b)]. Predictions of the echo PDF in this geometry therefore begins with a coherent phasor summation involving both types of scatterers. Calculating the echo statistics using the phasor sum method is done the same way as described in Sec. VII B, but by first rewriting Eqs. (6) and (7),

$$\tilde{e} = \left| \sum_{i=1}^N \tilde{e}_{iA} e^{j\Delta_{iA}} + \sum_{i=1}^M \tilde{e}_{iB} e^{j\Delta_{iB}} \right|$$

(phasor summation; interspersed aggregation). (54)

where the magnitude of the echo voltage from the i th scatterer of the k th type as received through the sensor system is

$$\tilde{e}_{ik} = \left| \int_{bs}^{c^{(ik)}} b(\theta_{ik}, \phi_{ik}) \right|$$

(55)

and Δ_{ik} and (θ_{ik}, ϕ_{ik}) are the phase and angular locations of the i th scatterer of the k th type, respectively. There are N and M type A and B scatterers, respectively. The term k corresponds to type A or type B scatterer in this example. Once \tilde{e} is calculated from Eq. (54) for many realizations, the echo PDF is formed.

3. Comparisons between echo PDFs from split and interspersed two-type aggregations

Echo PDFs are calculated using Monte Carlo simulations of Eq. (6) as described above for a range of parameters for both the split and interspersed aggregations involving two types of scatterers. Both types of scatterers are Rayleigh scatterers, but with two different mean scattering cross sections denoted by “weak” (smaller mean scattering cross section) and “strong” (larger mean scattering cross section). The difference of average scattering levels could be achieved through either a difference in boundary conditions (a weak scatterer with small contrast in material properties relative to surrounding medium and a strong scatterer with large contrast) or a difference in size (a weak scatterer being smaller than a strong scatterer). The ratio of *rms* magnitude of the scattering amplitudes of the strong (“S”) to weak (“W”) scatterers is given by

$$r_{SW} = \frac{\lambda_S}{\lambda_W},$$

(56)

where λ is the *rms* magnitude of the scattering amplitude of the denoted scatterer type [this notation is chosen to be consistent with that of Lee and Stanton (2014) and is not to be confused with λ_R of Eqs. (21)–(23) of this tutorial].

With the number of weak scatterers fixed at 2500, the number of strong scatterers is varied over the range 25–2500 for two values of r_{SW} (5 and 20). The resultant echo PDFs are shown to vary in shape over all combinations of these parameters (Figs. 20 and 21). All PDFs deviate significantly from the Rayleigh PDF. In each example, the tail of the PDF is elevated above the

Rayleigh PDF. The degree to which the tail is elevated is especially pronounced for the larger ratio of strong-to-weak scattering amplitude ($r_{SW} = 20$) in both types of aggregations and for the cases involving fewer numbers of strong scatterers in the interspersed aggregations. This is consistent with the intuition that the strong scatterers dominate the echo and can cause the echo to be non-Rayleigh when they are small in number. Also, very importantly, the PDFs with the same parameters, but different spatial distribution (split- and interspersed aggregation), are significantly different from each other. Note that, as with some of the previous simulations, the “noisy” characteristic in portions of some of the plots of PDF in Figs. 20 and 21 are due to the relatively low number of realizations in the Monte Carlo simulations that were within those particular log-spaced magnitude bins (i.e., when both p_e and $\tilde{e}/\langle \tilde{e}^2 \rangle^{1/2}$ are low).

With the many model parameters in these formulations, it is relatively easy to obtain a good fit to experimental data, even when using the “wrong” theoretical PDF (“wrong” in that the assumptions in the derivation of the theoretical PDF do not match the physical scenario). This was explored in Lee and Stanton (2014) where echoes from both split- and interspersed aggregations were simulated numerically. While allowing all parameters to vary freely, theoretical PDFs for each type of aggregation were then “fit” to simulations from both the corresponding appropriate aggregation and the other aggregation. Excellent fits were obtained in most cases (i.e., for both the “right” and “wrong” aggregations). For example, a mixture model could not only be successfully fit to echoes from a split aggregation (for which the mixture model is derived), but also could be “successfully” fit to an interspersed aggregation (which it was *not* derived for). However, when the theoretical PDF was fit to the wrong aggregation, the inferred parameters (that is, the ones required to obtain a good fit) were up to an order of magnitude in error [see Table I and Figs. 6 and 7 of Lee and Stanton (2014)]. The conclusion was that for accurate inference of model parameters from data, it is essential to model the spatial distribution of the scatterers appropriately, taking into account whether or not they are split or interspersed.

4. Many types of scatterers (general formulations)

The above simple cases involving two types of scatterers can easily be extended to the general case of K types of scatterers (where K is an integer, not to be confused with the K PDF). For the case in which each type of scatterer is partitioned separately in its own patch within the analysis window, the echo PDF from the entire analysis window is calculated using the following K -component mixture PDF:

$$p_e(\tilde{e}) = \sum_{k=1}^K w_k p_e^{(k)}(\tilde{e})$$

(mixture PDF; K types partitioned). (57)

where $p_e^{(k)}(\tilde{e})$ is the echo PDF of the patch associated with the k th type of scatterer, w_k is the weighting factor for the k th patch, and $\sum_{k=1}^K w_k = 1$.

For the case in which all types of scatterers are randomly and uniformly interspersed within the analysis window, the phasor sum for a single realization of echo is

Split Aggregation

$$N_w = 2500 \text{ (9.37)}$$

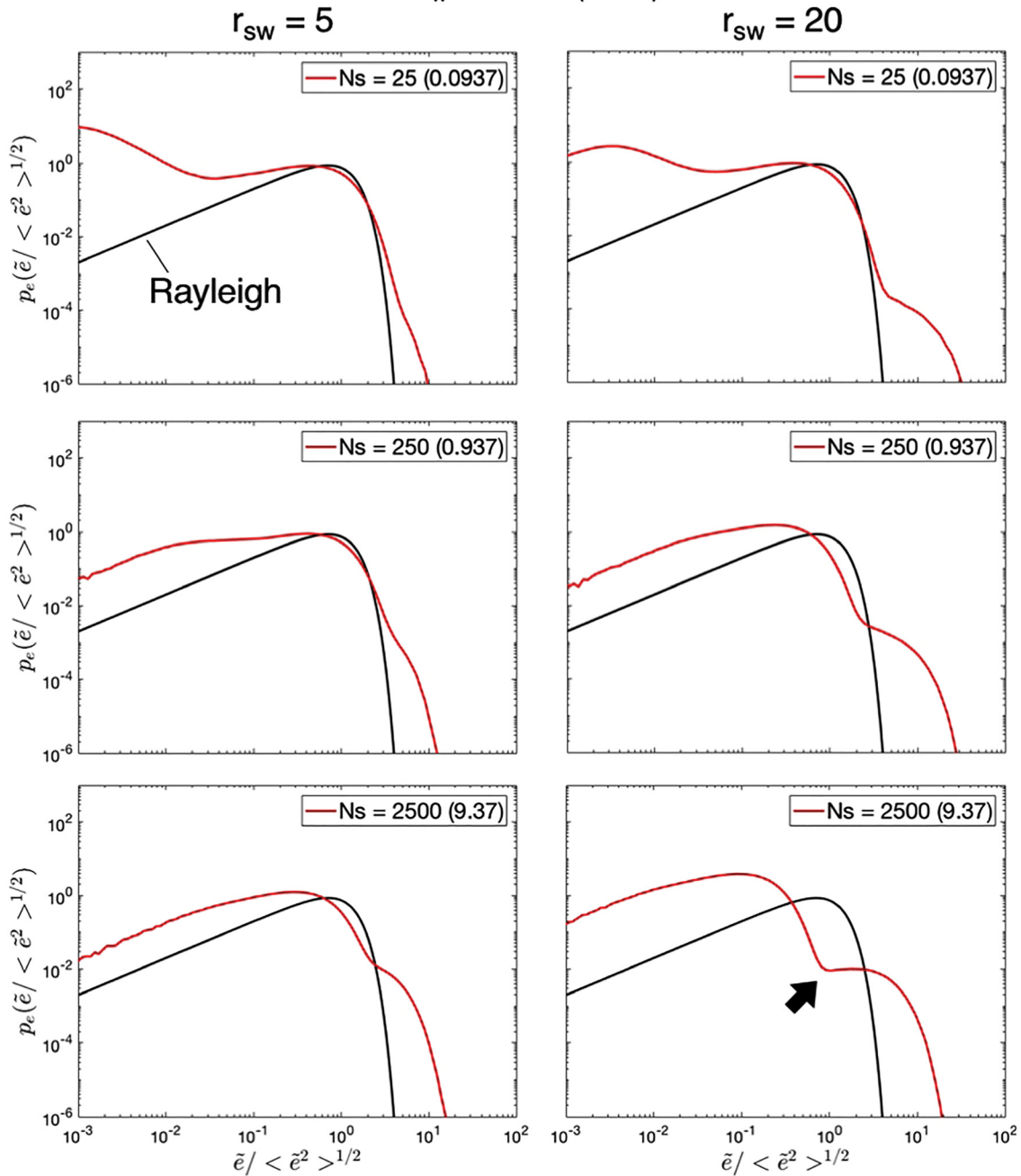


FIG. 20. (Color online) PDF of echo magnitude from multiple Rayleigh scatterers in a *split* aggregation in which the larger scatterers are separated from the smaller scatterers as illustrated in Fig. 19(a). The arrow in the lower right panel indicates an inflection in the PDF associated with having two types of scatterers. The beampattern is due to a circular aperture with $ka_T = 44.2511$, where the width of mainlobe (-3 to -3 dB; defined in Table I) of the composite (two-way) beampattern is 3° . The number of strong and weak scatterers, N_S and N_W , respectively, randomly and uniformly distributed in a thin hemispherical shell are given. Monte Carlo simulations (10^7 realizations) are used in each case using Eq. (6), where the scattering amplitude for each scatterer is Rayleigh distributed, but with different means, as indicated by the value of r_{sw} . The volume within which the strong scatterers occupy is 5% of the total volume (that is, $w_A = 0.05$ in Eq. (53), where “A” and “B” denote the patches of strong and weak scatterers, respectively). The value given in parentheses after each value of N_S and N_W is the corresponding number of strong and weak scatterers within the main lobe of the beam, as discussed in Table I. The software used to produce this figure is in the supplementary material at <https://doi.org/10.1121/1.5052255>. The software is also stored online (Lee and Baik, 2018), where it is subject to future revisions.

$$\tilde{e} = \left| \sum_{k=1}^K \sum_{i=1}^{N(k)} \tilde{e}_{ik} e^{j\Delta_{ik}} \right| \quad \text{(phasor summation; K types interspersed),} \quad (58)$$

where \tilde{e}_{ik} is given in Eq. (55) and $N(k)$ is the number of scatterers of the k th type. The echo is calculated for a large ensemble of independent realizations to form the echo PDF of the analysis window for the interspersed aggregation.

Interspersed Aggregation

$$N_w = 2500 \text{ (9.37)}$$

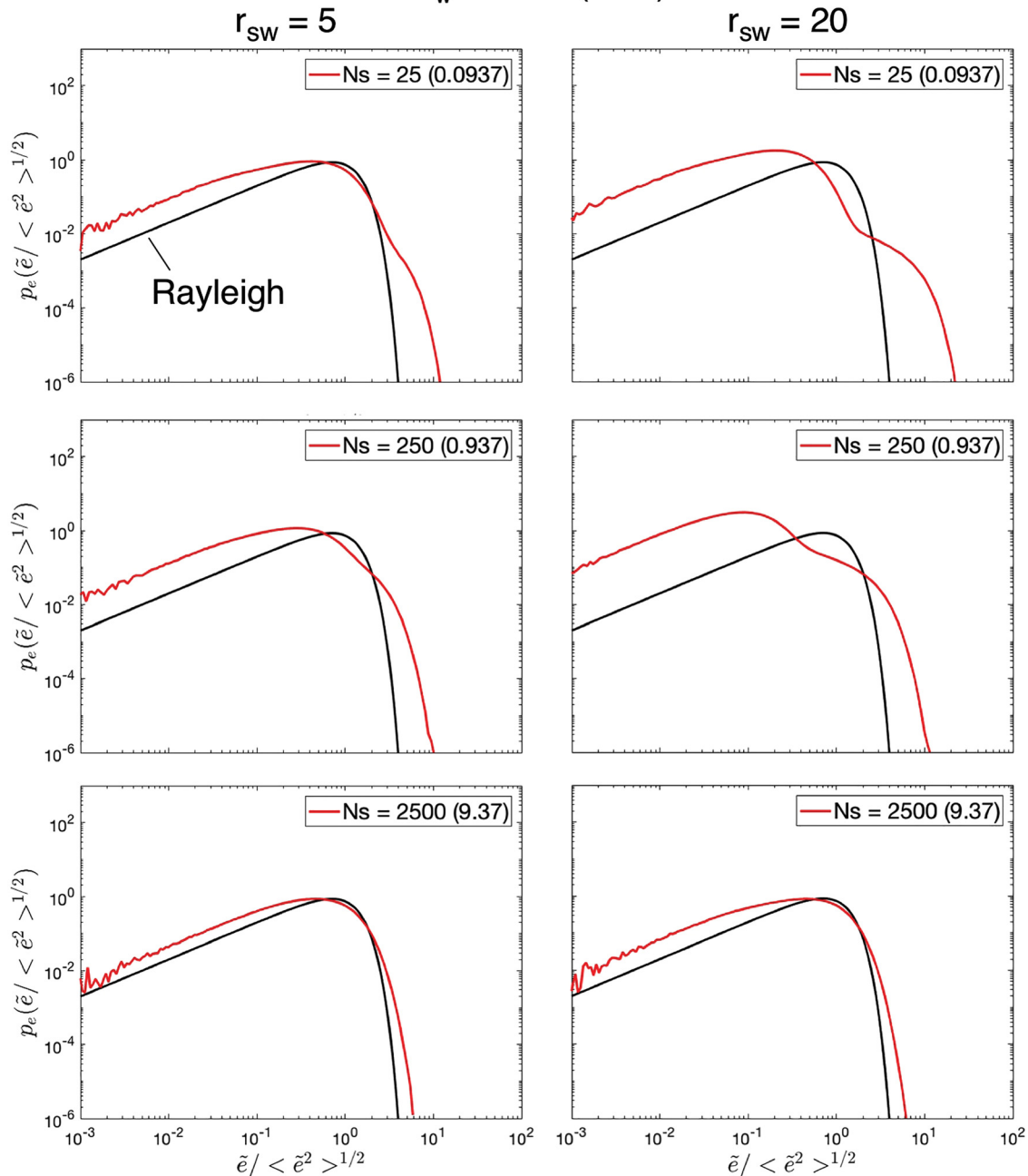


FIG. 21. (Color online) PDF of echo magnitude from multiple Rayleigh scatterers in an *interspersed* aggregation in which both the larger and smaller scatterers are uniformly and randomly interspersed throughout the analysis window as illustrated in Fig. 19(b). The inflections in these PDFs are less pronounced in this type of aggregation than in the split aggregations as noted by the arrow in Fig. 20. As with Fig. 20, Monte Carlo simulations (10^7 realizations) are used in each case using Eq. (6), where the scattering amplitude for each scatterer is Rayleigh distributed, but with different means, as indicated by the value of r_{sw} . All modeling parameters are the same as in Fig. 20 (except for w_A , which is specific to a split aggregation) and are described in the caption to that figure. Each type of scatterer occupies 100% of the volume with this case of interspersed aggregations. The software used to produce this figure is in the supplementary material at <https://doi.org/10.1121/1.5052255>. The software is also stored online (Lee and Baik, 2018), where it is subject to future revisions.

Finally, the above two equations can be used in concert to describe more complex cases such as when multiple patches of both monotype and interspersed aggregations are present.

VIII. SYSTEMS AND ENVIRONMENTS WITH MORE COMPLEXITY

All of the above involved relatively simple scenarios—single-frequency signals that are long enough so that echoes

from all scatterers completely overlapped and direct path geometries in which the medium is homogeneous and there is no interference from neighboring boundaries. While the results from these scenarios sufficiently approximate a wide range of applications, there are factors in other applications that sometimes must be accounted for in accurately predicting echo statistics. For example, signals in sensor systems are generally pulsed and the environments may be

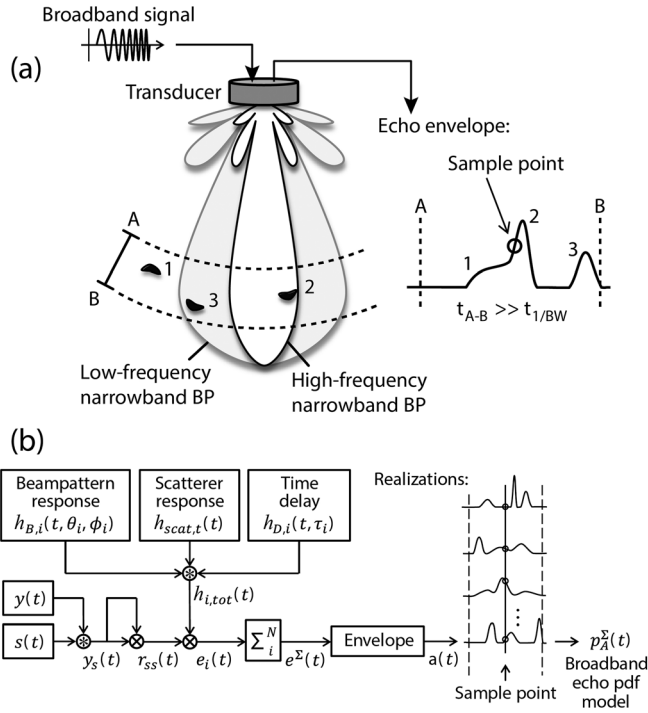


FIG. 22. Modeling considerations and processing flow for echo statistics associated with pulsed broadband signals. (a) Beamwidth that varies with frequency within a broadband signal is illustrated as well as partially overlapping echoes due to short signal. (b) Flow diagram illustrating system effects incorporated into echo statistics model. The echo time series shown in the right of (a) and (b) is the envelope of the pulse-compressed signal from match filter processing, which greatly increases temporal (range) resolution and increases the probability that the echoes will only partially overlap. The circled “*” and “×” symbols represent the convolution and cross correlation operations, respectively. From Lee and Stanton (2015), where terms in the illustration specific to that paper, are described.

heterogeneous and have boundaries. When pulsed signals are used, echoes from individual scatterers will generally partially overlap, or not overlap at all. The presence of a single boundary near a scatterer will be an added source of interference, and the presence of two parallel boundaries and/or heterogeneities will not only cause more interference, but also possibly waveguide effects.

The effects from these realistic conditions are described below as well as recommendations for physics-based predictions of the echo statistics.

A. Pulsed signals (partially overlapping echoes)

Once the signals are pulsed instead of continuous wave, the echoes from individual scatterers in an aggregation may only partially overlap or not overlap at all which can significantly affect the echo statistics (Figs. 22 and 23). This effect, in essence, translates to fewer effective scatterers in the mainlobe of the beam, which will tend to make the statistics of the pulsed signal more non-Rayleigh. Generally, the shorter the signal, the fewer the effective scatterers and, hence, the more non-Rayleigh the echo becomes. The signal can be shortened either by reducing the gate duration of the signal, or by increasing the bandwidth of the signal and applying matched filter processing as described below.

The bandwidth of a pulsed signal emitted by a system is inherently finite (i.e., non-zero bandwidth). The bandwidth can be exploited to further reduce the signal duration through signal processing such as matched filter processing where the received echo is cross correlated with a replica signal such as the transmitter waveform. This processing, which is sometimes referred to as “pulse-compression” processing, can shorten the duration of the processed echo down to the

Long narrowband vs short broadband signals

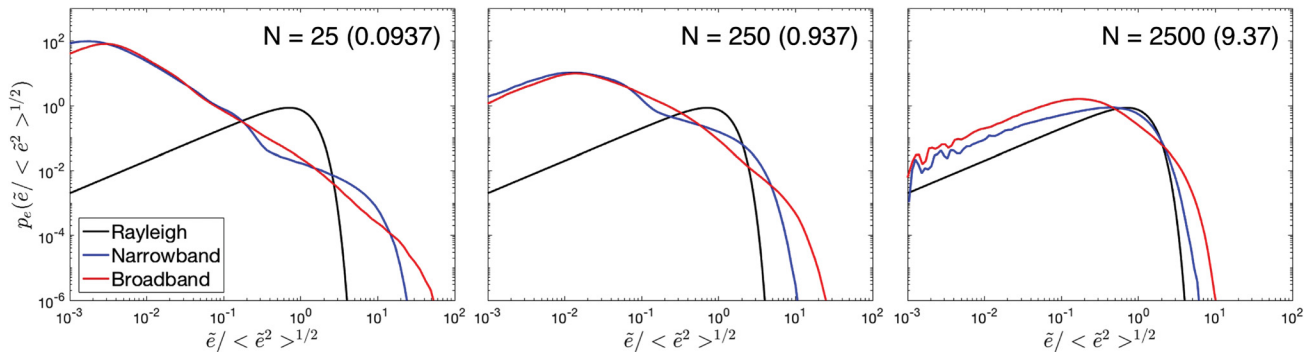


FIG. 23. (Color online) Comparisons between the PDFs of the echo magnitudes associated with long narrowband and short pulsed broadband signals with three cases of multiple scatterers. The broadband signal has an octave bandwidth centered about the frequency of the narrowband signal. The spectrum of the broadband signal has a constant value within the band and is equal to zero outside the band. The N Rayleigh scatterers are identical with the same mean and are randomly and uniformly distributed in a thin hemispherical shell. The narrowband signals are long enough so that the echoes completely overlap while, in contrast, there is generally only partial overlap between the echoes from the short broadband signals. The echo from the broadband signal is temporally compressed through matched filter processing so that its duration is approximately equal to the inverse of the bandwidth of the signal. Predictions for both the narrowband and broadband cases involve Monte Carlo simulations (10^6 realizations) in the time domain as illustrated in Fig. 22 and given in detail in Lee and Stanton (2015). In the simulations, the scattering amplitude of each scatterer (via Rayleigh PDF), time of return, and location in the beam pattern are randomized. The beam pattern is due to a circular aperture with $ka_T = 44.2511$ at the narrowband frequency and the center frequency of the broadband signal. The width of the mainlobe (-3 to -3 dB; defined in Table I) of the composite (two-way) beam pattern is 3.0° for $ka_T = 44.2511$. The value given in parentheses after the value of N is the number of scatterers within the main lobe of the 3.0° beam, as discussed in Table I. The width of the main lobe across all frequencies of the broadband signal varies from 2.1° to 4.2° . Note that these curves are qualitatively similar to the octave-band simulations in Fig. 3(b) of Lee and Stanton (2015) where the spectrum of the broadband signal is non-uniform due to the non-uniform transducer response. The software used to produce this figure is in the supplementary material at <https://doi.org/10.1121/1.5052255>. The software is also stored online (Lee and Baik, 2018), where it is subject to future revisions.

limit of the inverse bandwidth (Turin, 1960). In the common case in which the transmitter waveform is used as a replica, the cross-correlation between that signal and the echo (which contains the response of the system and scatterer) normally deviates from the autocorrelation function of the replica and that theoretical limit is never fully achieved. Either way, whether an ideal or practical waveform is used as a replica, generally the broader the bandwidth, the shorter the processed echo and, correspondingly, the finer the along-range resolution of the system becomes.

Because of the improvement in resolution of the compressed pulse, there will generally be even fewer scatterers in an aggregation contributing to a given (processed) echo than in the original pulsed signal which, in turn, can further increase the degree to which the echo is non-Rayleigh. This effect is particularly relevant to operational systems, as bandwidth is commonly increased in order to improve image resolution and signal-to-noise ratio (Gillman, 1997; Abraham and Lyons, 2002a,b; and Lee and Stanton, 2015).

Predicting the echo PDF for pulsed systems is complex. Generally, the system response is nonuniform across the frequency band, the transmitted signal is shaped in time and further modulated by the system response, and the echoes from the individual scatterers will only partially overlap, if at all. And, as indicated above, the broader the bandwidth, the less the echoes from the scatterers will overlap after pulse-compression processing, adding to the challenge of modeling the echo PDF.

Because of the complexity, treating the problem through a numerical, rather than analytical, approach may be best. In a recent study by Lee and Stanton (2015), a broadband pulsed system was simulated (Fig. 22). Parameters of the simulations were based on a known commercial system. The bandwidth of the system was roughly one octave (i.e., the upper frequency was approximately twice the lower frequency) and the system response was nonuniform (varying by more than 10 dB across the band). The transmission signal was linear frequency modulated (a “chirp”) across the band and the echoes were processed with matched filter processing, using the signal applied to the transmitter transducer as the replica. Key to the simulations was numerically convolving the applied signal with the system response (including frequency dependence of transducer and frequency dependence of beam pattern), convolving the resultant outgoing signal with the scatterer response, and delaying the echo from each randomized scatterer by a time that was randomized. The envelope of the matched filtered echo was sampled in the middle of the sample window (Fig. 22). The envelope was calculated using a Hilbert transform. The results of those simulations are illustrated in Figs. 2–5 of Lee and Stanton (2015) where direct comparisons are made between narrowband and broadband effects (Rayleigh scatterers), Rayleigh scatterers and randomly oriented rough prolate spheroids (broadband), and monotype and mixed assemblages of different types of scatterers (broadband).

In this tutorial, some of the simulations in Lee and Stanton (2015) are reproduced, but with the simplification of replacing the signal and system response that was specific to

a particular commercial system with a simple octave-bandwidth signal whose spectrum is uniform over the band. A different set of number of scatterers is also used. The echo PDFs illustrated in Fig. 23 of this tutorial are qualitatively similar to those predicted in Fig. 3(b) in Lee and Stanton (2015). Note that, as with some of the previous simulations, the “noisy” characteristic in portions of some of the plots of PDF in this figure are due to the relatively low number of realizations in the Monte Carlo simulations that were within those particular log-spaced magnitude bins (i.e., when both p_e and $\tilde{e}/\langle\tilde{e}^2\rangle^{1/2}$ are low).

The results of both sets of simulations in Lee and Stanton (2015) and this tutorial show that for any given set of parameters, the echo PDF of the broadband pulsed signal (after pulse-compression processing) deviates much more from the Rayleigh PDF than the corresponding PDF associated with a long single-frequency signal whose frequency is at the center of the spectrum of the broadband signal. This increase in the non-Rayleigh nature of the pulsed signal is due to the fact that the echoes are generally only partially overlapping or not overlapping, which reduces the number of effective scatterers whose echoes interfere with each other.

It is important to note that the echo was sampled in both sets of simulations at a single fixed point since this is an analysis involving first-order statistics, which is the focus of this tutorial. The analysis presented in this tutorial for Fig. 23 maintains generality and is not specific to any particular system or signal processing algorithm. For systems that involve a sampling method more advanced than sampling a single point, such as sampling a peak value within a sample window, the results in this tutorial can serve as a basis for modeling those methods, as discussed in Sec. VB.

B. Object near a rough boundary

When the scatterer of interest is close enough to a boundary so that echoes from the object overlap with echoes from the boundary, there will be interference between the two sets of echoes. In addition, there will be signals (and associated interference) involving secondary or “rescattered”

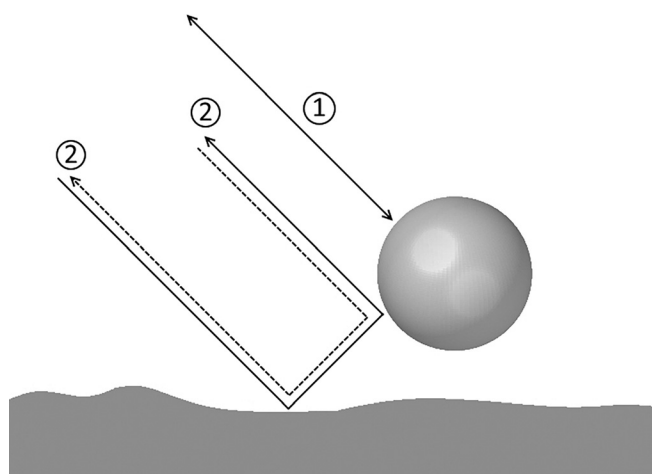


FIG. 24. Object near a rough boundary. The direction of propagation of the incident signal is at a shallow grazing angle relative to the boundary. Primary (1) and secondary (2) echoes are illustrated.

echoes following paths such as transmitter-boundary-scatterer-receiver and transmitter-scatterer-boundary-receiver (Fig. 24) (Williams *et al.*, 2010). Although some of the signal energy may be refracted into the boundary (for a penetrable boundary), these secondary echoes can be of comparable magnitude as the primary echoes that are directly from the scatterer. Accounting for these effects is specific to the particular geometry. One simple model is given below involving a single scatterer near a rough boundary with more complex solutions discussed.

The below treatment describes a simple model of the scattering involving use of rays. The statistics can be modeled by using an approximate ray-based method in which components of the echo are rays either involving scattering by the object (including object-boundary interaction) or by the boundary alone (not involving the object). The ray-based method is very intuitive and can lead to reasonable results over a wide range of important conditions. However, in general, the scattering in this complex geometry must be treated formally through various approaches involving solutions to the wave equation (Lim *et al.*, 2000; Zampolli *et al.*, 2008; Williams *et al.*, 2010). In those cases, the statistics can be formed through Monte Carlo simulations of the formal solutions.

One important geometry involves shallow grazing angles in which the incident signal is propagating in a direction nearly parallel to a rough boundary and the echo from the scatterer is comparable to or greater than that of the backscattered echo from the rough boundary (Fig. 24). The echo involving the object is the “signal” echo (i.e., echo of interest) and the boundary-alone echo is the “background” or noise-like echo. The magnitude of the total echo involves the coherent sum of the echoes from both the object and boundary,

$$\tilde{e} = \left| \sum_{i=1}^N \tilde{e}_i e^{j\Delta_i} + B e^{j\Delta} \right|, \quad (59)$$

where N is the number of rays that either involve a direct echo from the object or an echo involving interaction between the object and boundary. The terms \tilde{e}_i and Δ_i are the magnitude and phase shift, respectively, of the i th ray associated with the object. The terms B and Δ are the magnitude and phase shift, respectively, of the echo from the boundary only. Both \tilde{e}_i and B depend upon the beampattern. The term \tilde{e}_i is given by Eq. (7) (except that it represents the i th ray rather than the i th scatterer). The term B involves an integral of the beampattern, at constant range, over the boundary (Ogilvy, 1991).

All four of the terms in the right side of Eq. (59) are random variables. Since B is associated with diffuse scattering by the rough boundary, it is commonly assumed to be Rayleigh distributed. However, there is no restriction on its distribution and it could be, for example, K-distributed (Ferrara *et al.*, 2011) or one that is derived based on the scattering physics.

For the very simple case of a point scatterer near a rough boundary, an omnidirectional beam, no significant interactions between the scatterer and boundary ($N=1$), and a Rayleigh distributed echo from the boundary, the statistics of the echo magnitude in Eq. (59) can be described by the Rice PDF given in Eq. (26). The generalized K PDF, which

is conceptually similar to the Rice in that it involves a random signal with a preferred phase (such as due to the single scatterer in the presence of background reverberation), may also be used to approximate the echo statistics (Sec. VI A 3) (Jakeman and Tough, 1987; Ferrara *et al.*, 2011). For example, the generalized K PDF has been successfully used in an experimental study by Ferrara *et al.* (2011) to describe the statistics of radar echoes from ships and oil rigs on the sea surface (summary of their work in Sec. III A 2).

Beyond those simple scenarios with a closed-form solution such as the Rice and generalized K PDFs, the PDF of the magnitude of the echo in Eq. (59) generally must be determined numerically using physics-based methods. For example, once the directional characteristics of the beam are accounted for and the scatterer is now of complex shape and is randomly located in the beam, then the echo becomes a complex function of the sensor system and scatterer as described in Sec. VII and the problem may not have a closed form solution. In that case, the echoes from the rough boundary and scatterer are each (separately) non-Rayleigh. For these more general scenarios, the summation term in Eq. (59) can be determined through the phasor summation method using a scattering model of the rays associated with the object-boundary paths and the background term can be determined through a scattering model of the boundary alone. The two terms can be summed coherently for each realization, and an ensemble of realizations is calculated to form the echo PDF.

The method of characteristic functions, as described in Sec. IV C 5, may also be useful, especially if one or both terms in Eq. (59) has an assumed PDF. For example, it is common to assume a known statistical function (such as the Rayleigh or K PDF) for the echo from the boundary alone. In this case, the PDF associated with the summation term in Eq. (59) can still be determined using the phasor summation method. Assuming that the two terms within the absolute value sign in Eq. (59) are independent of each other and have random phase, the problem is reduced to the sum of two random complex independent variables whose individual PDFs (magnitude) are known.

C. Object(s) in a random waveguide

When a signal travels long enough distances, variability in the environment can play a significant role in the

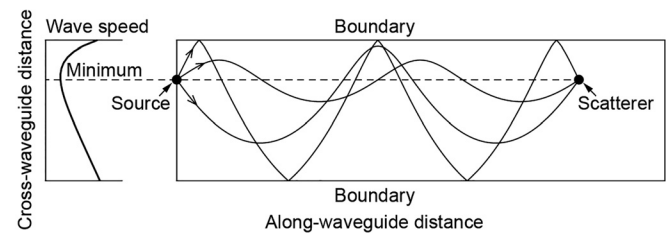


FIG. 25. Object in a waveguide. The signal propagates a long distance in the waveguide due to any combination of interacting with the boundaries and undulating about a minimum (when present) in wave speed. Although the waveguide illustrated involves physical boundaries and wave speed minimum, a similar scenario can occur without boundaries, but with the minimum in wave speed remaining (and corresponding undulations) that “traps” much of the signal energy within imaginary boundaries.

propagation. The presence of boundaries and heterogeneities in the medium will redirect the signal through various reflection, refraction, and scattering processes. In the case involving two parallel planar boundaries of infinite extent, a waveguide is formed, and a signal will naturally reflect repeatedly within the two boundaries as it travels along the length of the waveguide (Fig. 25). Under other conditions and without the presence of boundaries, variations in the medium can cause the signal to be “trapped” within an *effective* waveguide. In this latter case, there would be a cross-waveguide profile of wave speed that reaches a local minimum and the signals will undulate about that minimum through refraction (Snell’s Law) (Fig. 25). The space between the imaginary boundaries within which the signal undulates is also referred to as a waveguide. In some geometries, the propagation in an effective waveguide is further affected by the presence of one or more real boundaries and there can be repeated interaction with at least one of the boundaries every cycle of undulation (Fig. 25). Further complicating the propagation in all of the above cases, random variations of the surfaces (such as roughness) and of the properties of the medium (such as wave speed) will tend to randomize the phase of each ray. In general, in any waveguide, there are multiple rays due to multiple paths, and corresponding interference between the rays. Because of the inherent randomness of the natural environment, this interference will vary, causing ping-to-ping fluctuations.

For the case in which one or more objects of interest are in a waveguide (whether it involves real or imaginary boundaries), description of the signals incident upon the object(s) and receiver of the sensor system is quite complex. The signals will generally be random variables due to the variable nature of the waveguide that occurs naturally in the environment. There is a vast literature on this topic concerning both acoustic and electromagnetic fields and, because of the complexity, will generally require numerical modeling of both the random propagation and scattering. For example, fluctuations of signals due these phenomena, in general (any medium and type of field), are described in [Jakeman and Ridley \(2006\)](#). Formulations specific to sonar in the ocean and reviews of the literature are in [Jones et al. \(2014\)](#) and [Colosi \(2016\)](#). Analyses specific to wave propagation through the turbulent atmosphere (acoustics and electromagnetic) are given in [Tatarski \(1961\)](#). The modeling and measurements of propagation and bistatic scattering of medical ultrasound signals through tissue, treated as a continuous random medium, are reviewed by [Waag \(1984\)](#).

1. Some simple formulations

Several simple examples adapted from [Jones et al. \(2014\)](#) are described below to illustrate some of the interference phenomena associated with propagation and scattering in a real or effective waveguide. For simplicity, all examples are for long single-frequency signals (that is, echoes from all scatterers completely overlap).

The one-way propagation of a signal through a “frozen” waveguide due to a point source can be modeled through the simple equation

$$S_{inc}(\mathbf{R}) = H(\mathbf{R})S_{source} \quad (\text{one-way propagation}), \quad (60)$$

where $S_{inc}(\mathbf{R})$ is the (complex) signal in the waveguide incident at a scatterer at a location \mathbf{R} due to a source that is at the origin (Fig. 25), $H(\mathbf{R})$ is the transfer function of the waveguide between the source and location \mathbf{R} , and S_{source} is the source signal in the medium referenced to one meter from the source. Here, the “signal” in the medium could be a pressure or electromagnetic wave associated with an acoustic or electromagnetic sensor system, respectively. The term H is a function of the waveguide properties which include spatial variability of the wave speed and, when physical boundaries are present, material properties of the boundaries relative to those of the medium, and boundary roughness. Although generally the properties of waveguides can change temporally, this waveguide is considered “frozen” for simplicity, in that any temporal changes are considered negligible during the time of two-way propagation of the signal.

The transfer function can be written as the product of its magnitude $H_0(\mathbf{R})$ and an exponential term containing its phase shift δ ,

$$H(\mathbf{R}) = H_0(\mathbf{R})e^{j\delta} \quad (\text{one-way waveguide response}). \quad (61)$$

For an arbitrary spatial distribution of N scatterers within the waveguide at distances from the source much greater than the thickness of the waveguide, the magnitude of the echo received through two-way propagation due to a directional sensor system is

$$\tilde{e} = \left| \sum_{i=1}^N H_0^2(\mathbf{R}_i) |f_{bs}^{(i)}| b(\phi_i) e^{j\Delta_i} \right| \quad (\text{arbitrary distribution of scatterers}), \quad (62)$$

where the thickness of the waveguide is defined as the separation between the boundaries or, in the case of an effective waveguide with no physical boundaries, the amplitude of the undulation of the signal. The source level from Eq. (60) has been suppressed, as with all analyses earlier in this tutorial. In this two-way propagation, the square of the one-way transfer function is used due to the reciprocity of the waveguide. The term b is the two-way composite beam pattern due to the product of the directivity of the co-located source and receiver. As with Eq. (6), for simplicity in this formulation, all phase shifts associated with the i th scatterer are in the term Δ_i , which includes those due to the two-way propagation of the signal, the scatterer, and beamformer. For wavelengths of the acoustic/electromagnetic signal that are small compared with the differences in the along-range distances between the scatterers, Δ_i will generally be randomly and uniformly distributed in the range $[0, 2\pi]$ for randomly distributed scatterers.

At these great distances, generally only rays in a narrow range of angles within the plane normal to the waveguide boundaries (real or effective) and propagating nearly parallel to the boundaries will contribute to the signal at location \mathbf{R} . To simplify the formulation, those contributing rays are accounted for in the transfer function. As a result, the beam pattern at

these great ranges varies only in the azimuthal direction (the angle ϕ varies in the plane parallel to the boundaries). Because of the multiple rays that remain within the waveguide, the signal still varies as a function of distance from a boundary at these ranges. The scatterers described in Eq. (62) are arbitrarily distributed within the waveguide at arbitrary cross-waveguide and along-waveguide distances and location in the beampattern. In addition to being far from the source, the scatterers are assumed to be far enough from any boundary so that the scattering process does not significantly involve the proximity of a boundary (i.e., free field scattering is assumed).

Predicting the PDF of the echo for the arbitrary distribution of scatterers in Eq. (62) involves randomizing the location, scattering amplitude (as discussed previously), location in the beampattern, and phase. The resultant summed phasors are calculated for an ensemble of realizations resulting in the PDF for the magnitude of the echo.

At these large distances, the patch of scatterers may be small enough so that they all occur within a narrow range of azimuthal angles. In this geometry, the beampattern dependence can be taken out of the summation,

$$\tilde{\epsilon} = b(\phi) \left| \sum_{i=1}^N H_0^2(\mathbf{R}_i) |f_{bs}^{(i)}| e^{j\Delta_i} \right|$$

(patch within narrow range of azimuthal angles).

(63)

The expression can be further simplified for patches that are smaller than the correlation length of the waveguide. In this case, the magnitude of the waveguide transfer function is approximately constant within the small patch of scatterers and the function can be taken out of the summation

$$\tilde{\epsilon} = b(\phi) H_0^2(\mathbf{R}) \left| \sum_{i=1}^N |f_{bs}^{(i)}| e^{j\Delta_i} \right|$$

(patch smaller than correlation length).

(64)

The validity of the above phasor sum formulation to model echo statistics associated with scatterer(s) in a waveguide has been tested over a range of conditions in simulation and experimental studies in Jones *et al.* (2014) and Jones *et al.* (2017), respectively. In Jones *et al.* (2014), propagation and scattering of sound in ocean waveguides of various complexities were simulated using the PE (parabolic equation) and compared with the phasor summation method. In Jones *et al.* (2017), the analysis was extended to experimental data involving use of a directional long-range sonar to detect and classify aggregations of fish in an ocean waveguide. In this latter experimental study, random noise was added coherently to the phasor summation to simulate system noise and background reverberation to fit the low magnitude portion of the PDFs of the experimental echo data. In both studies, it was demonstrated that there was generally reasonable agreement (but with some departures) between the predictions of the echo magnitude PDF using the phasor summation and both the PE simulations and experimental data as a function of range in which there were both convergence and shadow zones present, and as a function of number of scatterers present.

In Jones *et al.* (2014), it was noted that the transfer function $H_0(\mathbf{R})$ of the waveguide should, in principal, be determined through numerical methods using formulations such as the PE. However, all applications of the phasor summation method in both papers by Jones *et al.* used limiting closed-form analytical forms of $H_0(\mathbf{R})$, which assumed the waveguide to be fully saturated, as discussed below. Although those solutions were based on a saturated waveguide, the phasor summation method using those limiting forms were reasonably successful, as noted above, as a function of range where the waveguide was not saturated.

The echo magnitude PDFs modeled through use of the phasor summation method were also shown to generally outperform the use of best-fit K PDFs (Figs. 15 and 16 of Jones *et al.*, 2014). A key element to the success of the phasor summation method was its ability to predict effects due to the directional sonar.

2. Closed form solutions for limiting cases involving a saturated waveguide

Regardless of simplification, calculation of the magnitude of the echo and its PDF will generally involve numerically determining the random phasors for an ensemble of realizations. However, there are some important cases which one can solve analytically or at least formulate into a closed-form solution (Jones *et al.*, 2014). For example, at sufficiently large ranges and associated multiple paths within the waveguide, the signal at location \mathbf{R} is “saturated” in that it can be described as the summation of many random phase $[0, 2\pi]$ signals. In this limit, the magnitude of the signal at location \mathbf{R} is Rayleigh distributed. Since the square of a Rayleigh distributed signal is exponentially distributed, then the square of the transfer function $H_0^2(\mathbf{R})$ is exponentially distributed.

In the case of the saturated waveguides, four examples are given below involving patches of scatterers smaller or larger than the correlation length of the waveguide and those patches either being fixed at a constant azimuthal angle or randomly distributed azimuthally across the entire beampattern. As discussed previously, simulations applying the phasor summation using these limiting solutions to signals in a realistic waveguide as a function of range are given in various figures in Jones *et al.* (2014) and Jones *et al.* (2017). The limiting solutions for different scenarios are also summarized in Table III of Jones *et al.* (2014).

a. Small patch of scatterers. For the case in which the patch of scatterers is smaller than the correlation length of the waveguide [Eq. (64)] and there are a large number of scatterers, each with echoes that have a random phase $[0, 2\pi]$, the magnitude of the summed expression in Eq. (64) is Rayleigh distributed. For a patch subtended by a narrow range of azimuthal angles so that $b(\phi)$ can be considered approximately fixed, then the statistics of the echo magnitude are determined by the product of the two random variables, $H_0^2(\mathbf{R})$ and the magnitude of the summed expression, whose distributions are exponential and Rayleigh, respectively. If that same patch is now randomly distributed

azimuthally, the product has a third random variable $b(\phi)$ as a factor, whose statistics are described by the beam pattern PDF given previously. PDFs of the above products of random variables can be derived using the closed-form expression in Sec. IVC 4.

b. Extended patch of scatterers. In another case when the patch of scatterers is larger than the correlation distance of the (saturated) waveguide, the transfer function remains in the summation [Eq. (63)]. For a large number of scatterers, each with echoes that have a random phase $[0, 2\pi]$, then the magnitude of the summed term in Eq. (63) is Rayleigh distributed. For the patch subtended by a narrow range of azimuthal angles so that $b(\phi)$ can be considered to be approximately fixed, then the magnitude of the echo is Rayleigh distributed. However, if the patch is randomly distributed azimuthally, then the echo is the product of the two random variables, $b(\phi)$ and the magnitude of the summed term, whose distributions are the beam pattern PDF and Rayleigh PDF as described previously, respectively. Section IVC 4, again, provides a closed form solution for the product of these two random variables.

IX. DISCUSSION AND CONCLUSIONS

There has been much success over the years across various types of sensor systems and applications in fitting generic statistical models to experimental echo data. However, since parameters of these models are not explicitly related to parameters of the sensor system, environment, or scattering process, the models are generally not predictive. Thus, a model fitted to experimental data within one scenario may not necessarily apply to another.

The use of physics-based models addresses this issue as these models are derived from physical principles and are predictive over a wide range of conditions. Parameters of the echo statistics formulas derived from this approach are explicitly related to parameters of the sensor system, environment, and scattering process. For example, for a given sensor system and scattering geometry, the shape parameter of the echo PDF is shown to be a direct function of beamwidth, type of signal, type of scatterer, and number of scatterers. These relationships between parameters are useful over a range of applications, from making inferences of scatterer characteristics from parameters of measured echo statistics data to understanding errors or uncertainties in predictions of signals that propagate through, and scatter in, a random or changing environment.

This tutorial presents many of the important concepts and formulas associated with physics-based echo statistics methods. Key formulas and illustrations of the major concepts are given, beginning with simple deterministic equations describing the scattering physics and properties of the sensor system. While all examples involved a sensor system with an axisymmetric beam pattern and a uniform distribution of scatterers, the formulations were general enough (with some explicitly given) to accommodate a non-axisymmetric beam pattern and non-uniform distribution of scatterers. Also, while the material focused

principally on the simple direct-path geometry using single-frequency signals that are long enough for significantly overlapping echoes and a homogeneous medium, cases were also presented involving short pulsed signals (narrowband and broadband) in which the echoes would only partially overlap, as well as geometries where the scatterer was near a boundary or in a waveguide and the medium was heterogeneous. Finally, discussions are given on how to extend these formulations to more complex environments and signal processing.

All formulations involved scalar fields applicable to both acoustic and electromagnetic phenomena. The general concepts involving scalar fields presented herein can also be applied or extended to cases involving elastic effects (shear waves in acoustics) and polarization (electromagnetic signals such as radar and laser).

An important aspect of the echo statistics is the degree to which the statistics deviate from the commonly used Rayleigh PDF. The non-Rayleigh nature of the statistics was shown to depend strongly upon the beamwidth, type of signal, type of scatterer, and number of scatterers. For example, the echo would become more non-Rayleigh under one or more of the following conditions: (1) the beamwidth is decreased, (2) the signal is shortened, (3) the number of scatterers is decreased, and/or (4) the type of scatterer is changed from one type of scatterer to another (such as from a point scatterer to a randomly oriented prolate spheroid).

In conclusion, regardless of complexity, the most accurate and predictive approach in modeling echo statistics requires beginning with a physical model of the sensor system, environment, and scattering process. The random nature of the parameters associated with the sensor system, environment, and scatterers can then be incorporated into the physical model and directly related to parameters of the statistical model of the echoes. The approach presented here progressed from deterministic solutions of the wave equation, randomizing the parameters of the solutions, to ultimately predicting the statistical nature of the echo. Through this physics-based approach, echo statistics can be predicted over a wide range of important conditions, as illustrated in this tutorial.

ACKNOWLEDGMENTS

The content of this work is based on research conducted in the past from years of support from the U.S. Office of Naval Research and the Woods Hole Oceanographic Institution, Woods Hole, MA. Writing of the manuscript by W.-J.L. was also supported by the Science and Engineering Enrichment and Development Postdoctoral Fellowship from the Applied Physics Laboratory, University of Washington, WA. The authors are grateful to Dr. Benjamin A. Jones of the Naval Postgraduate School, Monterey, CA for his thoughtful suggestions on an early draft of the manuscript. The authors are also grateful to the reviewer for the in-depth and constructive recommendations. W.-J.L. and K.B. contributed equally to this work.

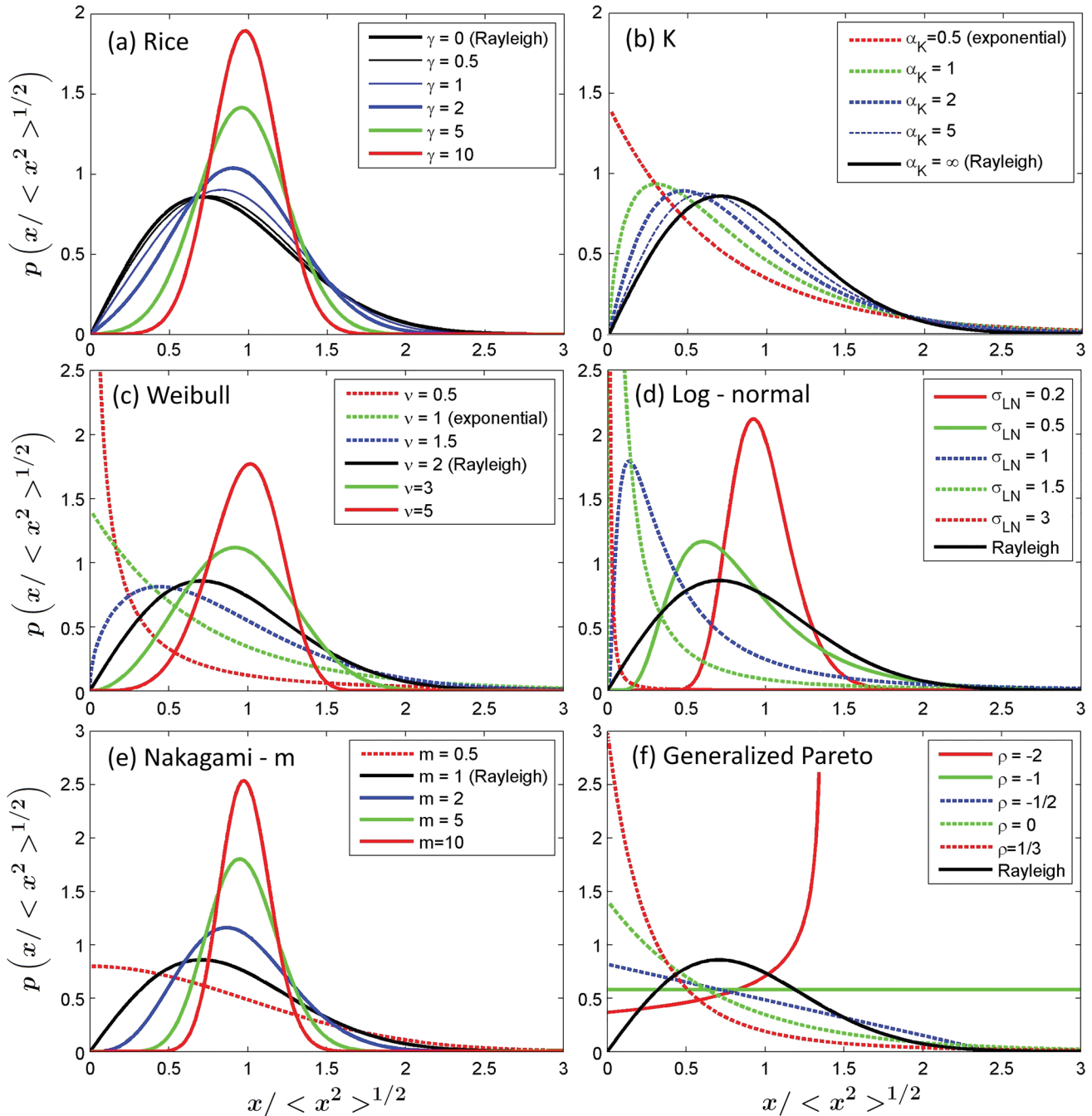


FIG. 26. (Color online) Comparison on a linear-linear scale between various generic PDFs commonly used to model echo magnitude statistics over a range of their shape parameters shown in the respective legends: (a) Rice, (b) K, (c) Weibull, (d) Log-normal, (e) Nakagami-m, (f) Generalized Pareto PDFs. The Rayleigh PDF is given in a thick solid black curve in each panel. The terms p and x are used to denote the PDF and its argument, respectively, for each of the different statistical functions. All curves are calculated using the analytical solutions given in the Appendix or main body of this tutorial. With each function plotted on a normalized scale, the curves are independent of the mean square magnitude of the signal and only depend upon their shape parameters (with the exception of the Rayleigh PDF which, once normalized, has no free parameters). The software used to produce this figure is in the supplementary material at <https://doi.org/10.1121/1.5052255>. The software is also stored online (Lee and Baik, 2018), where it is subject to future revisions.

APPENDIX: GENERIC OR COMMONLY USED STATISTICAL FUNCTIONS

As discussed in the main text, the majority of models used in various fields to describe echo statistics are generally not derived from first principals of scattering physics. However, for some of these “generic” models, there is some relation to the scattering, even if not direct, as they are connected to a Gaussian process. These include the Rayleigh,

Rice, K, Weibull, log normal, and Nakagami-m PDFs (Jakeman and Ridley, 2006; Destempes and Cloutier, 2010). Some of the commonly used PDFs are presented below. For completeness, the Rayleigh, Rice, and K PDFs are briefly summarized, with reference to their respective sections given above in which they are described in more detail. Intercomparisons between the below functions are in Figs. 26 and 27. Since there is not necessarily a rigorous connection between these PDFs and the magnitude of the

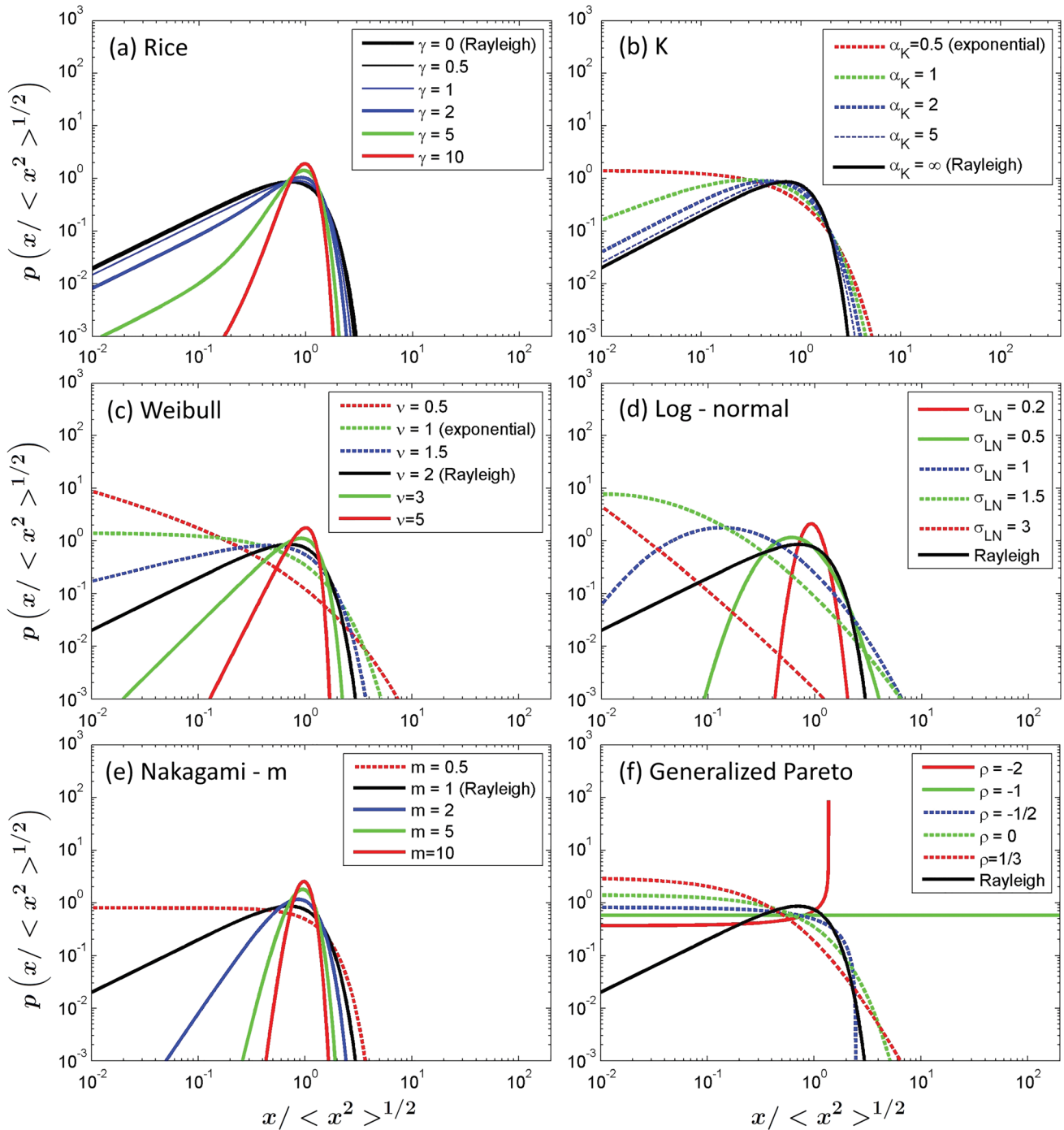


FIG. 27. (Color online) Same PDF curves as in Fig. 26, but on a logarithmic-logarithmic scale: (a) Rice, (b) K, (c) Weibull, (d) Log-normal, (e) Nakagami-m, and (f) Generalized Pareto PDFs. The software used to produce this figure is in the supplementary material at <https://doi.org/10.1121/1.5052255>. The software is also stored online (Lee and Baik, 2018), where it is subject to future revisions.

scattered signal, the term ψ (with subscript) is used to denote the argument of each PDF.

There are also a number of useful PDFs not presented below. For example, the Poisson-Rayleigh PDF (McDaniel, 1993; Fialkowski *et al.*, 2004), which involves a sum of Rayleigh PDFs weighted by the Poisson PDF. Also not presented, the following PDFs that can be described through compound representation are reviewed in Destempes and Cloutier (2010): Rician inverse Gaussian PDF (RiIG), generalized Nakagami, Nakagami-gamma (NG), and Nakagami-

generalized inverse Gaussian (NGIG). Here, the inverse Gaussian (IG) and generalized inverse Gaussian (GIG) PDFs are non-Gaussian functions with semi-heavy tails (Eltoft, 2006).

Considering the many types of generic PDFs that are applicable to echo statistics problems, Destempes and Cloutier (2010) have presented a unified review that describes many of these PDFs in terms of three key aspects of the compound representation: (1) the modulated distribution (Rice or Nakagami) whose parameters are

modulated by another distribution, (2) the modulating distribution (gamma, inverse Gaussian, or generalized inverse Gaussian) that is used to modulate one or more of the parameters of the modulated distribution, and (3) the modulated parameters (diffuse and/or coherent components) of the modulated distribution. See, for example, Table 2 of that paper that summarizes the three aspects for some of the PDFs.

1. Rayleigh PDF

In the limit of an infinite number of random phase sinusoids, the instantaneous amplitude (not magnitude) is a complex Gaussian in which both the real and imaginary components of the signal are Gaussian-distributed variables with the same variance. The magnitude of the instantaneous signal (i.e., its envelope) is Rayleigh distributed, whose equation is given in Eq. (21). In addition to being applied to modeling the statistics of white noise and, as discussed in Sec. IV C 6, this distribution can also be directly connected to the scattering physics in the case of a high number of scattering features whose echoes overlap and are of random phase (uniformly distributed $[0, 2\pi]$). The scattering features could be from multiple scatterers, a rough boundary, or an object with a complex shape or rough boundary.

2. Rice PDF

In the case of a single sinusoid of constant amplitude added to a signal whose magnitude is Rayleigh distributed, the magnitude of the instantaneous summed signal is Rice distributed, as given in Eq. (26). While originally developed to describe the statistics of a signal in the presence of white noise, it can also be directly related to the scattering physics. For example, as discussed in Sec. VIA 2, the constant signal could correspond to an individual scatterer of interest whose echo remains constant and the Rayleigh-distributed component could be the echo from a neighboring rough boundary or cloud of scatterers. In the limit of the scattering by the individual being strong or weak relative to the diffuse background scattering, the echo (Rice) PDF approaches a Gaussian or Rayleigh PDF, respectively.

3. K PDF

The K PDF, given in Eq. (29), can be derived several ways. Two approaches involve sums of sinusoidal signals: (a) when the number of sinusoids follows a negative binomial PDF and with the average number tending to infinity and (b) for a finite number of sinusoids whose amplitudes follow an exponential PDF. Two other approaches involve the “compound representation” that uses existing statistical functions where the K PDF can be derived from (c) the product of a Rayleigh-distributed random variable and a random variable that is chi distributed and (d) a Rayleigh PDF whose mean-square value is gamma distributed. Under certain limited conditions, the sinusoids in derivations (a) and (b) can be rigorously and directly related to the scattering physics by connecting the distribution of sinusoids to a corresponding

distribution of scatterers (whose echoes are convolved with the beampattern of the sensor system).

As discussed in Sec. VIA 3, the original K PDF is a two-parameter function and is associated with sinusoids with phases that are randomly and uniformly distributed $[0, 2\pi]$. The generalized K PDF (not shown) involves the more general case when the distribution of phases is not uniform and can be related to, for example, the echo from one or several large scatterers in the presence of an extended diffuse scatterer such as a rough boundary. This latter distribution, and a more restricted form (homodyned K PDF), have three parameters. While all of these K-based PDFs can be rigorously connected to the scattering physics under only a narrow range of conditions, these distributions have been demonstrated to reasonably fit experimental echo statistics data from objects and boundaries over a much wider range of conditions.

4. Weibull PDF

The distribution of intensity I_R (square of magnitude) of a Rayleigh-distributed random variable is a negative exponential PDF. Using the transformation $I_R = \psi_W^\nu$ yields the Weibull PDF

$$p_W(\psi_W) = \frac{\nu}{\lambda_R} \psi_W^{\nu-1} e^{-\psi_W^\nu/\lambda_R}, \quad (\text{A1})$$

where $\lambda_R = \langle I_R \rangle$ is the mean intensity of the original Rayleigh random variable as given in Eq. (21) (Jakeman and Ridley, 2006). This PDF for ψ_W , whose derivation involves a Gaussian process, has been used for both magnitude and intensity statistics. The PDF becomes a negative exponential (intensity-like) and Rayleigh PDF (magnitude-like) when ν is equal to 1 and 2, respectively. Furthermore, since the K PDF becomes a negative exponential when its shape parameter α_K in Eq. (29) is equal to 1/2, then the Weibull and K PDFs become the same PDF (negative exponential) when ν and α_K are equal to 1 and 1/2, respectively.

5. Log normal PDF

The log normal PDF involves a variable whose logarithm is Gaussian distributed. The magnitude ψ_{LN} can be written as $\psi_{LN} = Ce^x$ where x is Gaussian distributed with a mean and variance of zero and σ_{LN}^2 , respectively, and C is a constant. It follows that the PDF of ψ_{LN} is (Jakeman and Ridley, 2006)

$$p_{LN}(\psi_{LN}) = \frac{1}{\psi_{LN} \sqrt{2\pi\sigma_{LN}^2}} e^{-(\ln\psi_{LN} - \ln C)^2 / 2\sigma_{LN}^2}. \quad (\text{A2})$$

Although there is not a direct connection between this PDF and backscattering, the signal of a propagating field sometimes decreases exponentially, with x being a negative quantity in e^x above. The term x can be related to absorption and scattering-related loss of signal. The absorption and scattering may be variable, causing fluctuations or scintillation in the forward-propagating signal which, in turn, will result in fluctuations of the backscattered signal as it relates to the

local (fluctuating) value of the signal incident upon a scatterer. There will be additional fluctuations incurred in the backscattered signal as it propagates back to the sensor system. The PDF of intensity ψ_{LN}^2 takes on the same functional form as the above equation, but with different constant factors in the exponent (page 399 of [Goodman, 1985](#)).

6. Nakagami-m PDF (and related chi-squared and gamma PDFs)

The Nakagami-m, chi-squared, and gamma PDFs are related to each other, as they all involve incoherent processes in which the signal is composed of the incoherent addition (sum of squares) of m independent, Rayleigh-distributed variables. Or, equivalently, the signal is made up of the sum of the squares of $2m$ independent Gaussian-distributed variables. Although this incoherent process does not directly relate to a scattering process which involves the *coherent* sum of random variables (i.e., sum of complex signal), there has been success in using these PDFs to model echo statistics.

The Nakagami-m is concerned with the statistics of the magnitude of the signal whereas the chi-squared and gamma PDFs describe the PDF of the square (i.e., intensity) of the signal. The chi-squared PDF relates to an integer number of Rayleigh-distributed variables and the gamma PDF is an analytical continuation of that PDF for non-integer numbers of variables. The equations for all three PDFs have a similar form and are expressed in terms of a gamma function. This section will focus on the Nakagami-m PDF since it is most relevant to the magnitude statistics in this paper.

In this model, the random variable ψ_N is defined as the square root of the sum of the squares of m independent Rayleigh random variables. The resultant PDF of ψ_N is the Nakagami- m PDF ([Nakagami, 1960](#); [Karagiannidis et al., 2003](#); [Eltoft, 2006](#))

$$p_N(\psi_N) = \frac{2m^m \psi_N^{2m-1}}{\Gamma(m) \Omega^m} e^{-m\psi_N^2/\Omega}, \quad (\text{A3})$$

where Γ is the gamma function. The terms m and Ω are shape and scaling parameters, respectively, where $\Omega = \langle \psi_N^2 \rangle$. As with the gamma PDF, through analytical continuation, the term m can be a non-integer. And, as discussed above, while the Nakagami-m PDF is used to model fluctuations of signal magnitude, ψ_N does not rigorously represent the magnitude of the signal, as it is related to an incoherent (sum of squares), rather than a coherent (sum of complex variables) process associated with the scattering.

The Nakagami-m PDF reduces to the Rayleigh and “one-sided” Gaussian PDFs for $m = 1$ and $1/2$, respectively. Here, the one-sided Gaussian is a Gaussian PDF with its peak at an argument of zero and is only evaluated for non-negative values of argument. The Nakagami-m PDF also takes on qualitatively similar shapes to the Rice PDF for higher values of m (Nakagami-m) and γ (Rice) where both curves are Gaussian-like (Figs. 26 and 27). For example the Nakagami-m PDF, when calculated for the values $m = 3$,

3.9, and 5, looks similar to the Rice PDF when calculated for the values $\gamma = 5, 6.9, \text{ and } 9$, respectively (not shown).

7. Generalized Pareto PDF

The generalized Pareto PDF is based on extreme value theory, which focuses on either the minimum or maximum values of a signal ([Pickands, 1975](#); [La Cour, 2004](#)). In this case, the generalized Pareto PDF has been derived to describe the tails of the PDF (i.e., more than simply the maximum values). The generalized Pareto PDF is

$$p_{GP}(\psi_{GP}) = \frac{\left(1 + \frac{\rho \psi_{GP}}{\xi}\right)^{-(1/\rho)-1}}{\xi}, \quad (\text{A4})$$

where ρ and ξ are the shape and scale parameters, respectively. While this PDF is not specific to magnitude or intensity, this has been shown to successfully describe the tails of the intensity of non-Rayleigh echoes ([La Cour, 2004](#); [Gelb et al., 2010](#)). Note that this PDF can only be normalized for values of $\rho < 1/2$, otherwise the integration diverges. Also, when $\rho = -2$, the range of ψ_{GP} is limited to prevent the argument of the square root term from becoming negative above a certain value of ψ_{GP} .

- Abraham, D. A., Gelb, J. M., and Oldag, A. W. (2011). “Background and clutter mixture distributions for active sonar statistics,” *IEEE J. Ocean. Eng.* **36**(2), 231–247.
- Abraham, D. A., and Lyons, A. P. (2002a). “Reverberation envelope statistics and their dependence on sonar beamwidth and bandwidth,” in *Impact of Littoral Environmental Variability on Acoustic Predictions and Sonar Performance*, edited by N. G. Pace and F. B. Jensen (Kluwer Academic, Dordrecht, the Netherlands), pp. 539–546.
- Abraham, D. A., and Lyons, A. P. (2002b). “Novel physical interpretations of K -distributed reverberation,” *IEEE J. Ocean. Eng.* **27**(4), 800–813.
- Abraham, D. A., and Lyons, A. P. (2010). “Special issue on non-Rayleigh reverberation and clutter,” *IEEE J. Ocean. Eng.* **35**(2), 233–356.
- Agapiou, S., Paspaliopoulos, O., Sanz-Alonso, D., and Stuart, A. M. (2017). “Importance sampling: Intrinsic dimension and computational cost,” *Stat. Sci.* **32**(3), 405–431.
- Azzalini, A. (1996). *Statistical Inference Based on the Likelihood* (Chapman and Hall, London), Vol. 68, Chap. 3.
- Barakat, R. (1974). “First-order statistics of combined random sinusoidal waves with applications to laser speckle patterns,” *Opt. Acta* **21**, 903–921.
- Bhatia, S., Stanton, T. K., and Baik, K. (2015). “Non-Rayleigh scattering by a randomly oriented elongated scatterer randomly located in a beam,” *IEEE J. Ocean. Eng.* **40**(1), 169–176.
- Botev, Z. I., Grotowski, J. F., and Kroese, D. P. (2010). “Kernel density estimation via diffusion,” *Ann. Stat.* **38**(5), 2916–2957.
- Bowman, J. J., Senior, T. B. A., and Uslenghi, P. L. E. (1987). *Electromagnetic and Acoustic Scattering by Simple Shapes* (Hemisphere, New York).
- Chen, C.-C. (1998). “Electromagnetic resonances of immersed dielectric spheres,” *IEEE Trans. Ant. Propagat.* **46**(7), 1074–1083.
- Chu, D., and Stanton, T. K. (2010). “Statistics of echoes from a directional sonar beam insonifying finite numbers of single scatterers and patches of scatterers,” *IEEE J. Ocean. Eng.* **35**(2), 267–277.
- Clay, C. S. (1983). “Deconvolution of the fish scattering PDF from the echo PDF for a single transducer sonar,” *J. Acoust. Soc. Am.* **73**, 1989–1994.
- Colosi, J. A. (2016). *Sound Propagation Through the Stochastic Ocean* (Cambridge University Press, Cambridge).
- Crispin, J. W., Jr., and Siegel, K. M. (1968). *Methods of Radar Cross-Section Analysis* (Academic Press, New York).
- Destremes, F., and Cloutier, G. (2010). “A critical review and uniformized representation of statistical distributions modeling the ultrasound echo envelope,” *Ultrasound Med. Bio.* **36**(7), 1037–1051.

- Destrempes, F., and Cloutier, G. (2013). "Review of envelope statistics models for quantitative ultrasound imaging and tissue characterization," in *Quantitative Ultrasound in Soft Tissues*, edited by J. Mamou and M. Oelze (Springer, Dordrecht, the Netherlands), pp. 219–274.
- Devroye, L. (1986). "Inversion by numerical solution of $F(X) = U$," in *Non-uniform Random Variable Generation* (Springer-Verlag, New York), Sec. 2.2.
- Drumheller, D. M. (1999). "Padé approximations to matched filter amplitude probability functions," *IEEE Trans. Aerospace Electron. Syst.* **35**, 1033–1045.
- Eckart, C. (1953). "The scattering of sound from the sea surface," *J. Acoust. Soc. Am.* **25**, 566–570.
- Ehrenberg, J. E. (1972). "A method for extracting the fish target strength distribution from acoustic echoes," *Proc. Conf. Eng. Ocean Environ.* **1**, 61–64.
- Ehrenberg, J. E. (1989). "A review of target strength estimation techniques," in *Underwater Acoustic Data Processing*, edited by Y. Chan (Kluwer, Dordrecht, the Netherlands), pp. 161–175.
- Ehrenberg, J. E., Carlson, T. J., Traynor, J. J., and Williamson, N. J. (1981). "Indirect measurement of the mean acoustic backscattering cross section of fish," *J. Acoust. Soc. Am.* **69**, 955–962.
- Eltoft, T. (2006). "Modeling the amplitude statistics of ultrasonic images," *IEEE Trans. Med. Mag.* **25**, 229–240.
- Ferrara, G., Migliaccio, M., Nunziata, F., and Sorrentino, A. (2011). "Generalized-K (GK)-based observation of metallic objects at sea in full-resolution synthetic aperture radar (SAR) data: A multipolarization study," *IEEE J. Ocean. Eng.* **36**, 195–204.
- Fialkowski, J. M., Gauss, R. C., and Drumheller, D. M. (2004). "Measurements and modeling of low-frequency near-surface scattering statistics," *IEEE J. Ocean. Eng.* **29**, 197–214.
- Gallaudet, T. C., and de Moustier, C. P. (2003). "High-frequency volume and boundary acoustic backscatter fluctuations in shallow water," *J. Acoust. Soc. Am.* **114**, 707–725.
- Gelb, J. M., Heath, R. E., and Tipple, G. L. (2010). "Statistics of distinct clutter classes in midfrequency active sonar," *IEEE J. Ocean. Eng.* **35**, 220–229.
- Gillman, L. C. (1997). "First-order statistics of pulsed-sinusoid backscatter from random media: Basic elements of an exact treatment," *IEEE Trans. Ultrason. Ferroelectr. Freq. Control* **44**, 798–804.
- Goodman, J. W. (1985). *Statistical Optics*, 1st ed. (Wiley-Interscience, New York).
- Gurley, J. V., and Stanton, T. K. (1993). "Sound scattering by rough elongated elastic objects. III. Experiment," *J. Acoust. Soc. Am.* **94**, 2746–2755.
- Hackman, R. H. (1993). "Acoustic scattering from elastic solids," in *Physical Acoustics*, edited by A. D. Pierce and R. N. Thurston (Academic, New York), Vol. 22, pp. 1–194.
- Hogg, R. V., and Craig, A. T. (1978). *Introduction to Mathematical Statistics*, 4th ed. (Macmillan, New York).
- Jakeman, E., and Pusey, P. N. (1976). "A model for non-Rayleigh sea echo," *IEEE Trans. Antennas Propag.* **24**(6), 806–814.
- Jakeman, E., and Ridley, K. D. (2006). *Modeling Fluctuations in Scattered Waves* (Taylor and Francis, New York).
- Jakeman, E., and Tough, R. J. A. (1987). "Generalized K distribution: A statistical model for weak scattering," *J. Opt. Soc. Am.* **4**, 1764–1772.
- Jao, J. K., and Elbaum, M. (1978). "First-order statistics of a non-Rayleigh fading signal and its detection," *Proc. IEEE* **66**, 781–789.
- Jones, B. A., Colosi, J. A., and Stanton, T. K. (2014). "Echo statistics of individual and aggregations of scatterers in the water column of a random, oceanic waveguide," *J. Acoust. Soc. Am.* **136**, 90–108.
- Jones, B. A., Stanton, T. K., Colosi, J. A., Gauss, R. C., Fialkowski, J. M., and Jech, J. M. (2017). "Broadband classification and statistics of echoes from aggregations of fish measured by long-range, mid-frequency sonar," *J. Acoust. Soc. Am.* **141**, 4354–4371.
- Joughin, I. R., Percival, D. B., and Winebrenner, D. P. (1993). "Maximum likelihood estimation of K distribution parameters for SAR data," *IEEE Trans. Geosci. Remote Sens.* **31**, 989–999.
- Karagiannidis, G. K., Zogas, D. A., and Kotsopoulos, S. A. (2003). "On the multivariate Nakagami-m distribution with exponential correlation," *IEEE Trans. Commun.* **51**, 1240–1244.
- Kinsler, L. E., Frey, A. R., Coppens, A. B., and Sanders, J. V. (2000). *Fundamentals of Acoustics*, 4th ed. (Wiley, New York), Chap. 7.
- La Cour, B. R. (2004). "Statistical characterization of active sonar reverberation using extreme value theory," *IEEE J. Ocean. Eng.* **29**(2), 310–316.
- Le Chevalier, F. (2002). *Principles of Radar and Sonar Signal Processing* (Artech House, Boston).
- Lee, W.-J., and Baik, K. (2018). "leewujung/echo-stats-tutorial," <https://doi.org/10.5281/zenodo.1313729>.
- Lee, W.-J., and Stanton, T. K. (2014). "Statistics of echoes from mixed assemblages of scatterers with different scattering amplitudes and numerical densities," *IEEE J. Ocean. Eng.* **39**(4), 740–754.
- Lee, W.-J., and Stanton, T. K. (2015). "Statistics of broadband echoes: Application to acoustic estimates of numerical density of fish," *IEEE J. Ocean. Eng.* **41**(3), 709–723.
- Li, X., Xin, J.-Q., Donohue, K., and Bilgutay, N. M. (1992). "Rank determination of order statistic filters for ultrasonic flaw detection," in *Review of Progress in Quantitative Nondestructive Evaluation*, edited by D. O. Thomson and D. E. Chimenti (Plenum Press, New York), pp. 943–950.
- Lim, R., Williams, K. L., and Thorsos, E. I. (2000). "Acoustic scattering by a three-dimensional elastic object near a rough surface," *J. Acoust. Soc. Am.* **107**, 1246–1262.
- Marston, P. L. (1992). "Geometrical and catastrophe optics methods in scattering," in *Physical Acoustics*, edited by A. D. Pierce and R. N. Thurston (Academic, New York), Vol. 21, pp. 1–234.
- McDaniel, S. T. (1993). "Sea-surface reverberation fluctuations," *J. Acoust. Soc. Am.* **94**, 1551–1559.
- Medwin, H., and Clay, C. S. (1998). *Fundamentals of Acoustical Oceanography* (Academic, Boston).
- Moser, P. J., Murphy, J. D., Nagl, A., and Uberall, H. (1981). "Resonances and surface waves on conducting spheres with a dielectric coating," *Radio Sci.* **16**(3), 279–288, <https://doi.org/10.1029/RS016i003p00279>.
- Murphy, J. D., Moser, P. J., Nagl, A., and Uberall, H. (1980). "A surface wave interpretation for the resonances of a dielectric sphere," *IEEE Trans. Antennas Propag.* **AP-28**(6), 924–927.
- Nakagami, M. (1960). "The m-distribution—A general formula of intensity distribution of rapid fading," in *Statistical Methods in Radio Wave Propagation*, edited by W. C. Hoffman (Permagon, New York), pp. 3–36.
- Newton, R. G. (1982). *Scattering Theory of Waves and Particles* (Springer-Verlag, New York).
- Numrich, S. K., and Uberall, H. (1992). "Scattering of sound pulses and the ringing of target resonances," in *Physical Acoustics*, edited by A. D. Pierce and R. N. Thurston (Academic, New York), Vol. 21, pp. 235–318.
- Nussenzveig, H. M. (1969). "High-frequency scattering by a transparent sphere—Part I: Direct reflection and transmission, Part II: Theory of the rainbow and the glory," *J. Math. Phys.* **10**, 82–176.
- Oelze, M. L., and Mamou, J. (2016). "Review of quantitative ultrasound: Envelope statistics and backscatter coefficient imaging and contributions to diagnostic ultrasound," *IEEE Trans. Ultrason. Ferroelectr. Freq. Control* **63**, 336–351.
- Ogilvy, J. A. (1991). *Theory of Wave Scattering from Random Rough Surfaces* (Adam Hilger, Bristol).
- Ol'shevskii, V. V. (1978). *Statistical Methods in Sonar* (Consultants Bureau, New York).
- Papoulis, A. (1991). *Probability, Random Variables, and Stochastic Processes* (McGraw-Hill, New York).
- Pickands, J., Jr. (1975). "Statistical inference using extreme order statistics," *Ann. Statist.* **3**, 119–131.
- Rice, S. O. (1954). "Mathematical analysis of random noise," in *Selected Papers on Noise and Stochastic Processes*, edited by N. Wax (Dover, New York), pp. 133–294.
- Scott, D. W. (1992). *Multivariate Density Estimation: Theory, Practice, and Visualization* (Wiley, New York).
- Stanton, T. K. (1985). "Volume scattering: Echo peak PDF," *J. Acoust. Soc. Am.* **77**, 1358–1366.
- Stanton, T. K., and Chu, D. (1992). "Sound scattering by rough elongated elastic objects: II. fluctuations of scattered field," *J. Acoust. Soc. Am.* **92**, 1665–1678.
- Stanton, T. K., and Chu, D. (2010). "Non-Rayleigh echoes from resolved individuals and patches of resonant fish at 2–4 kHz," *IEEE J. Ocean. Eng.* **35**(2), 152–163.
- Stanton, T. K., Chu, D., Gelb, J. M., Tipple, G. L., and Baik, K. (2015). "Interpreting echo statistics of three distinct clutter classes measured with a midfrequency active sonar: Accounting for number of scatterers, scattering statistics, and beam pattern effects," *IEEE J. Ocean. Eng.* **40**, 657–665.
- Stanton, T. K., Chu, D., and Wiebe, P. H. (1998). "Sound scattering by several zooplankton groups II: Scattering models," *J. Acoust. Soc. Am.* **103**, 236–253.

- Stanton, T. K., and Clay, C. S. (1986). "Sonar echo statistics as a remote-sensing tool: Volume and seafloor," *IEEE J. Ocean. Eng.* **11**(1), 79–96.
- Tatarski, V. I. (1961). *Wave Propagation in a Turbulent Medium*, translated by R. A. Silverman (McGraw-Hill, New York).
- Tunis, A. S., Baddour, R. E., Czarnota, G. J., Giles, A., Worthington, A. E., Sherar, M. D., and Kolios, M. C. (2005). "Using high frequency ultrasound envelope statistics to determine scatterer number density in dilute cell solutions," in *Proceedings to IEEE Ultrasonics Symposium*, pp. 878–881.
- Turin, G. L. (1960). "An introduction to matched filters," *IRE Trans. Inf. Theory* **6**, 311–329.
- Uberall, H. (1973). "Surface waves in acoustics," in *Physical Acoustics*, edited by W. B. Mason and R. N. Thurston (Academic, New York), Vol. 10, pp. 1–60.
- Waag, R. C. (1984). "A review of tissue characterization from ultrasonic scattering," *IEEE Trans. Biomed. Eng. BME-13*, 884–893.
- Ward, K. D. (1981). "Compound representation of high resolution sea clutter," *Electron. Lett.* **17**(16), 561–563.
- Watts, S., and Ward, K. (2010). "Special issue on radar clutter," *IET Radar Sonar Nav.* **4**(2), 143–328.
- Williams, K. L., Kargl, S. G., Thorsos, E. I., Burnett, D. S., Lopes, J. L., Zampolli, M., and Marston, P. L. (2010). "Acoustic scattering from a solid aluminum cylinder in contact with a sand sediment: Measurements, modeling, and interpretation," *J. Acoust. Soc. Am.* **127**, 3356–3371.
- Zampolli, M., Tesei, A., and Canepa, G. (2008). "Computing the far field scattered or radiated by objects inside layered fluid media using approximate Green's functions," *J. Acoust. Soc. Am.* **123**, 4051–4058.